Reactivity of An Alkyl-substituted Al Anion

Kengo Sugita

Chapter 1

General introduction

1.1. Carbene and its analogue

Carbene is a carbon compound, which has two covalent bonds and one lone pair of electrons on the carbon center. The chemistry of carbene has been studied by today in a variety of research fields, such as physical organic chemistry, transition metal chemistry, main group chemistry, and synthetic organic chemistry.[1] The first example of an isolable carbene **A** was reported by Bertrand (Figure 1).[2a] Arduengo accomplished isolation and structural analysis of crystalline diamino-substituted cyclic carbene **B**,[2b] which can be easily prepared and is now commercially available. Subsequent efforts by Bertrand afforded cyclic (alkyl)(amino)carbene **C**,[2c] which has a higher σ-donating and π-accepting properties than those of diaminocarbene **B**, because the electropositive carbon atom could donate electrons to carbon center strongly and gives π-acceptor character on the carbon center of **C**. Recently, mono-substituted carbene **D** was isolated by using a bulky amino group bearing four CF_3-substituted terphenyls.[2d]

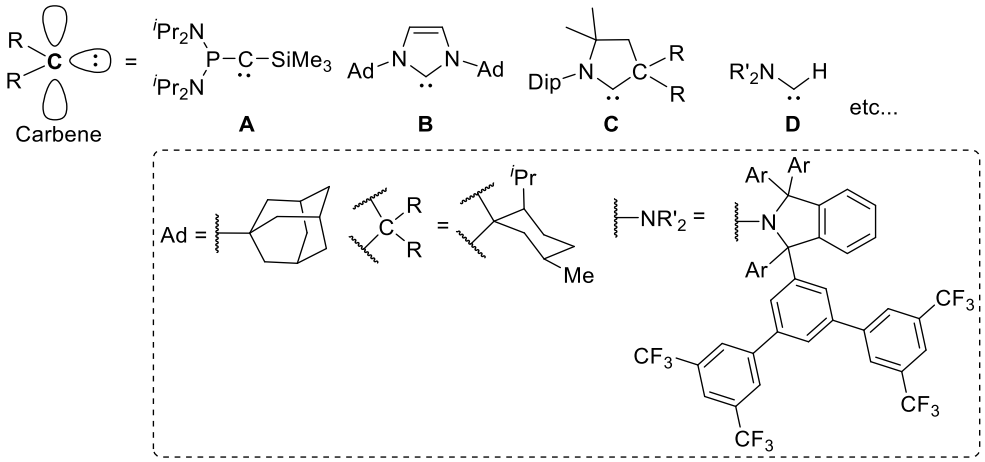

Figure 1. Selected examples of isolable carbene

In contrast to carbene family, their isoelectronic compounds made by a replacement of the carbon atom in carbene to other main group element are called "carbene analogues". For example, silicon-substituted carbene analogues are called silylene. Chemistry of isolable silylenes has been studied for their reactivity and photophysical properties.[3a-c] Since the group 13 elements have three valence electrons in contrast to that the group 14 elements have four, neutral group 13 element-substituted carbene analogues should have one lone pair of electrons, one covalent bond, and one coordination bond to construct six-electrons species, for example, base-stabilized borylene and alumylene.[3d] There are no report for the isolation of base-stabilized borylene having six electrons,[4] however, base-stabilized alumylene **E** has been synthesized.[5] In case of that the group 13 elements have two covalent bonds and one lone pair of electrons, they should have a negative charge on the element center to form anionic species, such as boryl and alumanyl anion (*vide infra*). These group 13 element-based anionic species have been isolated as a salt with cationic metal.

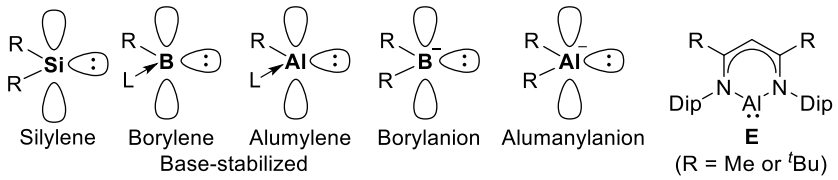

Figure 2. Carbene analogues

1.2. Introduction: Anionic group 13 carbene analogues

Anionic group 13 carbene analogues were isolated as salts with cationic alkali metals (Figure 3). These species are classified into (i) diamino-substituted 6-electron species (**Type-A**) and (ii) 8-electron species supported by Lewis base(s) (**Type-B**). In **Type-A** species, two nitrogen atoms attached to the main group center stabilized these species by their π-donating and σ-accepting character. Gallyl anion **1** is the first example of anionic group 13 carbene analogue and it was prepared by two-electron reduction of the corresponding halogenated precursor.[6] After that, boryl anions (**2**[7a-c], **3**[7d]), an indyl anion (**4**[8]), and alumanyl anion dimers (**5**[9a], **6**[9b]) were isolated by similar procedures. The 8-electron boryl and alumanyl anions shown in **Type-B** were synthesized by a complexation with Lewis base to occupy the vacant orbital on the boron or aluminum center (**7**-**14**)[10, 11]. In contrast to the anionic group 13 carbene analogues in **Type-A** and **Type-B**, Yamashita group accomplished the synthesis of dialkyl-substituted alumanyl anion **15**,[12] which is a new class of compounds apart from **Type-A** and **Type-B**.

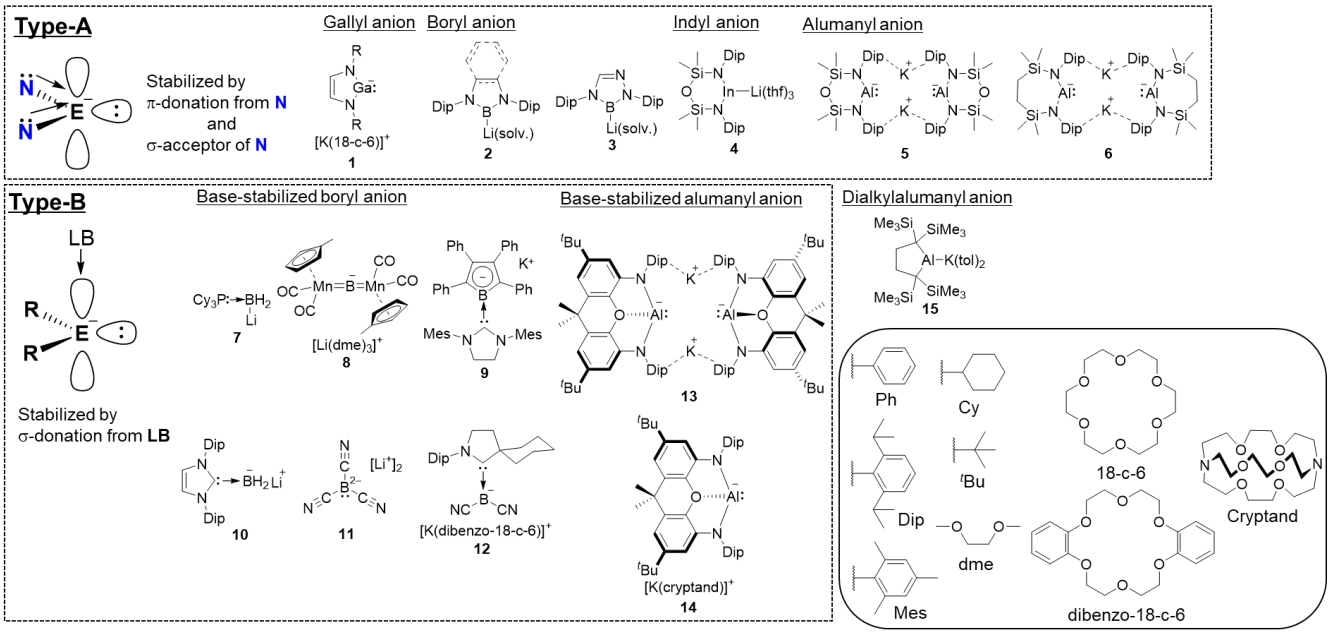

Figure 3. Group 13 element anionic species

1.3. Reactivity of group 13 anion species

The group 13 element anion species behaves as a nucleophile and a Brønsted base. Reactions of diaminoboryllithium **2** with electrophiles, such as benzaldehyde, benzoyl chloride, methyl trifluoromethanesulfonate, hexafluorobenzene, and carbon dioxide, gave the corresponding organoboron compounds **16**-**20** (Scheme 1), while a halophilic attack of **2** toward BnBr took place to afford bromoborane **21**.[7b]

Scheme 1. Reactivity of **2** with organic compounds

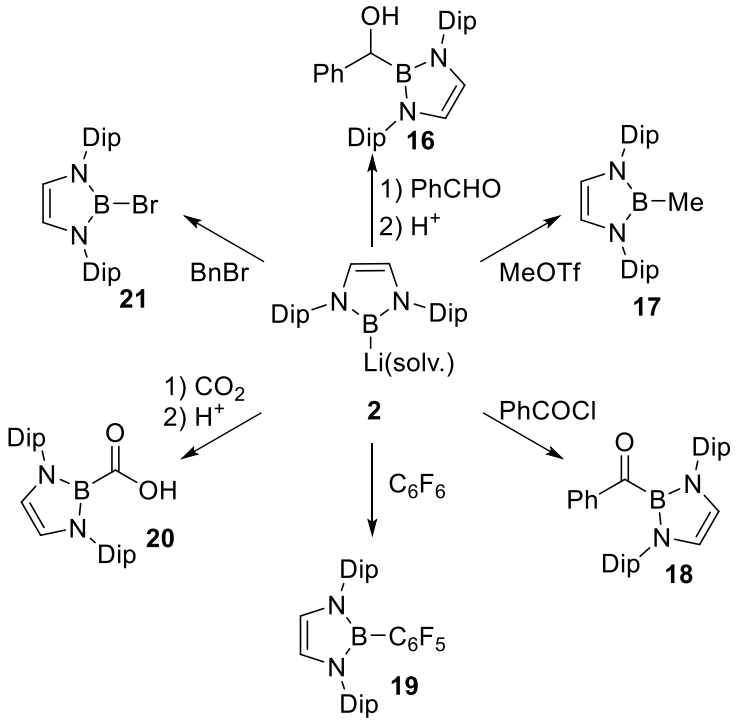

Transition metal-boryl complexes, where the transition metal bonds to boron atom, were important class of compounds in synthetic organic chemistry and transition metal chemistry. For example, they worked as catalysts for borylation reaction of unactivated substrates and nucleophilic boron reagents.[13] However, the synthetic methods for transition metal-boryl complexes were limited to the following four types (Scheme 2); (i) nucleophilic attack of ate complexes toward boron electrophiles,[14] (ii) oxidative addition of X–[**B**] (X = halogen, hydride, and boron) toward low-oxidation state metal center,[15] (iii) photo-induced metathesis reaction of methyl-substituted metal complexes with hydroborane,[16] (iv) oxygen atom-assisted metathesis reaction between metal alkoxide and diborane(4).[17] One can expect that a nucleophilic substitution of metal halide with boron nucleophiles would be a potential method to form boryl-substituted transition metal complexes (Scheme 2 (v)).

Scheme 2 Strategies for the synthesis of transition metal boryl complexes

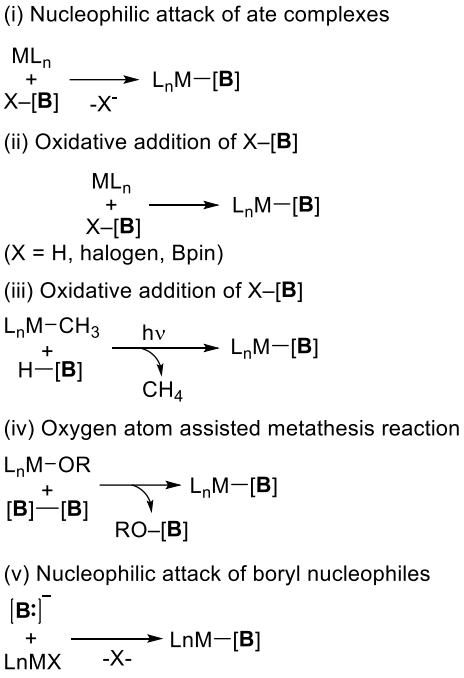

In fact, transition metal boryl complexes could be easily accessed by a nucleophilic substitution of metal electrophiles with **2** (Scheme 3). Group 11 metal-boryl complexes **22**-**24** were obtained by a transmetallation of **2** to group 11 metal chlorides.[18a] Similarly, **2** attacked to titanium tetraisopropoxide to afford boryltitanium triisopropoxide **25**.[18b] In the same manner, the reaction of **2** with (η^5-cyclopentadienyl)hafnium trichloride followed by an alkylation furnished borylhafnium complex **26**. A combination of the complex **26** with $[Ph_3C][B(C_6F_5)_4]$ is applicable as a catalyst for polymerization of ethylene and 1-hexene. The reaction between **2** and cationic rare earth metal complexes furnished the corresponding rare earth metal-boryl complexes **27**-**30**.[18c,d] Double nucleophilic borylation on metal center proceeded by using group 12 metal dibromide to give homoleptic diborylmetal complexes **31**-**33**.[18e,f] An iron complex **34** was prepared by nucleophilic attack of **2** to carbonyl center and subsequent CO elimination under heating condition.[18h] Formation of metal-boron bond on **22**-**33** were the most widely applicable strategy for the synthesis of metal-boryl complexes. Thus, boryllithium **2** enabled the synthesis of unprecedented transition metal complexes.

Scheme 3. Synthesis of metal-boryl complexes via nucleophilic borylation by using diaminoboryl anion **2**

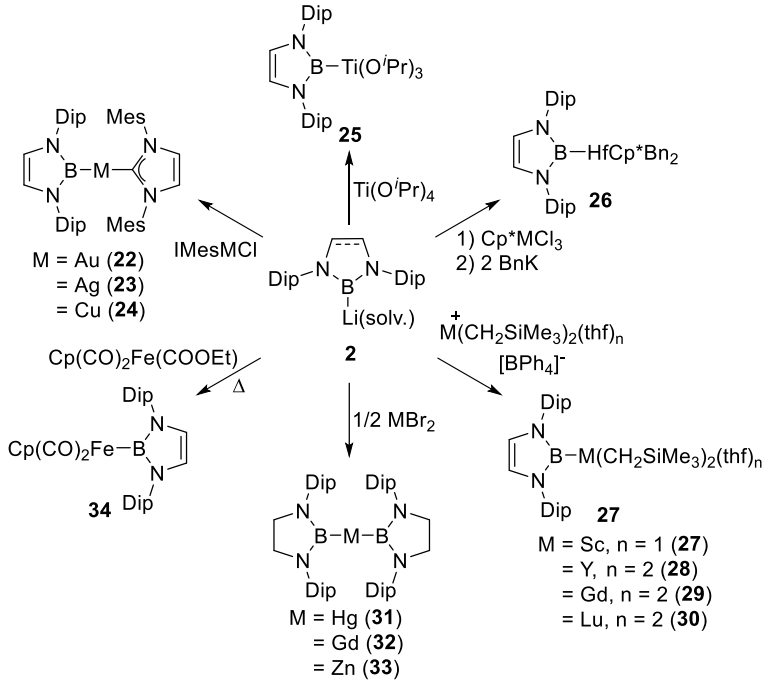

Diaminoalumanyl anion showed a different reactivity from that of the boryl anion (Scheme 4). For example, a (1+2) cycloaddition reaction between **5** and cyclooctatetraene furnished a three-membered ring compound **35**.[9a] Oxidation of **5** with elemental selenium gave anionic Al=Se compound **36**,[19a] which is an isoelectronic structure of carbonyl compounds. Treatment of **5** with N_2O similarly gave an anionic Al=O bond compound **37**. A four-membered ring compound **38** was provided by a reaction with CO_2 via the formation of intermediate **37**.[19b] The reaction of **5** with mesityl azide gave anionic Al=N compound **39** along with elimination of nitrogen molecule.[19c] The seven-membered ring alumanyl anion **14** also reacted with cationic nacnac-ligated group 2 metal complexes to afford the corresponding stable calcium and magnesium complexes **40-Ca, Mg**.[9b] The vacant orbital of aluminum atom in **5** and **6** would be responsible to form cyclized products (**35**, **38**) and Al=E multiply bonded compounds (**36**, **37**, **39**).

Scheme 4. Reactivity of diaminoalumanyl anion **5** and **6** as Al(I) species and transmetallating Al(I) anion with cyclooctatetraene, main group compounds, and group 2 metals.

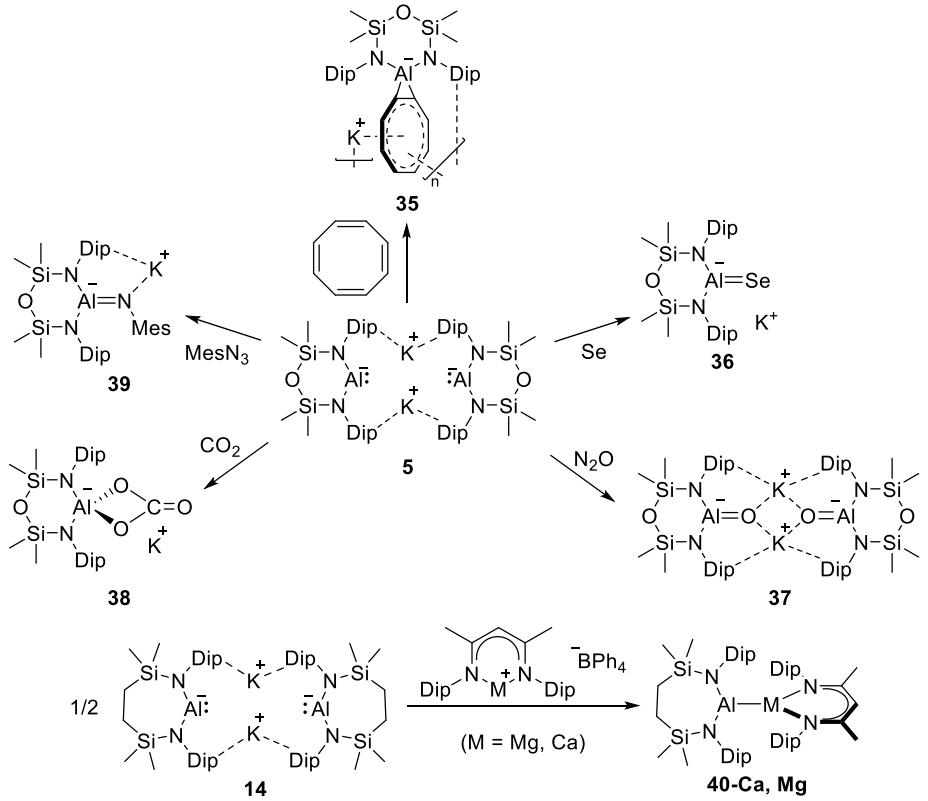

Base-stabilized borylanion also reacted with electrophiles as a boron-centered anion species (Scheme 5). A tricyclohexylphosphine-coordinated boryl anion **7** attacked to benzaldehyde and trimethylsilyl chloride to give boron-containing alcohol **41** and silylborane **42**, respectively.[10a] A manganese-bridged boryl anion **6** reacted with methyl iodide or gold chloride afforded methylborane **43**[10b] or borylgold complex **44**.[20] An NHC-stabilized borole anion **9** attacked to ammonium chloride or methyl reagent to give NHC-stabilized hydroborane **45** and NHC-stabilized methylborane **46**, respectively.[10c] The reaction between NHC-stabilized dihydroboryllithium **10** and diethyl carbonate furnished boryl ester **47** through a nucleophilic attack to the carbonyl center.[10d] This compound **10** also acts as a boron nucleophile with a wide range of electrophiles such as ethyl acetate, *p*-chlorobenzaldehyde, epoxide, alkenyl halide, 2-iodopropane, 2-iodoadamantane, hexafluorobenzene. The dianion **11** did not react with THF under 100 °C, but reacted at 120 °C to give a ring-opening product **48**.[10f] The CAAC-supported dicyanoboryl anion **12** attacked to isopropyl iodide to afford the corresponding substituted product **49**.[10f] Reaction of **12** with trimethylphosphine-ligated gold chloride induced a similar nucleophilic attack of boron center to gold atom to afford borylgold complex **50**.[10g]

Scheme 5. Reactivity of base-stabilized boryl anion **7**-**12** with electrophiles as boron-centered nucleophiles

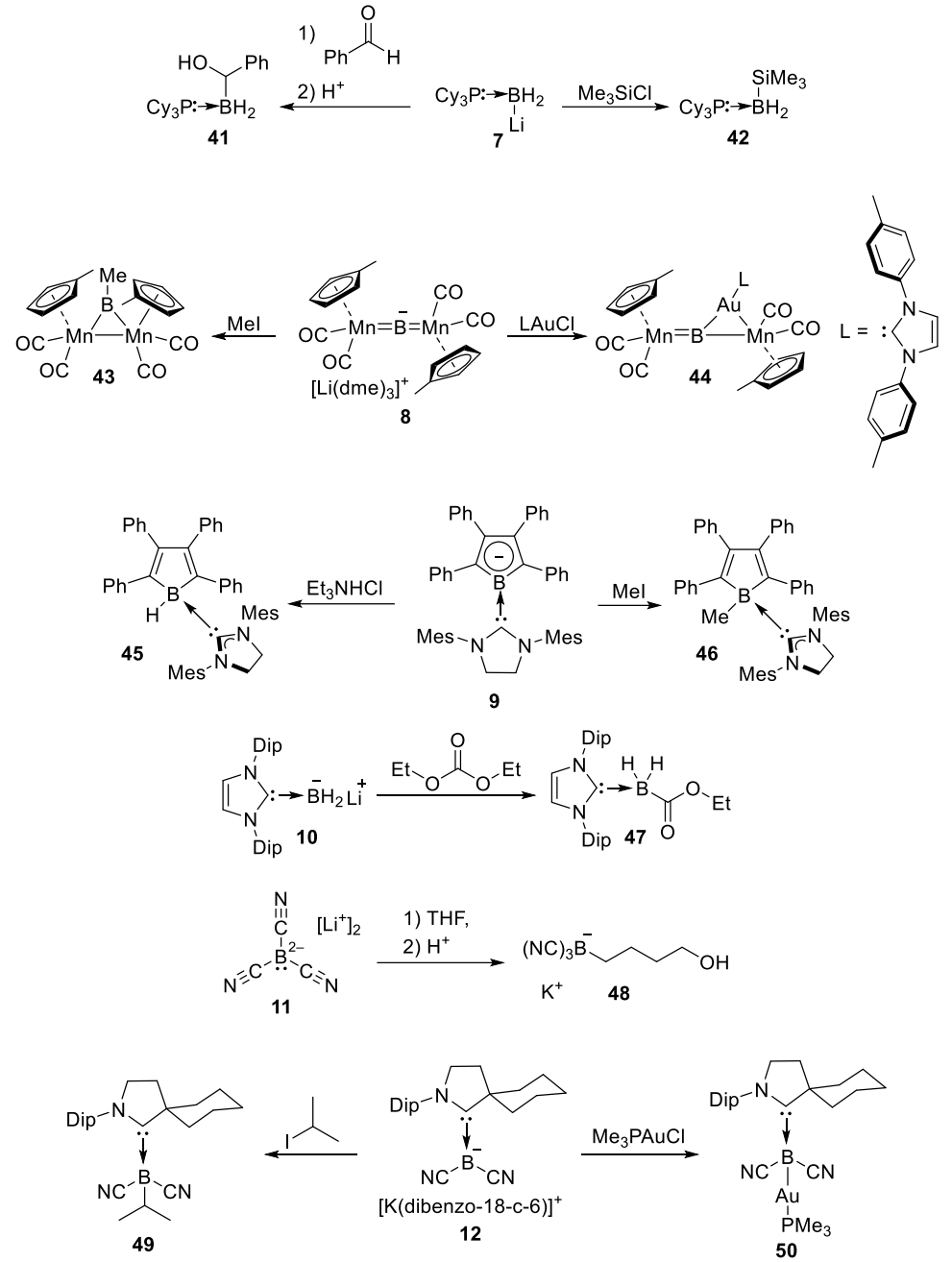

The base-stabilized 8-electron alumanylanion dimer **13** has a nucleophilicity on the Al center and reacts as an aluminum(I) compound (Scheme 6). It reacted with MeOTf as a nucleophilic aluminum(I) giving four-coordinated methylalumane **51**.[11a] This compound **13** cleaved dihydrogen molecule to furnish dihydroaluminate **52**, in which the Al(I) center underwent oxidative addition of H–H bond. An alumanylgold complex **53** was obtained by a reaction of **13** with an electron-rich gold iodide.[21b] Reaction of **13** with nitrous oxide gave an anionic and nucleophilic aluminum oxide **54**.[21b] The resulting **54** can be considered as an intermediate for the formation of **55** and **56** derived from the reaction of **13** with CO_2 and PhNCO. The reaction of **13** with organic azide gave aluminum-substituted amide **57** possessing a high basicity to deprotonate the benzyl proton of toluene.[21c] The monomeric base-stabilized alumanyl anion **14** cleaved the C–C bond of benzene at room temperature to furnish an Al-incorporated seven-membered ring compound **58**.[11b] At a higher

temperature, **14** activated C–H bond of benzene to give thermodynamically stable (hydrido)(phenyl) aluminate **59**.

Scheme 6. Reactivity of base-stabilized alumanyl anion **13** and **14** as tri-coordinated aluminum nucleophiles

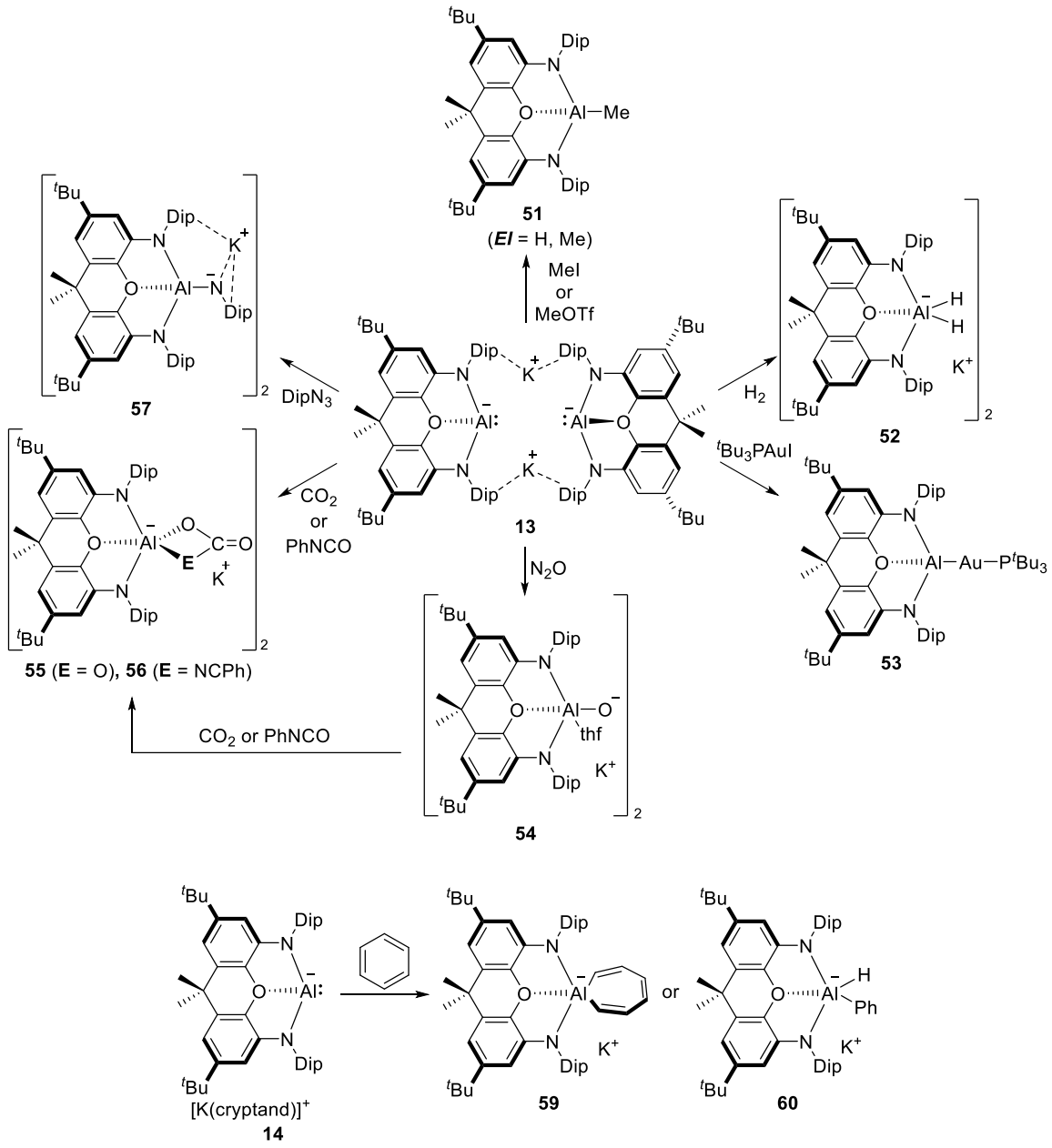

Similarly, dialkylalumanylpotassium **15** reacted with electrophiles or arenes as a nucleophilic alumanylanion or a Brønsted base (Scheme 7).[12] The reaction with methyl trifluoromethanesulfonate afforded trialkylalumane **60**. Dialkylalumanyl anion **15** also had nucleophilicity. Halophilic attack proceeded by the reaction between **15** and benzyl chloride to give tetraalkylaluminate **61**. On the other hand, **15** deprotonated benzene to give (hydrido)(phenyl) dialkylaluminate **62** at room temperature for 2.5 h, being shorter time than the case of **13**. A nucleophilic aromatic substitution with **15** proceeded by using hexafluorobenzene as a substrate to give mono- and bis-Al-adducts **63** and **64**. Thus, dialkylalumanylpotassium **15** behaved as a strongly basic aluminum(I) nucleophile.

Scheme 7. Reactivity of dialkyalumanylpotassium **15** toward electrophiles and arenes (***Si*** = $SiMe_3$)

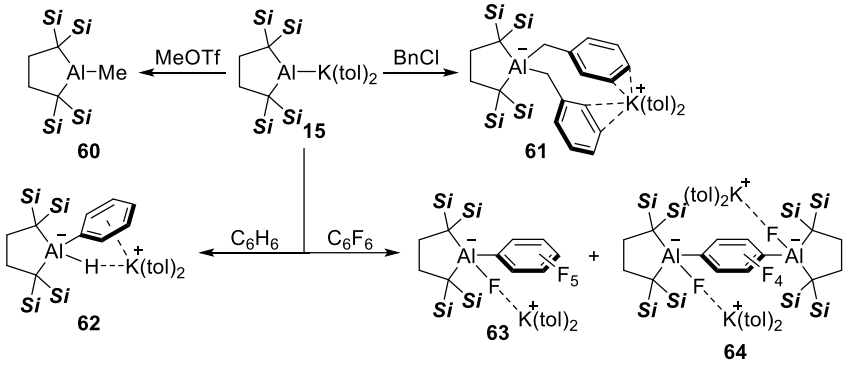

The alumanyl anions **13**, **14** and **15** showed different reactivity toward benzene (Scheme 8). The C–H cleavage of benzene by **13** to afford penta-coordinated (hydrido)(phenyl)aluminate dimer **65** required a high temperature (60 °C) and long time (4 days) (Scheme 8(a)) probably due to slow dissociation of dimeric structure to the corresponding monomer upon coordination of benzene to the potassium cation. In contrast, dialkylalumanyl anion **15** cleaved the C–H bond of benzene at room temperature with a shorter time than that for **13** to afford (hydrido)(phenyl)dialkylaluminate **60** (Scheme 8b). Exchange of potassium-coordinated toluene with benzene proceeded smoothly followed by a concerted nucleophilic aromatic substitution as supported by DFT calculations.[22] These results indicated that the carbon-substituted alumanyl anion **15** has stronger basicity than that of **13** due to lower electronegativity of carbon atoms bonding to the Al atom than those of nitrogen atom (Pauling, C:2.55, N:3.04). Apart from **13** and **15**, monomeric 8-electron diaminoalumanyl anion **14**, existing as a separated ion pair, reacted with benzene to cleave its C–C bond giving 7-membered ring compound **58** (Scheme 8(c)). DFT calculations of model compound **14'**, having Me groups instead of ^{t}Bu groups, proposed that the (1+2) cycloaddition proceeded in a concerted manner via a transition state $\mathbf{TS_{14\text{-}A}}$ to afford aluminacyclopropane intermediate **14-A** followed by a formation of **58'** via $\mathbf{TS_{58'}}$ (Scheme 8(d)). This reactivity of compound **14** is similar to Büchner ring expansion of carbene[23] and silylene. [24] Thus, the Al center in **14** behaved as a Lewis acid rather than Brønsted base.

Scheme 8. Comparison in reactivity of **13**, **14** and **15** toward benzene

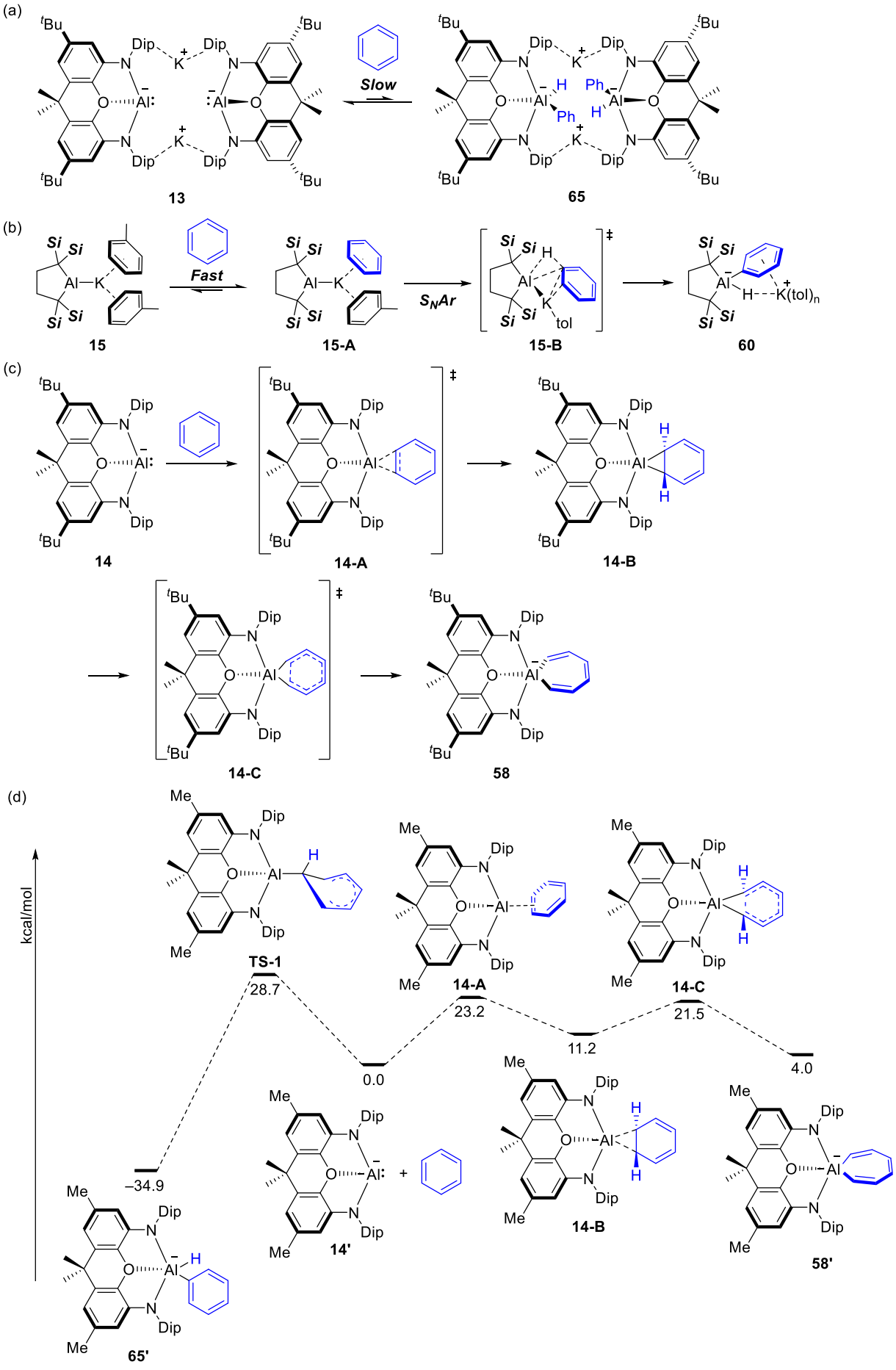

1.4. Outline of this thesis

In this doctoral thesis, the author revealed three reaction modes of dialkylalumanylpotassium **15** (Scheme 8). In chapter 2, the reaction of **15** with unsaturated hydrocarbons was investigated. It was found that (1+2) or (1+4) cycloaddition proceeded to afford four-coordinated anionic aluminum-containing benzonorbornadiene derivatives and three-membered ring compounds which contain four-coordinated anionic aluminum atom. In chapter 3, **15** attacked to a cationic yttrium complex as an aluminum-centered nucleophile to furnish alumanylyttrium complex having unprecedented Al–Y single bond. The resulting alumanylyttrium complex exhibited a characteristic absorption in visible region due to the overlapping two vacant orbitals between Al and Y atoms, although the complex does not have any π-electrons. In chapter 4, **15** reacted with group 4 metal complexes as an one-electron reductant reagent affording trivalent group 4 metal complexes. The resulting complexes are inactive for NMR spectroscopy and exhibited an intense color due to the existence of an unpaired electron, The Chapter 5 summarized this Ph.D. thesis.

Scheme 9. Outline of the present doctoral thesis (***Si*** = $SiMe_3$)

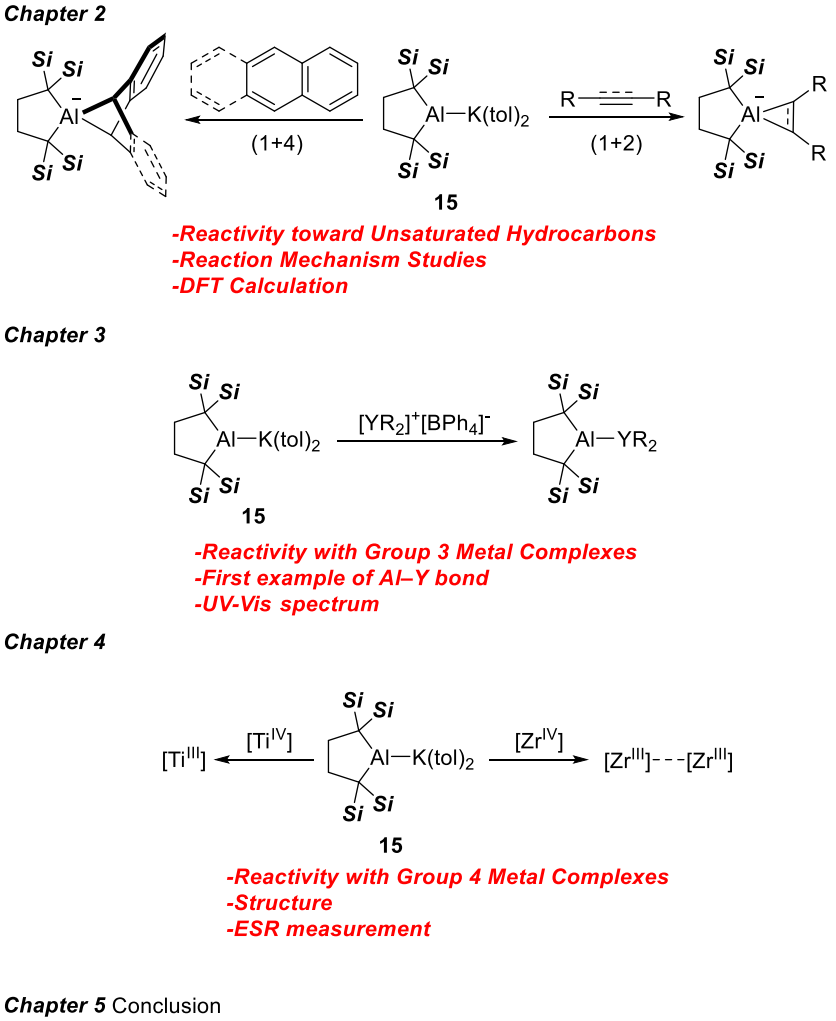

1.5. References

1. (a) Sander, W.; Bucher, G.; Wierlacher, S.; *Chem. Rev.* **1993,** *93,* 1583-1621; (b) Bourissou, D.; Guerret, O.; Gabbaï, F.; Bertrand, G.; *Chem. Rev.* **2000,** *100,* 39-91; (c) Hirai, K.; Itoh, T.; Tomioka, H. *Chem. Rev.* **2009,** *109,* 3275-3332; (d) Hopkinson, N. M.; Ritcher, C.; Schedler, M.; Glorius, F. *Nature* **2014,** *510,* 485-496; (e) Hahn, F. E.; *Chem. Rev.* **2018,** *118,* 9455-9456; (f) Huynh, V. H. *Chem. Rev.* **2018,** *118,* 9457-9492. (g) Vivancos, Á.; Segarra, C.; Albrecht, M.; *Chem. Rev.* **2018,** *118,* 9493-9586.

2. (a) Gillette, R. G.; Baceiredo, A.; Bertrand, G. *Angew. Chem. Int. Ed. Engl.* **1990,** *29,* 1429-1431. (b) Arudengo, J. A. III; Harlow, L. R.; Kline, M. *J. Am. Chem. Soc.* **1991,** *113,* 361-363; (c) Gillette, R. G.; Baceiredo, A.; Bertrand, G. *Angew. Chem. Int. Ed. Engl.* **1990,** *29,* 1429-1431; (d) Nakano, R.; Jazzar, R.; Bertrand, G. *Nat. Chem.* **2018,** *10,* 1196-1200.

3. (a) Haaf, M.; Schmedake, A. T.; West, R. *Acc. Chem. Res.* **2000,** *33,* 704-714; (b) Hill, J. N.; West, R.; *J. Orgmet. Chem.* **2004,** *689,* 4165-4183; (c) Mizuhata, Y.; Sasamori, T.; Tokitoh, N. *Chem. Rev.* **2009,** *109,* 3479-3511; (d) Asay, M.; Jones, C.; Driess, M. *Chem. Rev.* **2011,** *111,* 354-396.

4. (a) Bissinger, P.; Braunschweig, H.; Kraft, K.; Kupfer, T.; *Angew. Chem. Int. Ed.* **2011,** *50,* 4704-4707; (b) Wang, Y.; Robinson, H. G. *Inorg. Chem.* **2011,** *50,* 12326-12337; (c) Bissinger, P.; Braunschweig, H.; Damme, A.; Dewhurst, D. R.; Kupfer, T.; Radacki, K.; Wagner, K. *J. Am. Chem. Soc.* **2011,** *133,* 19044-19047. (d) Curran, P. D.; Boussonnière A.; Geib, J. S.; Lacôte, E. *Angew. Chem. Int. Ed.* **2012,** *51,* 1602-1605; (e) Dahcheh, F.; Martin, D.; Stephan, W. D.; Bertrand, G. *Angew. Chem. Int. Ed.* **2014,** *53,* 13159-13163; (f) Braunschweig, H.; Claes, C.; Damme, A.; Deißenberger, A.; Dewhurst, D. R.; Hörl, C.; Kramer, T. *Chem. Comm.* **2015,** *51,* 1627-1630; (g) Ledet, D. A.; Hudnall, W. T. *Dalton. Trans.* **2016,** *45,* 9820-9826; (h) Arrowsmith, M.; Böhnke, J.; Braunschweig, H.; Gao, H.; Légaré M.-A.; Paprocki, V.; Seufert, J. *Chem. Eur. J.* **2017,** *23,* 12210-12217; (i) Légaré M.-A.; Bélanger-Chabot, G.; Dewhurst, D. R.; Welz, E.; Krummenacher, I.; Engels, B.; Braunschweig, H. *Science* **2018,** *359,* 896-900. (j) Légaré M.-A.; Rang, M.; Bélanger-Chabot, G.; Schweizer, I. J.; Krummenacher, I.; Bertermann, R.; Arrowsmith, M.; Holthausen, C. M.; Brausnschweig, H. *Science* **2019,** *363,* 1329-1332.

5. (a) Cui, C.; Roesky, W. H.; Schmidt, H.-G.; Noltemeyer, M.; Hao, H.; Cimpoesu, F. *Angew. Chem. Int. Ed.* **2000,** *39,* 4274-4276; (b) Li, X.; Cheng, X.; Song, H.; Cui, C. *Organometallics* **2007,** *26,* 1039-1043.

6.(a) Schmidt, S. E.; Jockisch, A.; Schmidbaur, H. *J. Am. Chem. Soc.* **1999,** *121,* 9758-9759; (b) Baker, J. R.; Farley, D. R.; Jones, C.; Kloth, M. Murphy, M. D. *J. Chem. Soc., Dalton Trans.,* **2002,** 3844-3850.

7. (a) Segawa, Y.; Yamashita, M.; Nozaki, K.; *Science* **2006,** *314*, 113-115; (b) Segawa, Y.; Suzuki, Y.; Yamashita, M.; Nozaki, K. *J. Am. Chem. Soc.* **2008**, *130*, 16069-16079; (c) Yamashita, M.; Nozaki, K. In *Synthesis and Application of Organoboron Compounds*, Ferna´ndez, E.; Whiting, A., Eds. Springer International Publishing: **2015**, *49*, 1-37; (d) Lu, W.; Hu, H.; Li, Y.; Ganguly, R.; Kinjo, R. *J. Am. Chem. Soc.* **2016,** *138,* 6650-6661.

8. Schwamm, J. R.; Anker, D. M.; Lein, M.; Coles, P. M.; Firchett, M. C. *Angew. Chem. Int. Ed.* **2018,** *57,* 5885-5887.

9. (a) Schwamm, R. J.; Anker, M. D.; Lein, M.; Coles, M. P. *Angew. Chem. Int. Ed.* **2019,** *58*, 1489-1493; (b) Schwamm, J. R.; Coles, P. M.; Hill, S. M.; Mahon, F. M.; McMullin, L. C.; Rajabi, A. N.; Wilson, S. S. A. *Angew. Chem. Int. Ed.* **2020,** in press. doi:10.1002/anie.201914986.

10. (a) Blumenthal, A.; Bissinger, P.; Schmidbaur, H. *J. Orgmet. Chem.* **1993,** *462,* 107-110; (b) Imamoto, T.; Hikosaka, T. *J. Org. Chem.* **1994,** *59,* 6753-6759; (c) Braunschweig, H.; Burzler, M.; Dewhurst, D. R.; Radacki, K. *Angew. Chem. Int. Ed.* **2008,** *47,* 5650-5653; (d) Braunschweig, H.; Chiu, C.-W.; Radacki, K.; Kupfer, T. *Angew. Chem. Int. Ed.* **2010,** *49,* 2041-2044; (e) Monot, J.; Solovyev, A.; Bonin-Dubarle, H.; Derat, É, Curran, P. D.; Robert, M.; Fensterbank, L.; Malacria, M.; Lacôte, E. *Angew. Chem. Int. Ed.* **2010,** *49,* 9166-9169; (f) Bernhardt, E.; Bernhardt-Pitchougina, V.; Willner, H.; Ignatiev, N. *Angew. Chem. Int. Ed.* **2011,** *50,* 12085-12088; (g) Ruiz, A. D.; Ung, G.; Melaini, M.; Bertrand, G.; *Angew. Chem. Int. Ed.* **2013,** *52,* 7590-7592.
11. (a) Hicks, J.; Vasko, P.; Goicoechea, J. M.; Aldridge, S. *Nature* **2018,** *557*, 92-95; (b) Hicks, J.; Vasko, P.; Goicoechea, J. M.; Aldridge, S. *J. Am. Chem. Soc.* **2019,** *141*, 11000-11003.
12. Kurumada, S.; Takamori, S.; Yamashita, M. *Nat. Chem.* **2020,** *12*, 36-39.
13. Mkhalid, A. I. I.; Barnard, H. J.; Marder, B. T.; Murphy, M. J.; Hartwig, F. J. *Chem. Rev.* **2010,** *110,* 890-931.
14. Nöth, H.; Schmid, G. *Angew. Chem. Int. Ed. Eng.* **1963,** *2,* 623.
15. Schmid, G.; Nöth, H.; *Z. Naturforsch. B.* **1965,** *20b,* 1008.
16. Kawano, Y.; Yasue, T.; Shiomi, M. *J. Am. Chem. Soc.* **1999,** *121,* 11744-11750.
17. Takahashi, K.; Ishiyama, T.; Miyaura, N. *J. Orgmet. Chem.* **2001,** *625,* 47-53.
18. (a) Segawa, Y.; Yamashita, M.; Nozaki, K. *Angew. Chem. Int. Ed.* **2007**, *46*, 6710-6713; (b) Terabayashi, T. Kajiwara, T. Yamashita, M. Nozaki, K. *J. Am. Chem. Soc.* **2009,** *131*, 14162-14163. (c) Saleh, L. M. A.; Birjkumar, K. H.; Protchenko, A. V.; Schwarz, A. D.; Aldridge, S.; Jones, C.; Kaltsoyannis, N.; Mountford, P. *J. Am. Chem. Soc.* **2011,** *133*, 3836-3839. (d) Li, S.; Cheng, J.; Chen, Y.; Nishiura, M. Hou, Z. *Angew. Chem. Int. Ed.* **2011,** *50,* 6360-6363. (e) Kajiwara, T.; Terabayashi, T.; Yamashita, M.; Nozaki, K. *Angew. Chem. Int. Ed.* **2008,** *47,* 6606-6610. (f) Protchenko, V. A.; Dange, D.; Schwarz, D. A. Tang, Y. C.; Phillips, N.; Mountford, P.; Jones, C.; Aldridge, S. *Chem. Comm.* **2014,** *50,* 3841-3844; (g) Frank, R.; Howell, J.; Tirfoin, R.; Dange, D.; Jones, C.; Mingos, P. D. M.; Aldridge, S. *J. Am. Chem. Soc.* **2014,** *136,* 15730-15741.
19. (a) Anker, D. M.; Coles, P. M. *Angew. Chem. Int. Ed.* **2019,** *58,* 13452-13455; (b) Anker, D. M.; Coles, P. M. *Angew. Chem. Int. Ed.* **2019,** *58,* 18261-18265; (c) Anker, D. M.; Schwamm, J. R.; Coles, P. M. *Chem. Comm.* **2020,** *56*, in press. doi: 10.1039/C9CC09214E
20. Braunschweig, H.; Brenner, P.; Dewhurst, D. R.; Kaupp, M.; Müller, R.; Östreicher, S. *Angew. Chem. Int. Ed.* **2009,** *48,* 9735-9738.
21. (a) Jamie, H.; Mansikkamäki, A.; Vasko, P.; Goicoecha, M. J.; Aldridge, S. *Nat. Chem.* **2019,** *11,* 237-241; (b) Hicks, J.; Heilmann, A.; Vasko, P.; Goicoecha, M. J.; Aldridge, S. *Angew. Chem. Int. Ed.* **2019,** *58,* 17265-17268; (c) Heilmann, A.; Hicks, J.; Vasko, P.; Goicoecha, M. J.; Aldridge, S. *Angew. Chem. Int. Ed.* **2020,** *59,* in press, doi: 10.1002/anie.201916073.
22. Kurumada, S.; Nakano, R.; Yamashita, M. *manuscript in preparation.*
23. (a) Buchner, E.; Curtius, T. *Ber. Dtsch. Chem. Ges.* **1885,** *18,* 2377−2379; (b) Perera, T. A.; Reinheimer, E. W.; Hudnall, T. W. *J. Am. Chem. Soc.* **2017,** *139,* 14807−14814.
24. (a) Suzuki, H.; Tokitoh, N.; Okazaki, R. *J. Am. Chem. Soc.* **1994,** *116,* 11572−11573; (b) Kira, M.; Ishida, S.; Iwamoto, T.; Kabuto, C. *J. Am. Chem. Soc.* **2002,** *124,* 3830−3831.

Chapter 2

Reactivity of Dialkylalumanylpotassium toward Unsaturated Hydrocarbons

2.1. Introduction

Main group element compounds, especially in low oxidation state, have been known to undergo oxidative addition at the main group element center to give oxidized compounds.[1] Among them, aluminum-containing molecules in the low-oxidation state have been extensively studied in the last three decades,[2] especially for dialumane derivatives having an Al–Al bond,[3] oligomeric form of aluminum(I) species,[4] and Al=Al doubly bonded compounds.[3o-s, 5] While the parent monomeric halogenated Al(I) species "AlX" are unstable and only can be handled in matrics,[6] isolation of monomeric and nucleophilic Al(I) species are still limited to a handful of examples (Figure 1), including, CpAl(I) species **A**,[7] nacnac (β-diketiminate)-substituted species **B**,[8] Al(I) hydride **C** stabilized by two CAAC ligands,[9] diaminoalumanyl anions (**D**[10], **E**[11]), and base-stabilized diaminoalumanyl anions (**F**[12], **G**[13]). Yamashita group recently reported the synthesis of dialkylalumanyl anion (**1**),[14] featuring strong basicity to deprotonate benzene at room temperature as an anionic aluminum nucleophile.

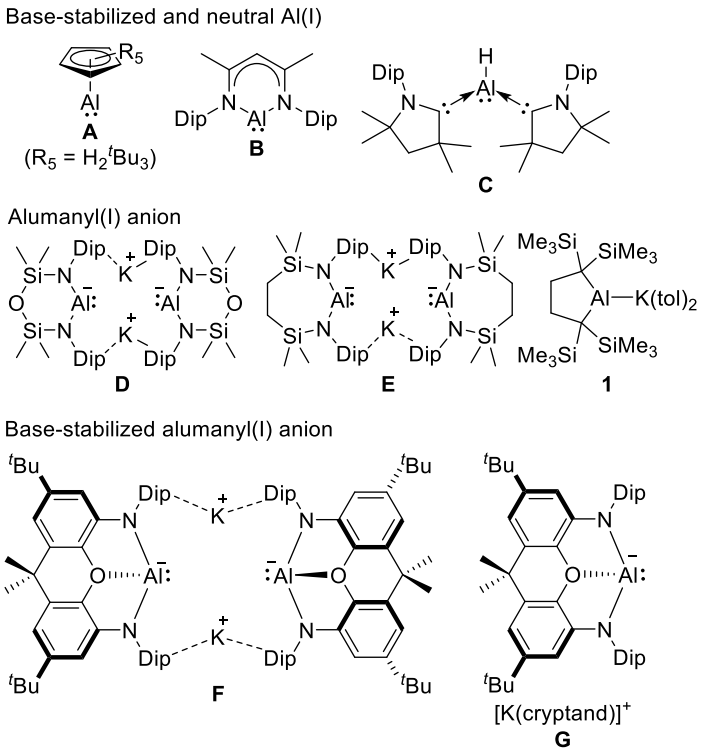

Figure 1. Isolated examples of monomeric Al(I) compounds

Some of these Al(I) compounds in Figure 1 reacted with unsaturated hydrocarbons to give the corresponding cycloadducts (Scheme 1). The nacnac-stabilized Al(I) species **B** underwent (1+2) cycloaddition with alkynes and alkenes to form Al-containing three-membered ring compound **H**.[15] Diamino-Al anion **D** cyclized with cyclooctatetraene to give **I** via (1+2) cycloaddition.[10] Similarly, the monomeric form of oxygen-stabilized Al anion **G** reacted with ethylene to form (1+2) cycloadduct **J**. On the other hand, **B** also reacted with a benzene complex of [nacnac-Ca^{+}] to furnish an alumanonorbornadiene product **K**.[16] The anionic bicyclic compound **I** rearranged to the (1+4) product **L** upon addition of 18-crown-6.[10a]

Scheme 1. Cyclization of monomeric Al(I) compounds with unsaturated hydrocarbons

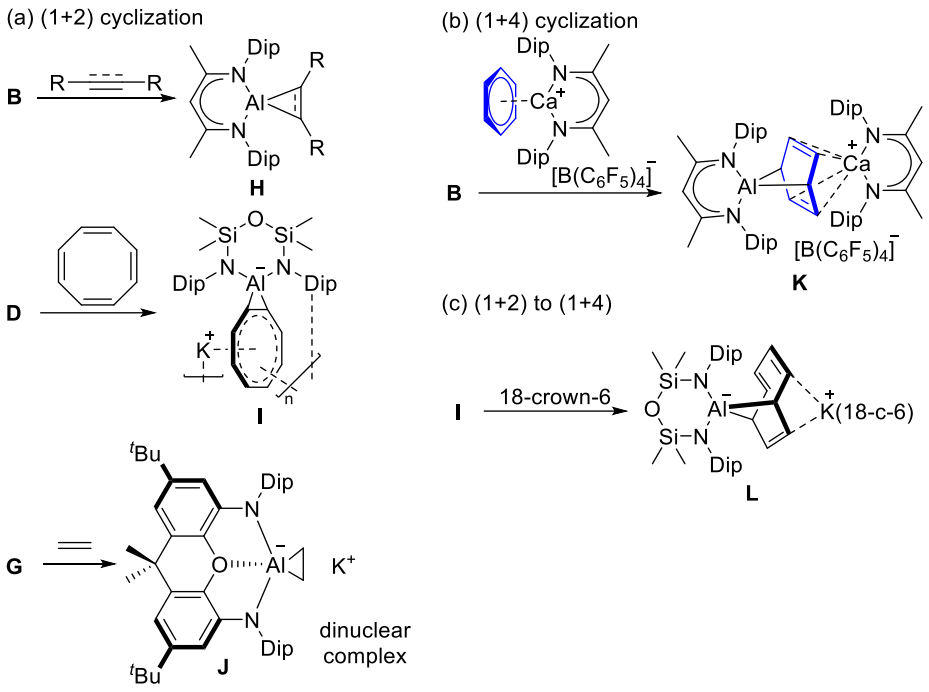

In this chapter, it showed that dialkyl-substituted Al anion **1** undergoes oxidative cycloaddition in both (1+4) and (1+2) modes to give the corresponding Al-containing norbornadiene, cyclopropene, and cyclopropane compounds. From the structure of the products and DFT calculations, possible reaction mechanisms for the cycloaddition reaction were proposed.

2.2. This work

The Reaction of **1** with naphthalene at room temperature gave an aluminum-containing benzoborbornadiene derivative **2** as colorless crystals in 96% isolated yield, through (1+4) cyclization reaction (Scheme 2). This is in contrast to that **G** reacted with naphthalene at 80 °C to form an isomeric mixture of (naphthyl)(hydrido)-aluminate **M** and **N** (Scheme 3),[13] and to that the isoelectronic dialkylsilylene (**O**[17]) bearing the same ‘‘helmet’’ substituents reacted with naphthalene to furnish mono- or bis-(1+2) adducts under the irradiation of visible light (Scheme 4).[18]

Scheme 2. Reaction of **1** with naphthalene

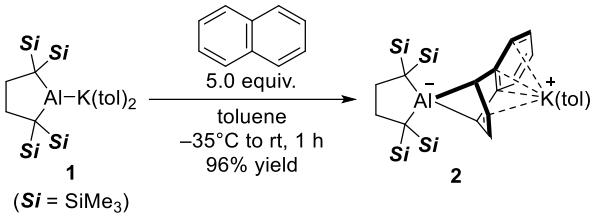

Scheme 3. The reaction of **G** with naphthalene

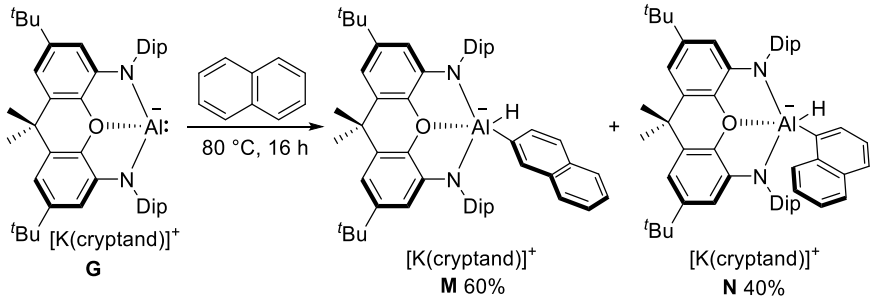

Scheme 4. The reaction of dialkylsilylene **O** with naphthalene (***Si*** = $SiMe_3$)

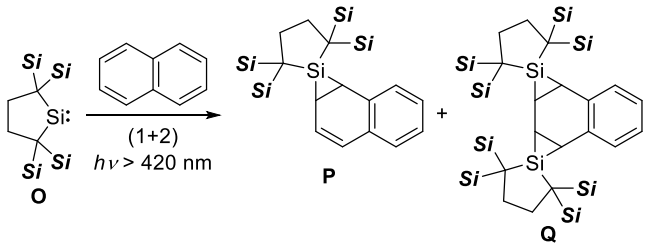

The ^{1}H NMR spectrum of **2** in THF-d_8 exhibited a C_s symmetrical pattern which is matched with the anionic part of the crystal structure of **2** *(vide infra)* with a characteristic multiplet signal of two bridgehead protons at δ 2.89 ppm which is correlated with a signal of alkenyl protons at δ 5.99 ppm (Figure 2).

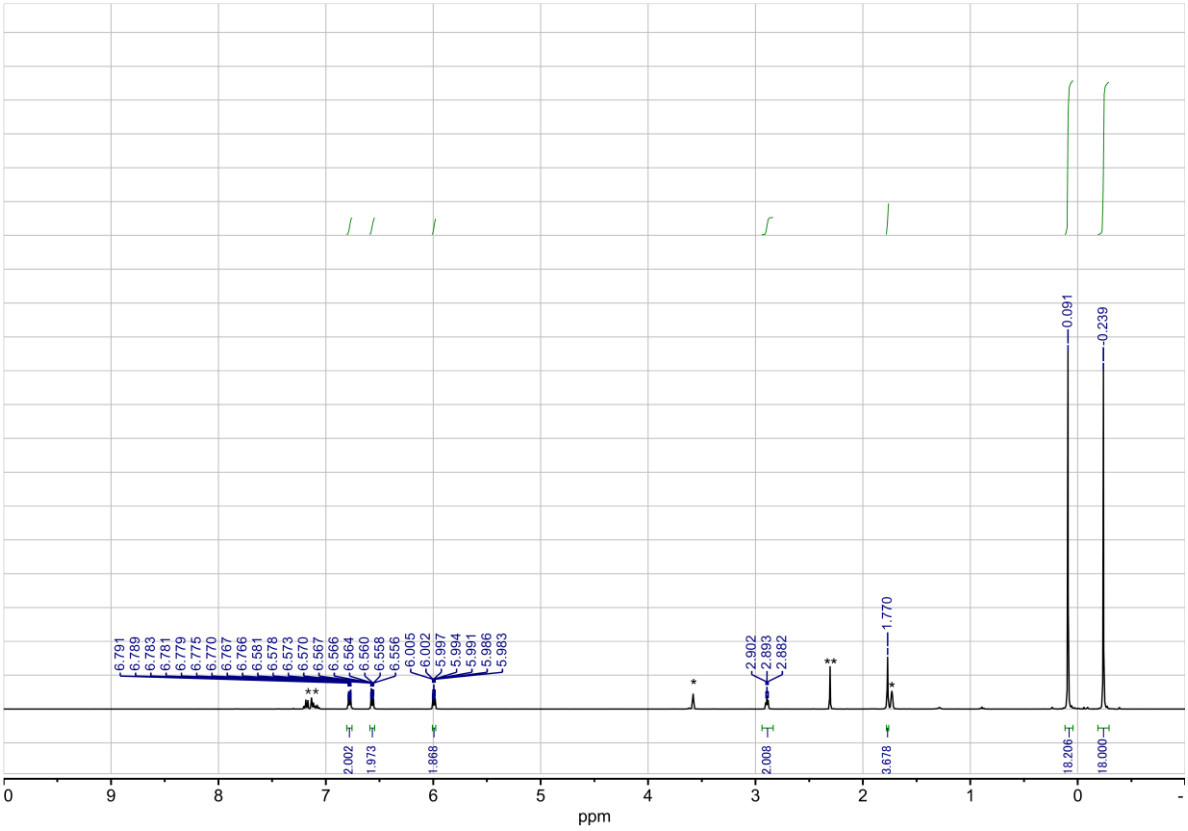

Figure 2. The ^{1}H NMR spectrum of **2** (*THF-d_7, **free toluene dissociated from **2**)

Similarly, **1** was treated with anthracene to afford (1+4) cyclization product **3** as a colorless solid in 66% yield (Scheme 5). In the case of **3**, the ^{1}H NMR exhibited one singlet signal of magnetically equivalent four TMS groups and one singlet signal of the bridgehead protons at δ 3.34 ppm, indicating the C_{2v}-symmetrical aluminadibenzonorbornadiene structure (Figure 3). The bicyclic structure of **2** and **3** were unambiguously confirmed by a single crystal X-ray diffraction analysis (*vide infra*)

Scheme 5. Reaction of **1** with anthracene

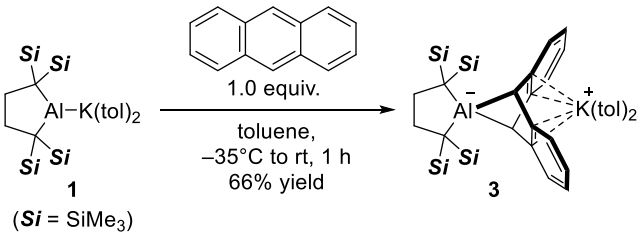

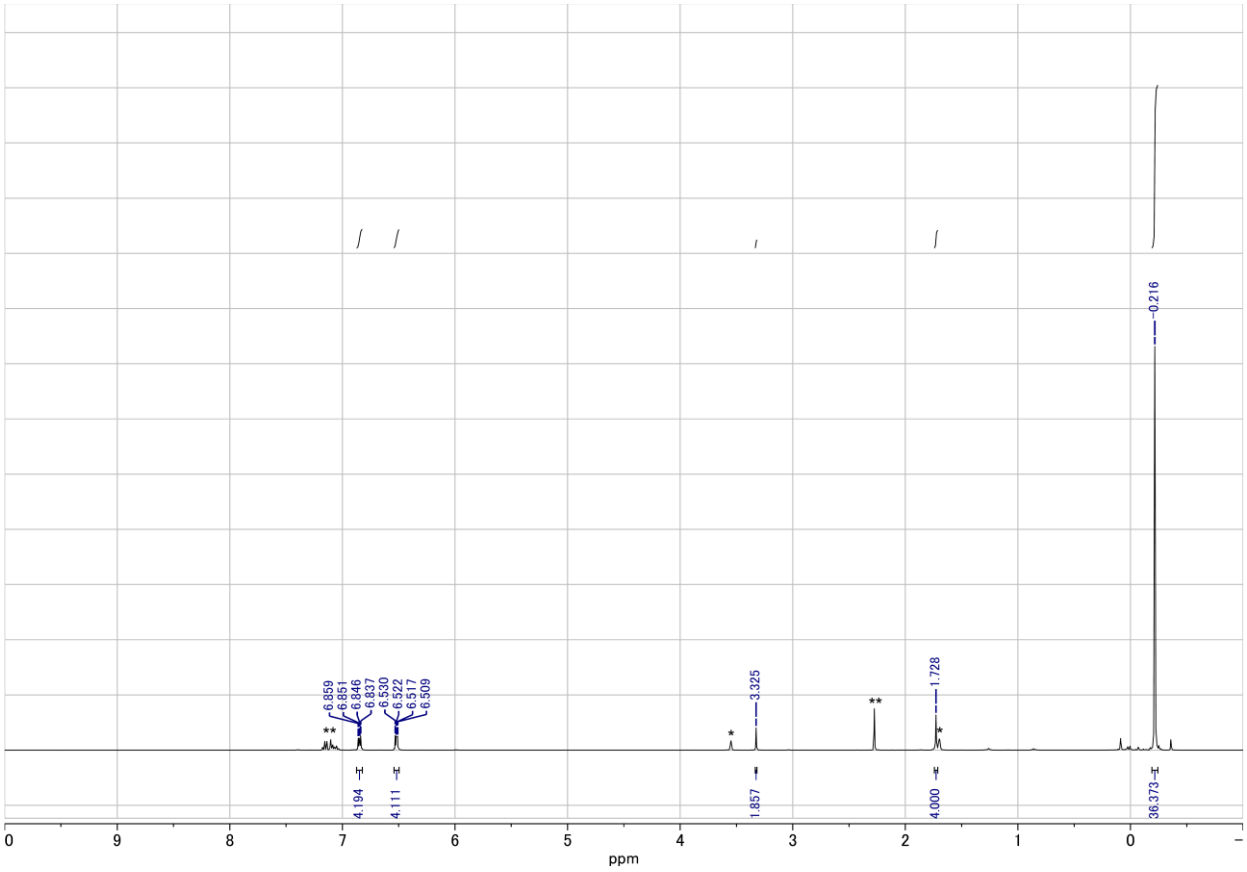

Figure 3. The ^{1}H NMR spectrum of **3** (*THF-d_7, **free toluene dissociated from **3**)

The reaction of **1** with phenanthrene was investigated (Scheme 6). The resulting ^{1}H NMR spectrum is shown in Figure 4. two singlets for the TMS groups in 1:1 (18H:18H) and a broadened methylene signal on 5-membered ring (4H) was observed. In the aromatic region, seven new signals were observed. The methine proton of anionic aluminacyclopropane (*trans*-**8,** *vide infra*) was observed in 2.57 ppm in THF-d_8, indicating the present crude product would have methine protons. These results implied that the observed products may be (1+2) cycloadducts **4**.

Scheme 6. The reaction of **1** with phenanthrene

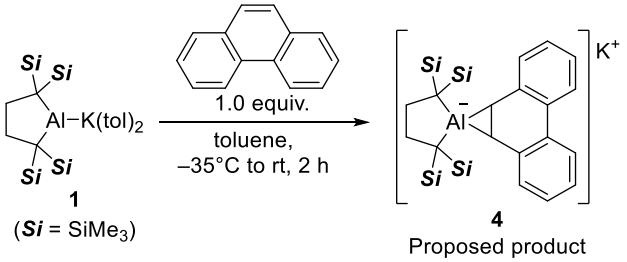

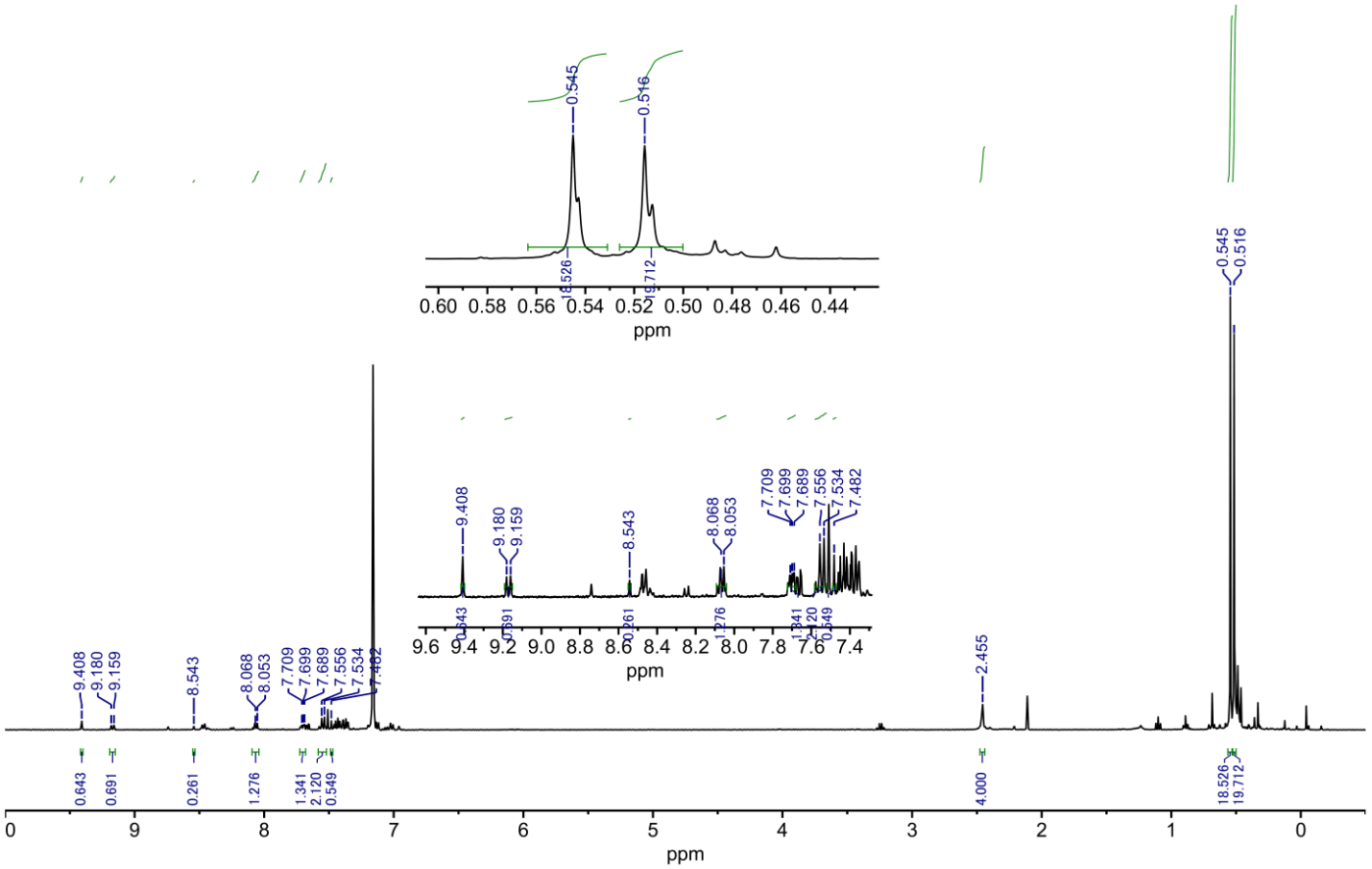

Figure 4. The ^{1}H NMR of crude products by the reaction of **1** with phenanthrene

The reaction of **1** with diphenylacetylene furnished a (1+2) cyclized product, diphenylaluminacyclopropene **5**, which was recrystallized from Et_2O. Similarly, **1** was treated with diborylacetylene to afford a diborylaluminacyclopropene **6** (Scheme 7), which was recrystallized after complexation with [2.2.2]-cryptand. The ^{1}H NMR spectra of **5** and **6** suggested C_{2v}-symmetrical structures of **5** (Figure 5) and **6** (Figure 6) similar to the case of **3**. X-ray crystallographic analysis revealed the three membered ring structures of **5** and **6** (*vide infra,* Figure 9c, d). DFT calculations of **5** exhibited that the HOMO is contributed by two Al–C σ-bonds (Figure 7), leading to a carbanionic character of **5**, as confirmed by a hydrolysis to give (*Z*)-stilbene (Scheme 7). It should be noted that compound **6** is the first example of tetrasubstituted alkene having only boron and aluminum substituents. Existence of two different types of bond (Al–C and B–C bonds) would provide synthetic methods for the formation of C–E bond (E = C, N, O…etc).[2b, 19] Being applicable to diverse synthesis of alkenes for materials and medicines (Scheme 8).

Scheme 7. The reaction of **1** with diphenylacetylene and diborylacetylene

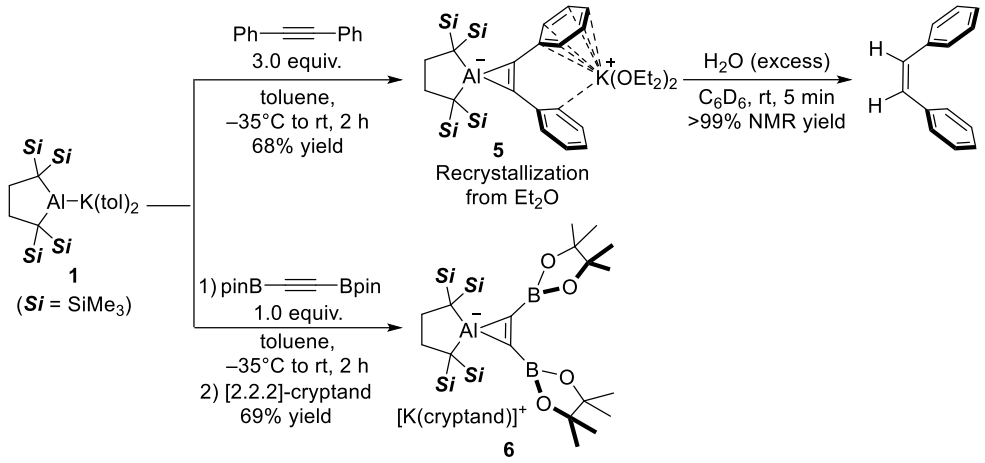

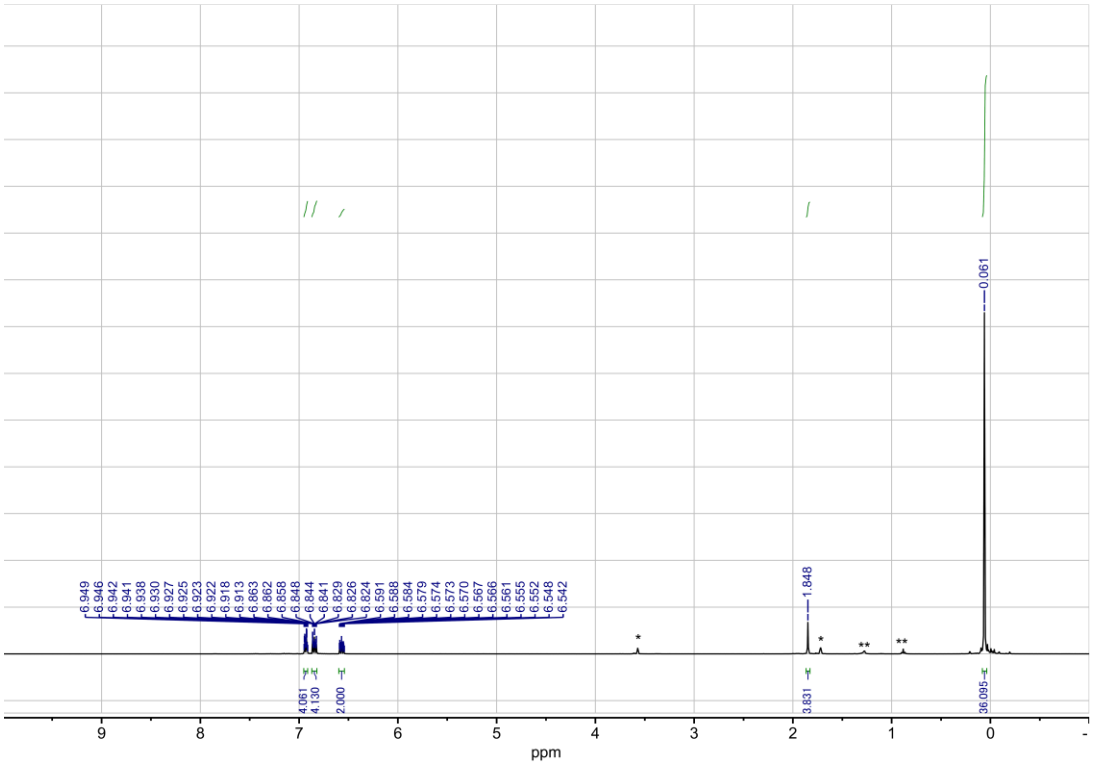

Figure 5. The ^{1}H NMR spectrum of **5** (*THF-d_7, **hexane from glovebox atmosphere)

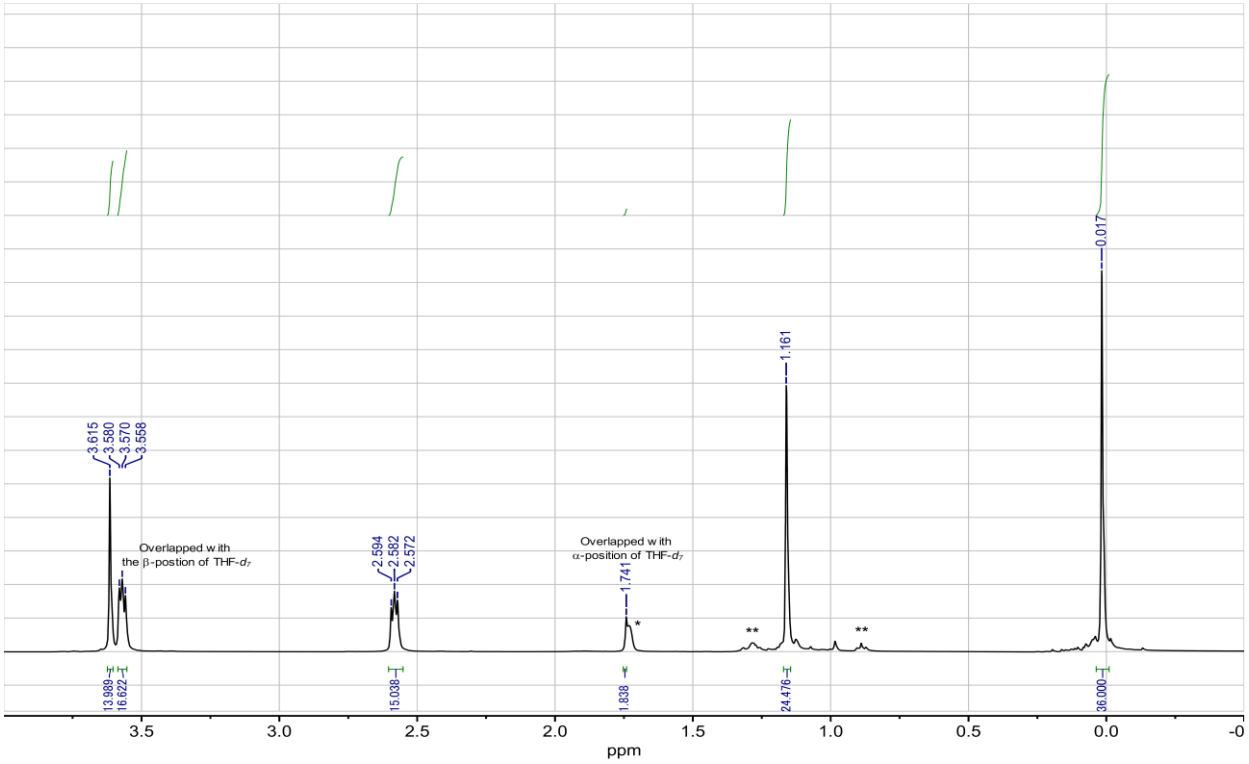

Figure 6. The ^{1}H NMR spectrum of **6** (*THF-d_7, **hexane from glovebox atmosphere)

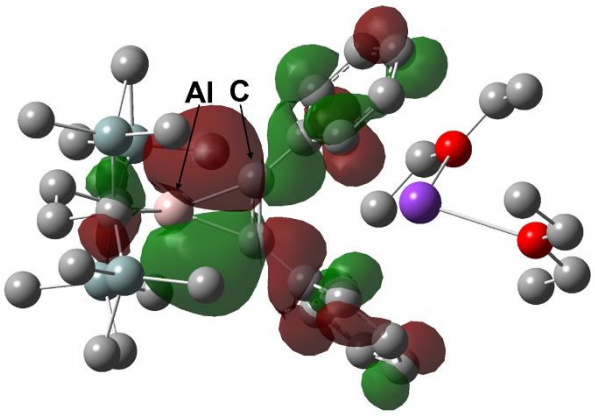

Figure 7. HOMO of **5** (B3LYP/6-31+g(d))

Scheme 8. Potential application of compound **6** for organic synthesis

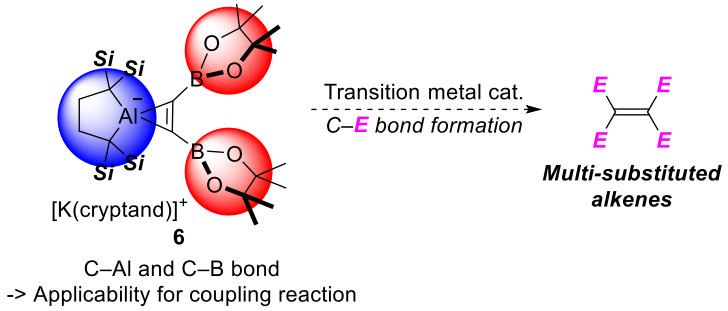

C–Al and C–B bond
-> Applicability for coupling reaction

To reveal the effect of substituents on alkynes, the reaction of **1** with 4-octyne was investigated (Scheme 9). The ^{1}H NMR spectrum of the crude reaction mixture showed a complicated pattern (Figure 8). Since alkyl

substituents having no π-electrons did not stabilize K^+, possible intermediates would be too unstable to obtain the expected product.

Scheme 9. Reaction of **1** with 4-octyne

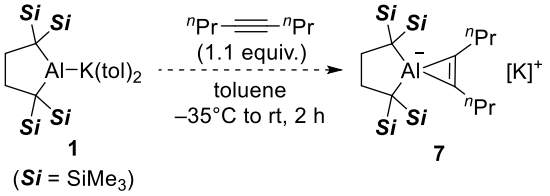

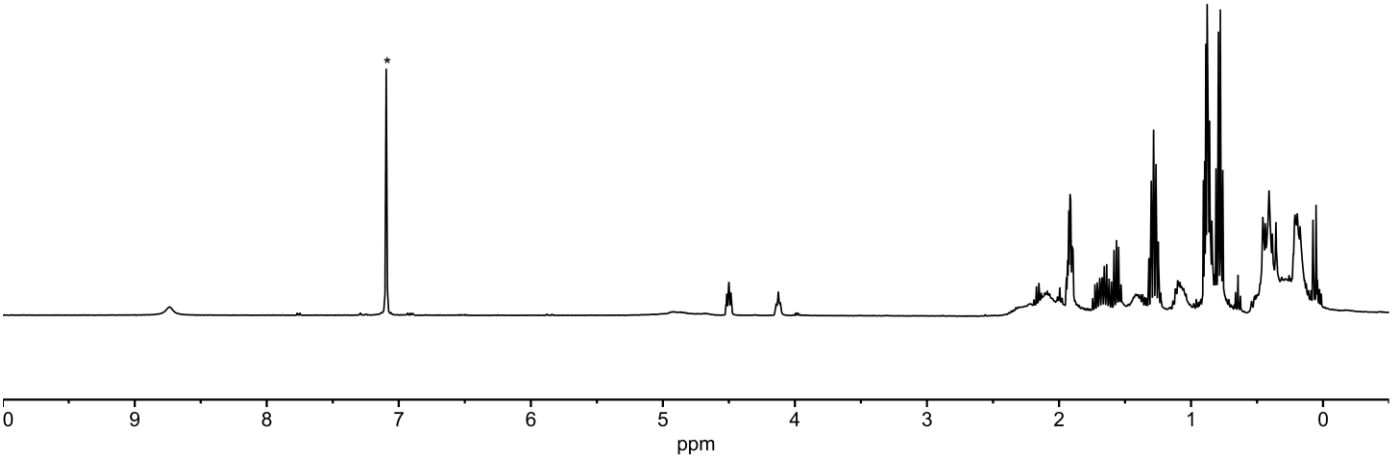

Figure 8. The ^{1}H NMR spectrum of the crude mixture (*C_6D_5H)

Cyclization of **1** also took place with (*Z*)- or (*E*)-stilbenes to give the same single product (Figure 9), *trans*-diphenylaluminacyclopropane (*trans*-**8**), which was crystallized after complexation with [2.2.2]-cryptand. (Scheme 10). X-ray diffraction study unambiguously confirmed the *trans* stereochemistry of two phenyl substituents in *trans*-**8** (Figure 10e). Note that corresponding *cis* product was not observed by NMR measurements, indicating that the (1+2) cyclization of **1** with stilbenes took place in a stepwise manner to give a thermodynamically stable *trans* isomer. It should be noted that the reaction of **1** with (*E*)-stilbene under dark also proceeded to afford *trans*-**8**. It has been reported that **O** did not react with (*Z*)- and (*E*)-2-butenes at <10 °C under the dark but reacted with them at a slightly higher temperature or upon irradiation of visible light (>420 nm) to afford the corresponding stereoretained silacyclopropane derivatives *cis*-**R** and *trans*-**R** respectively (Scheme 11).[20]

Scheme 10. The reaction of **1** with stilbenes

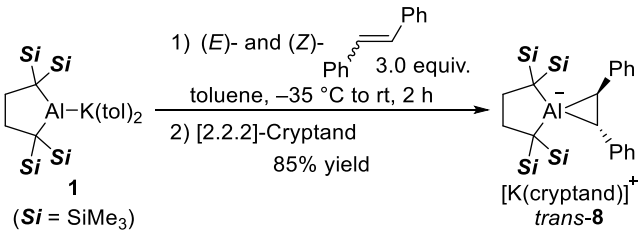

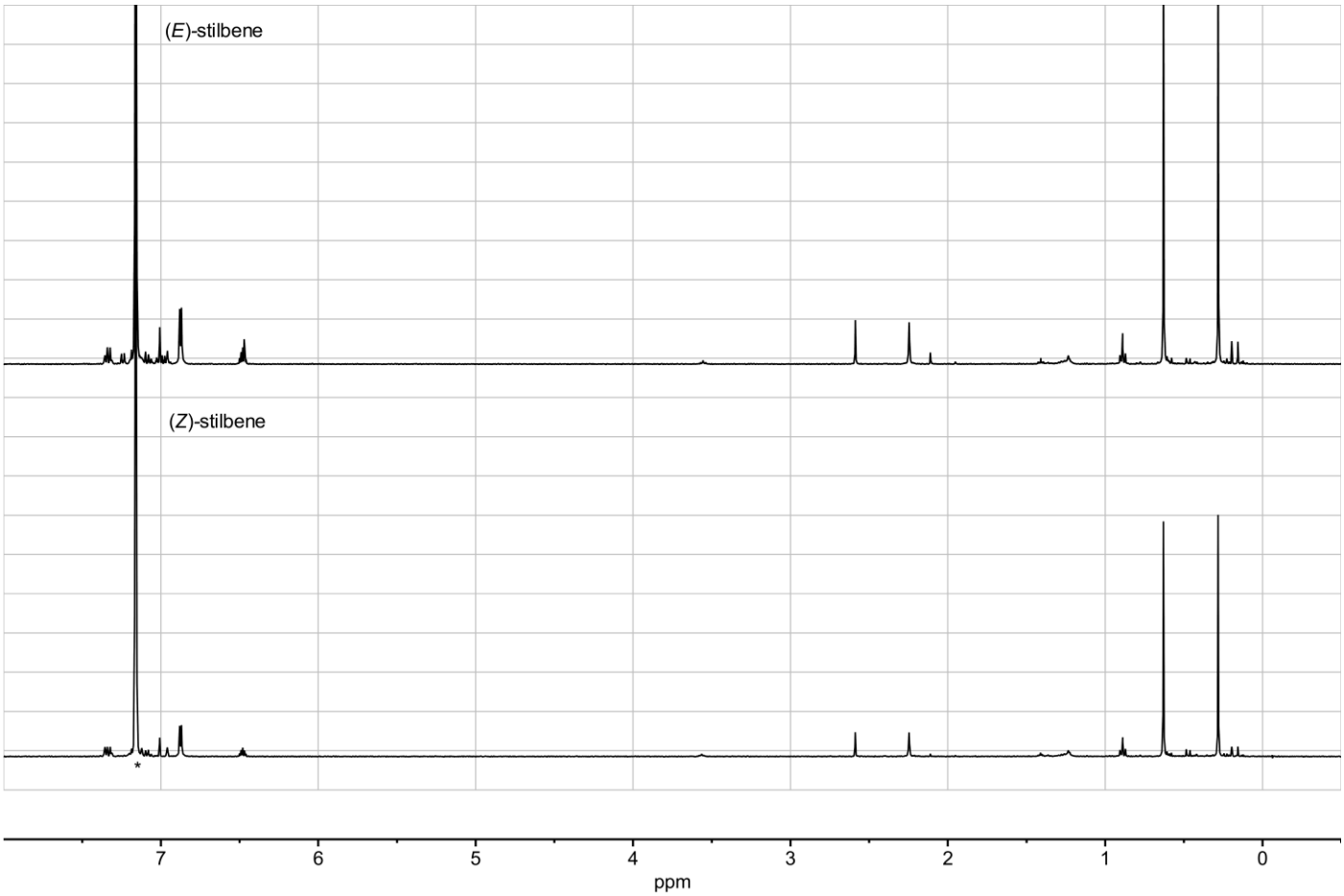

Figure 9. The ^{1}H NMR spectra of the crude product for the reaction of **1** with (*E*)- or (*Z*)-stilbenes (*C_6D_5H)

Scheme 11. Stereoretained (1+2) cycloaddition of dialkylsilylene **O** with butenes

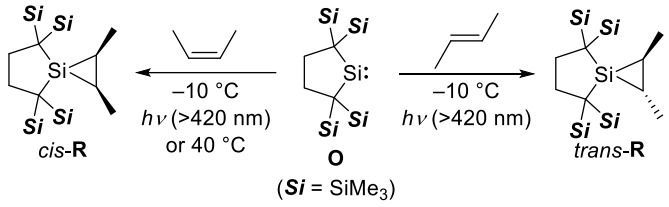

The single crystal X-ray diffraction analysis revealed characteristic structural parameters of **2**, **3**, **5**, **6**, and *trans*-**8** in comparison with those of reference compounds (Table 1). Compounds **2** and **3** are the first examples of anionic aluminanorbornadiene derivatives. Two newly formed Al–C(bridgehead) bonds of **2** and **3** [**2**: 2.1118(15), 2.1087(15) Å; **3**: 2.1125(12), 2.1154(15) Å] are longer than those of the previously reported Al-incorporated bicyclic compounds [**K**: 2.060(3), 2.073(3) Å,[16] **L**: 2.025(3), 2.044(3) Å,[10a] **S**: 2.055(4), 2.059(5) Å[21]] reflecting the steric repulsion between four trimethylsilyl substituents and benzoannulated moiety in **2** and **3**. As a result, the C–Al–C angles in **2** and **3** [**2**: 75.10(6)°; **3**: 75.21(6)°] are slightly smaller than those of reference compounds. (**K**:77.2(1)°, **L**:88.1(1)°, and **S**:81.5(1)°). Similar tendencies were found in the Al–C bonds and C–Al–C angles of **5** and *trans*-**8** in comparison with those of reference compounds (**H1**-**H6**,[15] **I**). One exception from these structural tendencies could be found in the structure of reference compound **T** probably due to the steric hindrance among bulky $CH(SiMe_3)_2$ substituents.[22]

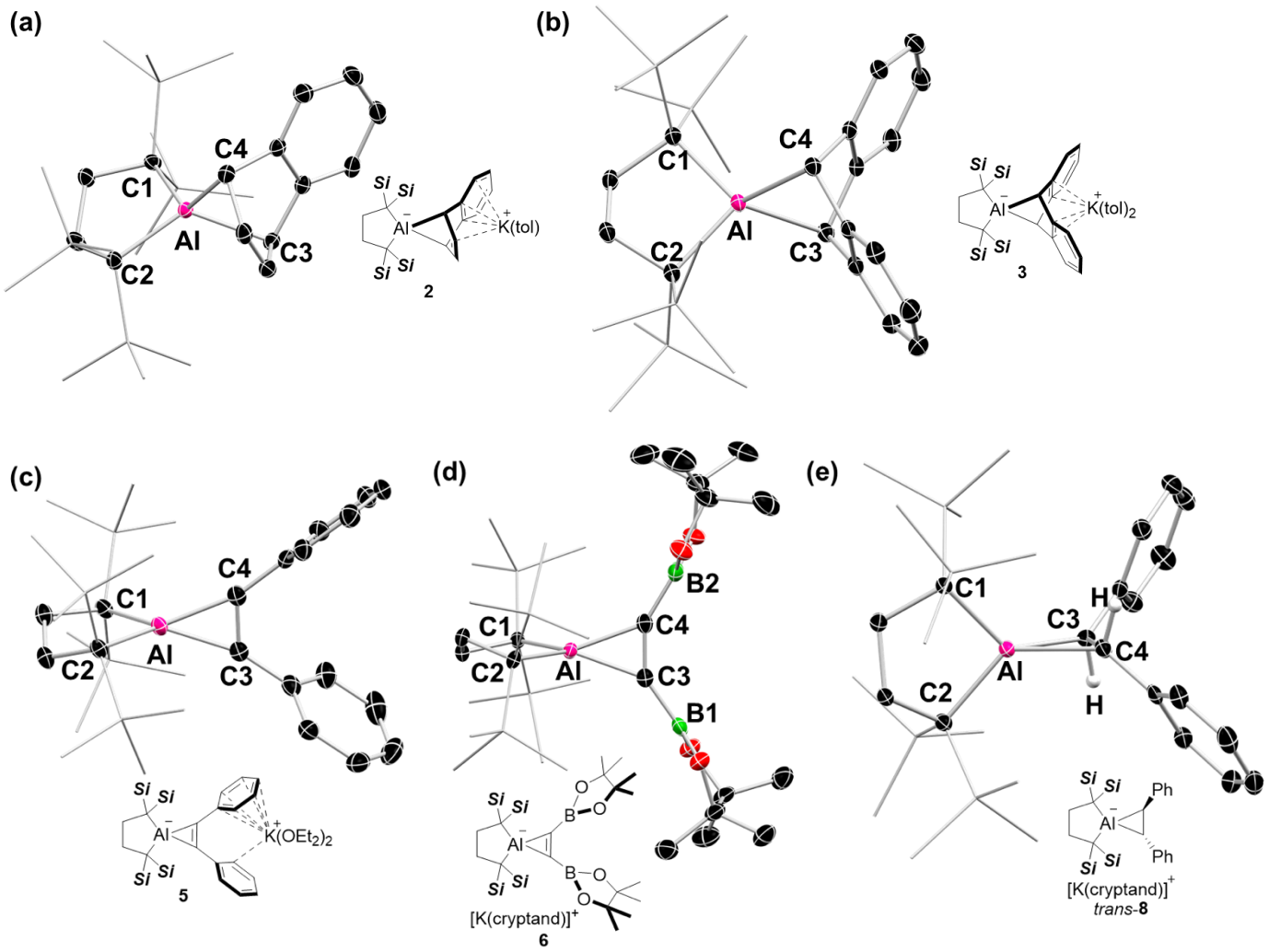

Figure 10. Molecular structure of (a) **2**, (b) **3**, (c) **5**, (d) **6** and *trans*-**8** (hydrogen atoms except methane protons on *trans*-**8** and K^+ units were omitted for clarity)

Table 1. Structual parameters (Å, °) of **2**, **3**, **5**, **6** and *trans*-**8** with those of reference compounds **S**, **H1-6** and **T**.

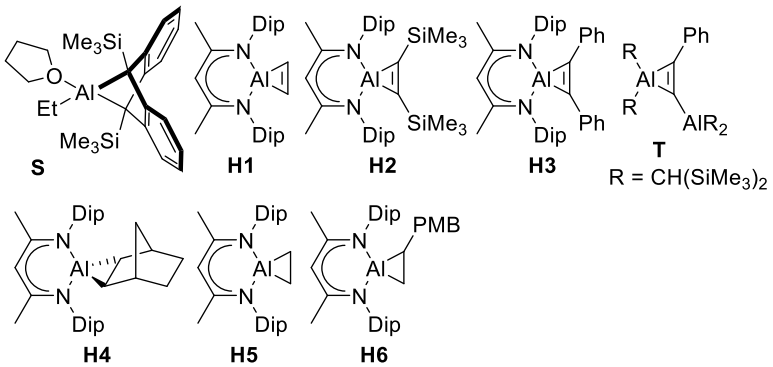

cpd	2	3	S	K	L	
Al–C (Å)	2.1118(15) 2.1087(15)	2.1125(12) 2.1154(15)	2.059(4) 2.055(4)	2.060(3) 2.073(3)	2.025(3) 2.044(3)	
C–Al–C (°)	75.10(6)	75.21(6)	81.5(1)	77.2(1)	88.1(1)	
cpd	**5**	**6**	**H1**	**H2**	**H3**	**T**
Al–C (Å)	1.945(3) 1.940(3)	1.9666(17) 1.9707(16)	1.885(2) 1.878(2)	1.899(3) 1.908(3)	1.889(3) 1.894(3) 1.887(3) 1.886(3)	2.052(3) 1.951(3)
C–Al–C (°)	41.10(14)	40.49(7)	42.30(7)	42.57(11)	42.02(14) 42.56(14)	37.6(1)
cpd	*trans*-**8**	**H4**	**H5**	**H6**	**I**	
Al–C (Å)	2.0178(18) 1.9953(19)	1.940(4) 1.948(3)	1.9209(18) 1.9163(19)	1.920(3) 1.924(3)	2.061(3) 2.071(3)	
C–Al–C (°)	45.43(14)	49.35(17)	48.54(8)	48.78(12)	42.0(1)	

In contrast, compound **1** did not react with cyclohexene, probably due to electron richness on the C=C double bond, Instead, **1** reacted with toluene solvent to afford **10** (Scheme 12). DFT calculations indicated that the the reaction giving **10** proceeded through an S_NAr mechanism as shown in Figure 10.[23] First of all, toluene molecule in the ground state **1** rotates for 60 degrees to give a slightly less stable **1'**. Then, the anionic aluminum center in **1** attacks to the *meta*-position of toluene to give the *meta*-cleaved product **10** in a concerted mechanism via a Meisenheimer-type transition state (**TS-A**).[24] The activation energy for the direct substitution of *para*-position (**path B**) from **1** is slightly higher than that for **path A** (Figure 11(a)). The electronic and structural details of **TS-A** and **TS-B** are shown in Figure 11(b). The NBO analysis revealed that the NPA charge on the *ipso*-carbon of methyl group in **TS-A** is less negative than that in **TS-B** and a longer C_a–H_a bond in **TS-A** than that in **TS-B** indicates that hyperconjugation from C_a–H_a σ-bond to vacant *p*-orbital of aluminum atom would stabilize **TS-A**.

Scheme 12. The reaction of **1** with cyclohexene

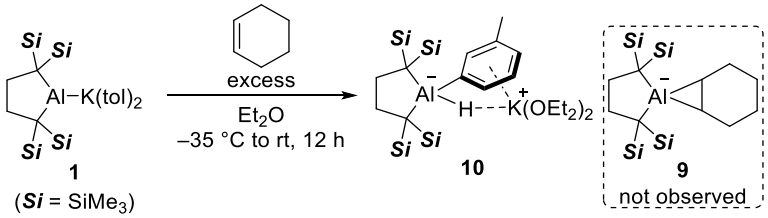

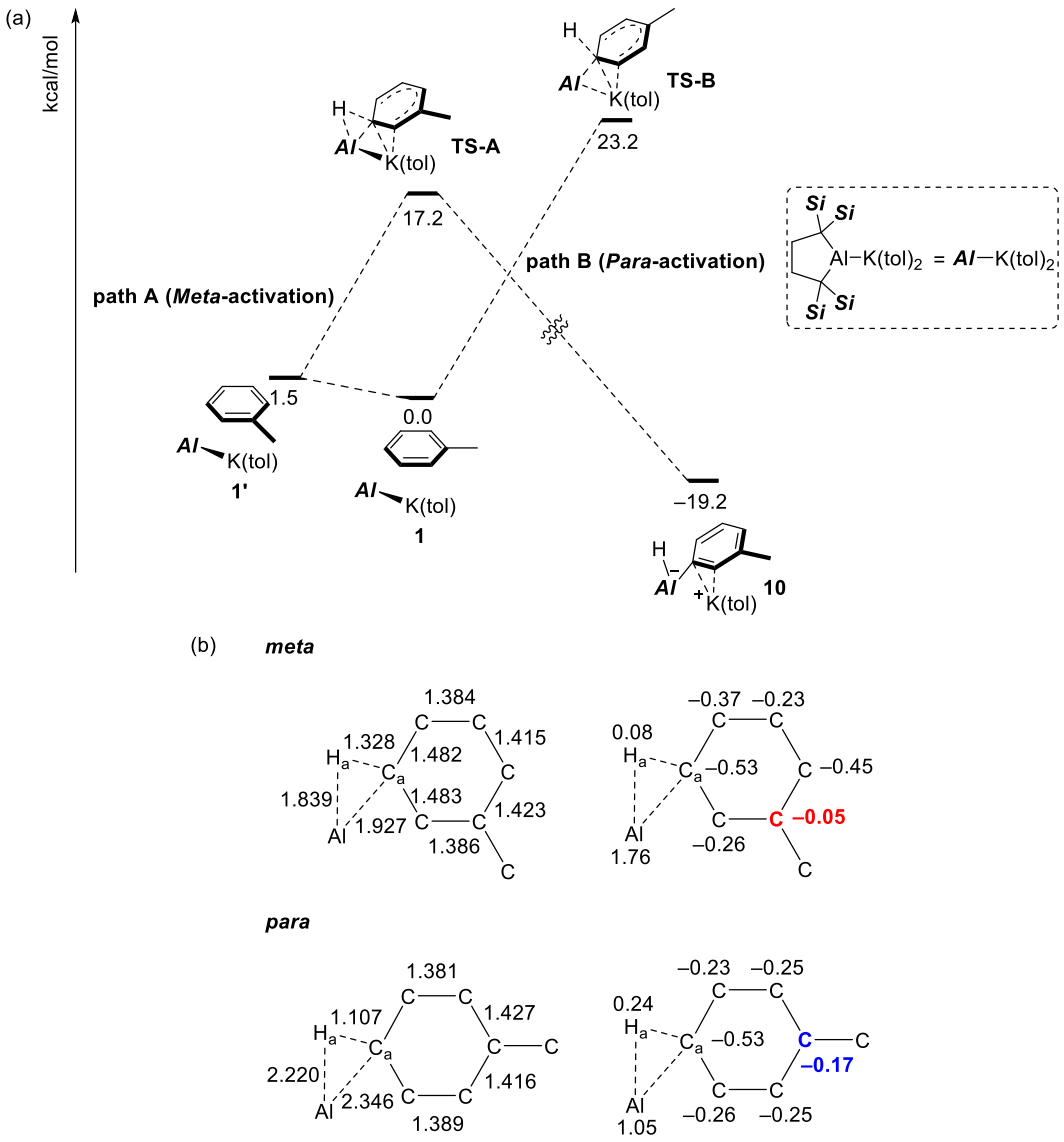

Figure 11. (a) Energy profile for *meta*- and *para*-selective C–H cleavage of toluene by using **1**, (b) Interatomic distances and distribution of NPA charges in **TS-A** and **TS-B**

To explore the utility of the cycloaddition by **1**, diboryldiyne was investigated as a substrate. This diyne is useful for the synthesis of five-membered zirconacycles (**U**) by (1+2+2) cycloaddition of "zirconium(II)" species with the diyne as shown in Scheme 13.[25] However, the reaction of **1** with the diboryldiyne did not afford (1+2+2) cycloadducts **11**, but afforded double (1+2) adduct **12**. The molecular structure of **12** was confirmed by a preliminary single-crystal X-ray diffraction analysis (Scheme 14).

Scheme 13. (1+2+2) cycloaddition of zirconocene(II) with boryl-substituted diyne

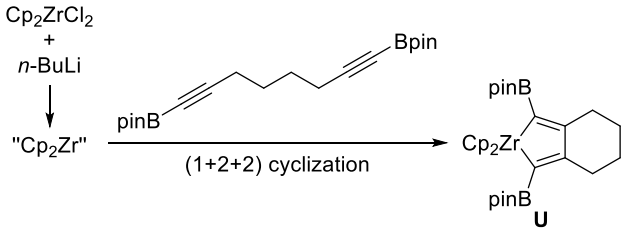

Scheme 14. Trial for the (1+2+2) cycloaddition of **1** toward the diboryldiyne

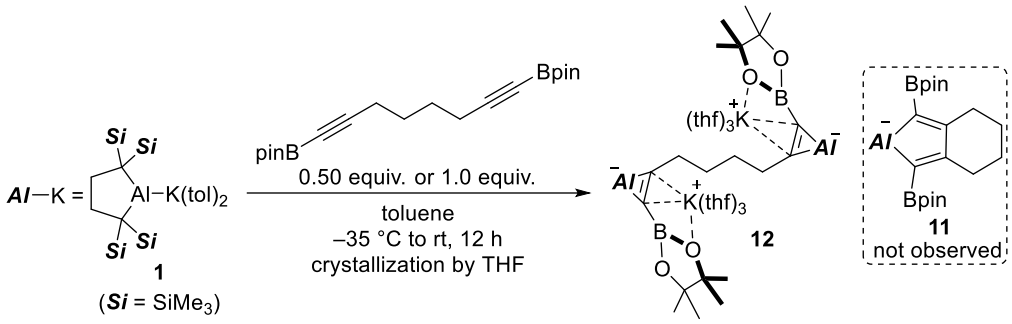

To gain insights on the electronic character of transition structures for the present cycloadditions, DFT computations were conducted for the reactions of naphthalene, diphenylacetylene, and (*E*)-, and (*Z*)-stilbenes. Initial structures of these reactions were generated by replacing one of two toluene molecules in **1** with the reactant. In the reaction of naphthalene, (1+2) cycloaddition via **naph_TS_12add** occurs, followed by a ring-expanding isomerization to (1+4) cycloadduct in concurrence of potassium migration (Figure 12). Although the second step of (1+2) to (1+4) isomerization did not provide the exact transition structures, the reaction pathway search performed with AFIR method followed by locally updated plane (LUP) relaxation[26] provided approximate minimum energy pathways (MEPs) (Figure 13). As a result, two pathways, (i) direct isomerization from **naph_12a** and (ii) potassium migration to **naph_12b** prior to isomerization were found. In both cases, the activation barriers were roughly estimated about 15 kcal/mol, which is apparently smaller than that for **naph_TS_12add**, indicating the (1+2) step should be the rate-determining step. This result is consistent with that no intermediate was detected in the experimental study.

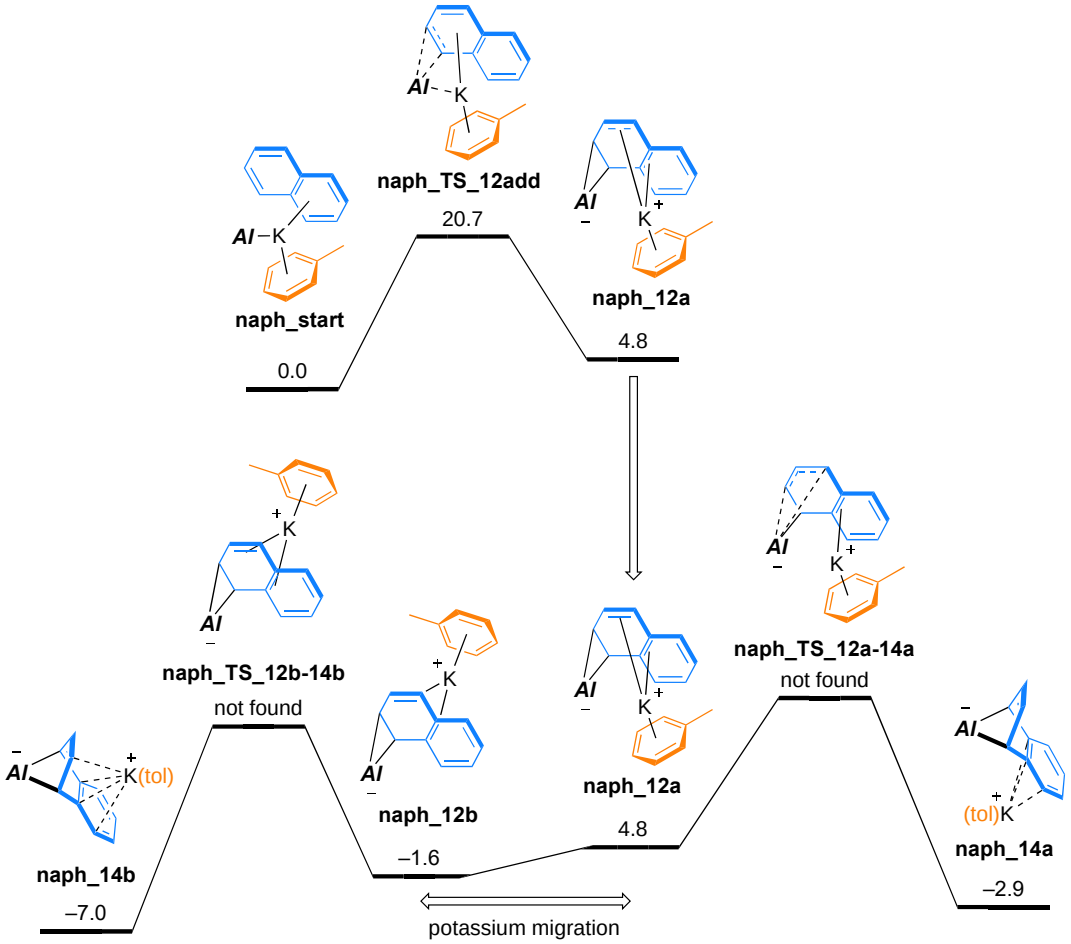

Figure 12. Free energy profile of cycloaddition of naphthalene

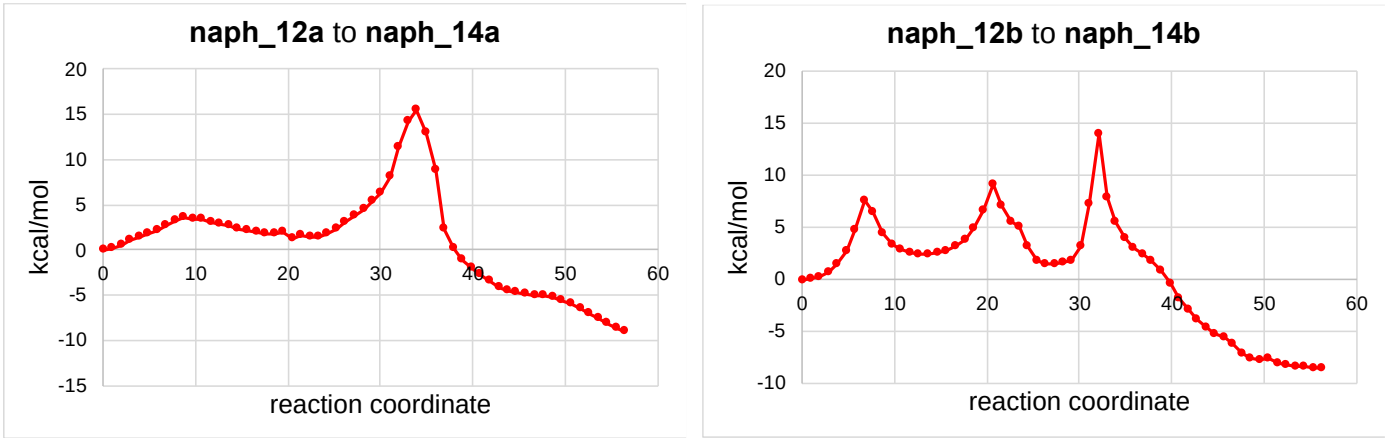

Figure 13. LUP paths of isomerization from (1+2) to (1+4) cycloadducts.

For the cycloaddition of diphenylacetylene and *(E)*-stilbene, one transition structure was found with a reasonable activation barrier in each case (Figures 14 and 15). In both of the transition structures (**PhCCPh_TS** and **E_TS**), the anionic Al atom is attacking to the carbon atom which attaches to the potassium-bound benzene ring. IRC analysis from both transition structures indicated the concerted cyclization to form the Al–C–C three-membered ring.

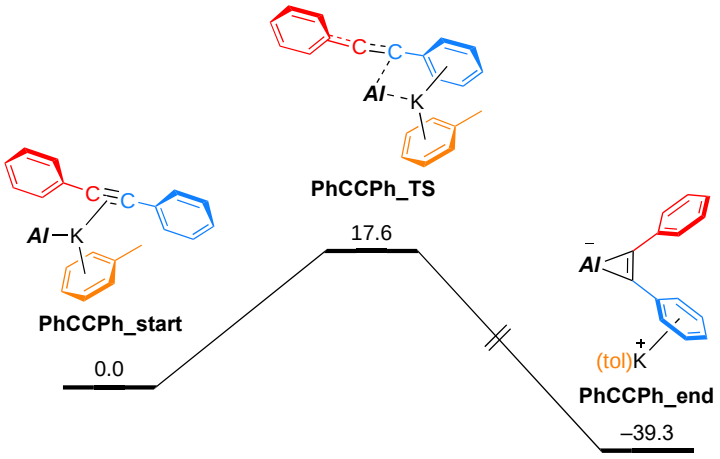

Figure 14. Free energy profile of cycloaddition of diphenylacetylene.

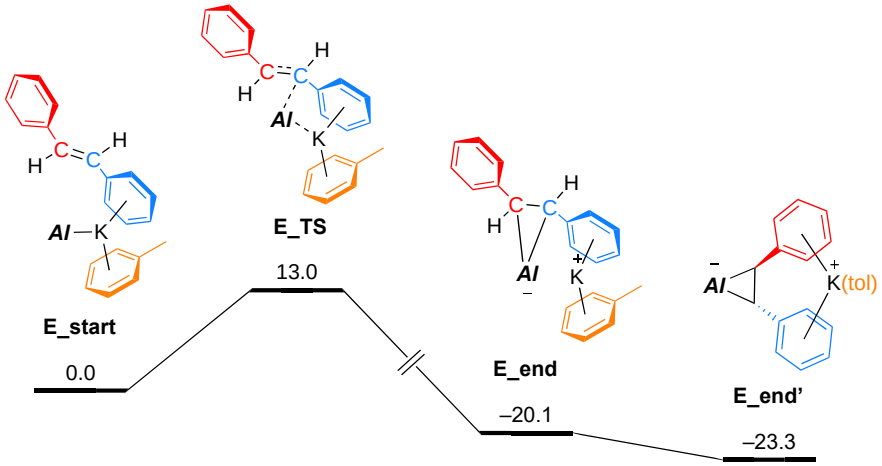

Figure 15. Free energy profile of cycloaddition of (*E*)-stilbene.

For the cycloaddition of (*Z*)-stilbene, the IRC analysis resulted in a stationary point (**Z_int**) which is very close to the transition structure (**Z_TS1**) (Figure 16). The transition states of the 2nd steps could not be obtained, due to the small activation barriers and the large size of the molecules. The reaction pathway search performed with AFIR method followed by LUP relaxation provided MEP (Figure 17). Note that the transition state **Z-TS1** in Figure S16 was obtained from the highest point of the MEPs (Figure 17), and both ends of the MEP are same as the starting structure **Z-start** and the final structure **Z-end** in Figure 16. The MEP suggested the 2nd step of carbanion addition to aluminum is a rotational TS of C–C bond and thus may have a very small activation barrier.

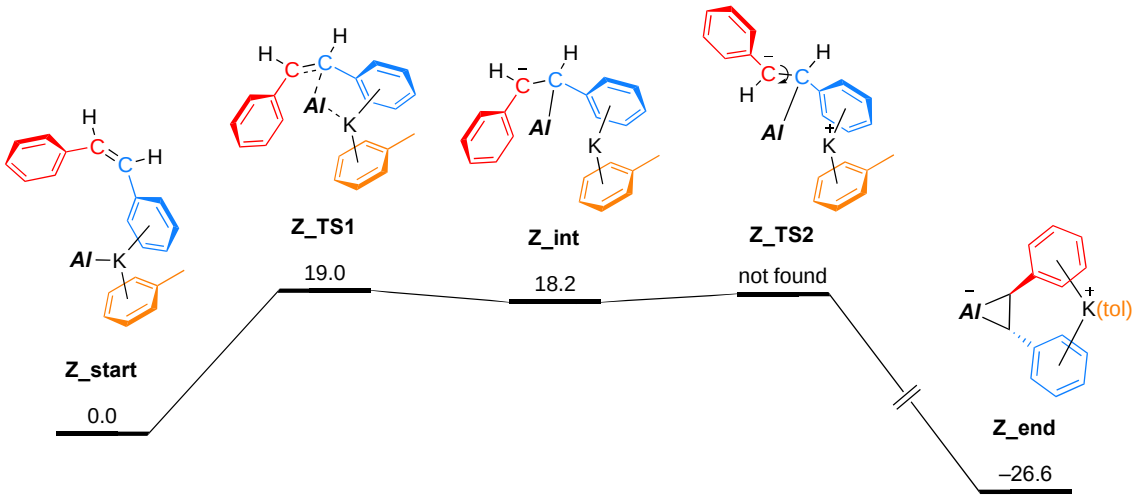

Figure 16. Free energy profile of cycloaddition of (*Z*)-stilbene.

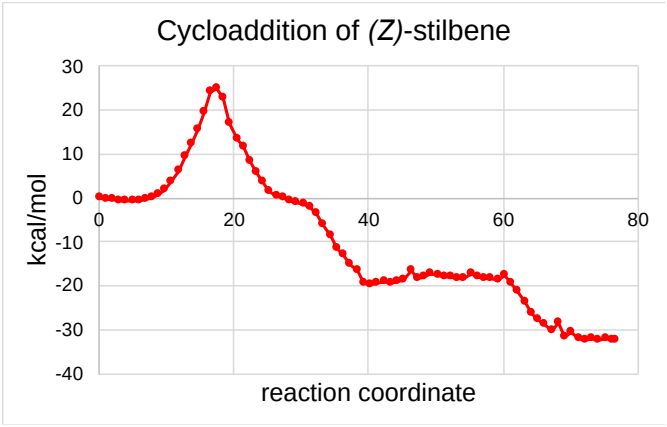

Figure 17. LUP path of (*Z*) -stilbene cycloaddition.

The carbanionic nature of the transition structure of cycloaddition of diphenylacetylene, *(E)*- and *(Z)*-stilbene is supported as follows (Table 2). The natural charges obtained by NBO analysis on those unsaturated compounds in the transition structures are summarized in Table 2. Both of the half attaching on the aluminum (blue part) and the half not attaching to the aluminum (red part) bear negative overall charge, while toluene coordinating to the potassium (yellow part) bears slight positive charge. Also, it should be noted that the C_1-C_2 bond lengths are slightly shortened compared to free substrate, suggesting that anion delocalization over the phenyl ring.

Table 2. Natural charges and selected bond lengths (Å) in the transition structures and free reactant.

reactant	PhCCPh	*(E)*-stilbene	*(Z)*-stilbene
Charge on Al attached half (blue)	–0.30091	–0.38684	–0.28283
Charge on Al unattached half (red)	–0.08457	–0.22751	–0.14422
Charge on toluene (yellow)	0.00199	0.00464	0.00138
C-C bond length in TS	1.40732	1.44266	1.45255
C-C bond length in free reactant	1.42631	1.46562	1.47478

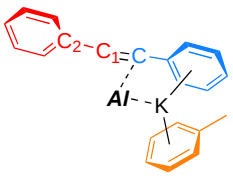

2.3. Conclusion

In conclusion, cycloaddition of **1** toward unsaturated hydrocarbons was investigated. Reactions of **1** with naphthalene and anthracene furnished anionic aluminabenzonorbornadiene through (1+4) cycloaddition. Diphenylacetylene, diborylacetylene and stilbenes gave Al-containing three-membered ring compounds. The reaction of (*E*)- and (*Z*)-stilbene solely gave *trans*-isomer. DFT calculations suggested a carbanionic character of transition states explaining the selectivity toward *trans*-**8**.

2.4. Experimental Section

General

All manipulations involving the air- and moisture-sensitive compounds were carried out under an argon atmosphere using glovebox (Korea KIYON) technique. All glasswares and glass fiber filter (ADVANTEC, GC-50) were dried for 20 min in the 250 °C oven before use. Toluene, hexane, Et_2O, and THF was purified by passing through a solvent purification system (Grass Contour). C_6D_6, was dried by mixing with sodium/benzophenone and subsequent vacuum distillation. THF-d_8 was dried by mixing with sodium/potassium alloy and subsequent filtration through a pre-activated neutral alumina. The nuclear magnetic resonance (NMR) spectra were recorded on JEOL ECS-400 (399 MHz for ^{1}H, 100 MHz for ^{13}C). Chemical shifts are reported in δ ppm relative to the residual protiated solvent for ^{1}H, deuterated solvent for ^{13}C used as references. The absolute values of the coupling constants are given in Hertz (Hz). Multiplicities are abbreviated as singlet (s), doublet (d), triplet (t), multiplet (m), and broad (br). Melting points were determined on Optimelt (SRS) and were uncorrected. X-ray crystallographic analysis was performed on XtaLAB Synergy/Hypix-6000HE diffractometer. Elemental analyses were performed on a Perkin Elmer 2400 series II CHN analyzer. Tetraalkyldialumane **S1**[14], diborylalkyne[27], diborylidiyne[28] was prepared by literature method. Naphthalene (Sigma-Aldrich), anthracene (Kanto), diphenyl acetylene (TCI), (*E*)-stilbene (TCI), (*Z*)-stilbene (TCI), and [2.2.2]-Cryptand (TCI).

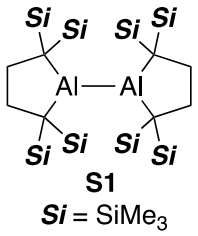

S1
Si = $SiMe_3$

Synthesis of 2

In a glovebox, pre-cooled (–35 °C) crystalline tetraalkyldialumane **S1** (50.0 mg, 67.0 μmol) and potassium graphite (50.0 mg, 369 μmol) were placed in a 3 mL vial with a glass stirring bar, then pre-cooled toluene/THF (1.50 mL, v/v = 100/1) was added to the mixture and the resulting suspension was stirred at –35 °C for 2 days. After the filtration by using a pre-cooled (–35 °C) plastic syringe with glass fiber filter, a red solution of **1** was obtained. To a precooled (–35 °C) toluene (1.00 mL) solution of naphthalene (86.0 mg, 670 μmol) in a 15 mL vial, the solution of **1** was added. The resulting orange solution was stirred for 1 h at room temperature and then volatiles were evaporated under reduced pressure. To the residue, hexane was added and volatiles were removed in vacuo. This addition/evaporation cycle was repeated for three times. The obtained crude material was washed with hexane to afford **2** as colorless solids (81.7 mg, 129 μmol, 96%). Single crystals suitable for X-ray analysis were obtained by recrystallization from toluene at –35 °C. ^{1}H NMR (Figure 2, 399 MHz, THF-d_8, 304 K) δ –0.24 (s, 18H, Si(CH_3)$_3$), 0.09 (s, 18H, Si(CH_3)$_3$), 1.77 (s, 4H, CH_2), 2.89 (m, 2H, bridgehead C*H*), 5.99 (m, 2H, alkenyl C*H*), 6.56 (m, 2H, aromatic), 6.78 (m, 2H, aromatic); ^{13}C NMR

(Figure 18, 100 MHz, THF-d_8, 304 K) δ 3.64 (Si(CH_3)$_3$), 4.33 (Si(CH_3)$_3$), 9.12 (4°, C(Si(CH_3)$_3$)$_2$), 33.5 (CH_2), 34.4 (CH_2), 52.5 (bridgehead C) 120.4 (ArH), 121.6 (ArH), 127.0 (alkenyl CH), 149.4 (4°); mp. 233-278 °C (decomp.); Anal. Calcd for $C_{26}H_{45}AlKSi_4$·0.86(toluene) [estimated by ^{1}H NMR spectrum after evacuation]: C, 62.20; H, 8.95; found: C, 62.11; H, 9.12.

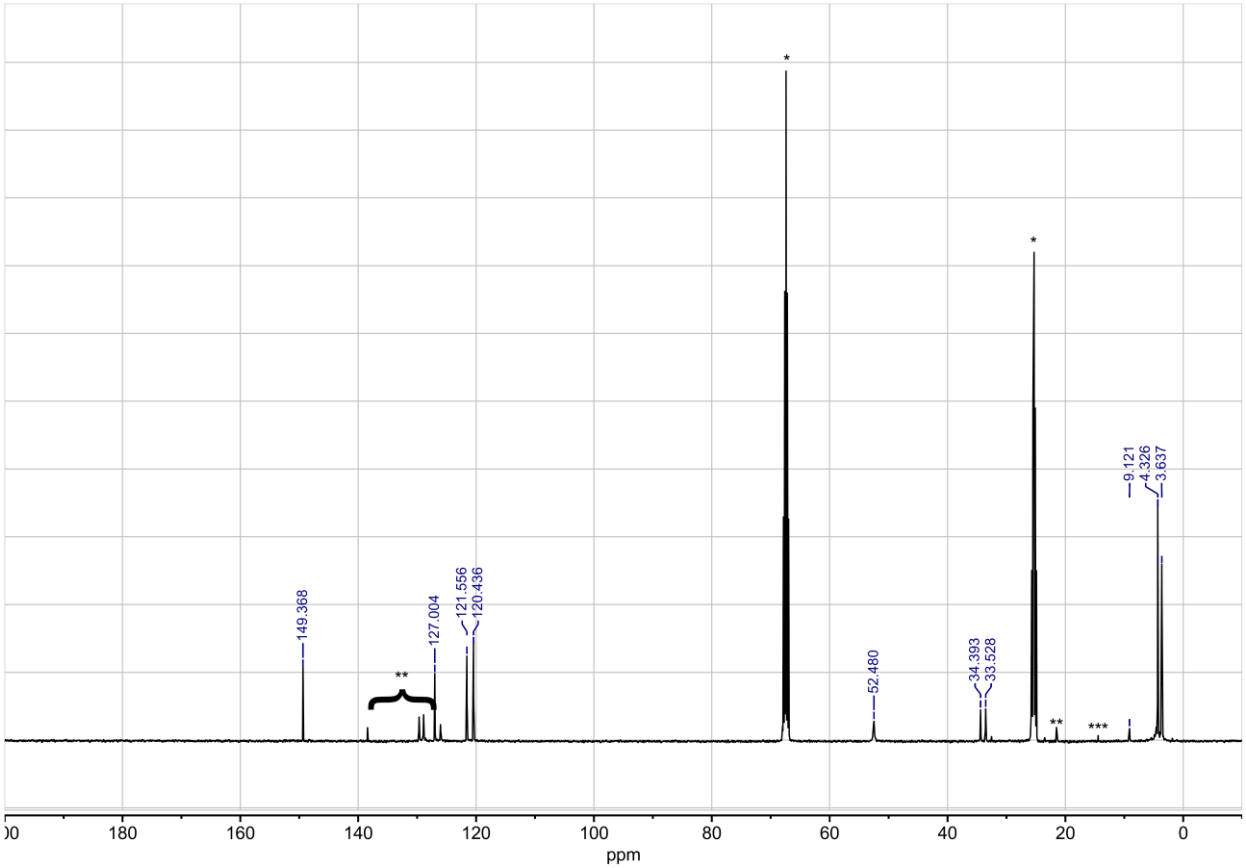

Figure 18. The ^{13}C NMR spectrum of **2** (*THF-d_8, **free toluene dissociated from **2**, ***hexane from glovebox atmosphere)

Synthesis of 3

In a glovebox, pre-cooled (–35 °C) crystalline tetraalkyldialumane **S1** (50.0 mg, 67.0 μmol) and potassium graphite (50.0 mg, 369 μmol) were placed in a 3 mL vial with a glass stirring bar, then pre-cooled toluene/THF (1.50 mL, v/v = 100/1) was added to the mixture and the resulting suspension was stirred at –35 °C for 2 days. After the filtration by using a pre-cooled (–35 °C) plastic syringe with glass fiber filter, a red solution of **1** was obtained. Precooled 3.0 mL toluene solution of anthracene (24.0 mg, 134 μmol) were placed in 15 mL vial, then pre-cooled solution of **1** was added to the solution. The resulting orange solution was stirred for 1 hour at room temperature and then volatiles were evaporated under reduced pressure. The residues were washed by hexane to afford **3** as yellow solids (68.8 mg, 89.0 μmol, 66% yield). Single crystals suitable for X-ray analysis were obtained by recrystallization from vapor diffusion by toluene and pentane in a sealed vial. ^{1}H NMR (Figure 3, 399 MHz, THF-d_8, 304 K) δ -0.20 (s, 36H, Si(CH_3)$_3$), 1.75 (s, 4H, CH_2), 3.34 (s, 2H, bridgehead CH), 6.53 (m, 4H, aromatic), 6.94 (m, 4H, aromatic); ^{13}C NMR (Figure. 19, 100 MHz, THF-d_8) δ 3.86 (SiCH_3)$_3$), 3.90 (Si(CH_3)$_3$), 6.96 (4°), 34.51 (CH_2), 55.0 (bridgehead C), 120.7 (aromatic), 122.7 (aromatic), 122.9 (aromatic), 148.5 (aromatic) mp 228-251 °C (decomp.); Anal. Calcd for

$C_{30}H_{50}AlKSi_4 \cdot 0.60$(toluene) [estimated by ^{1}H NMR spectrum after evacuation]: C, 63.74; H, 8.57: found; C, 63.45; H, 8.66.

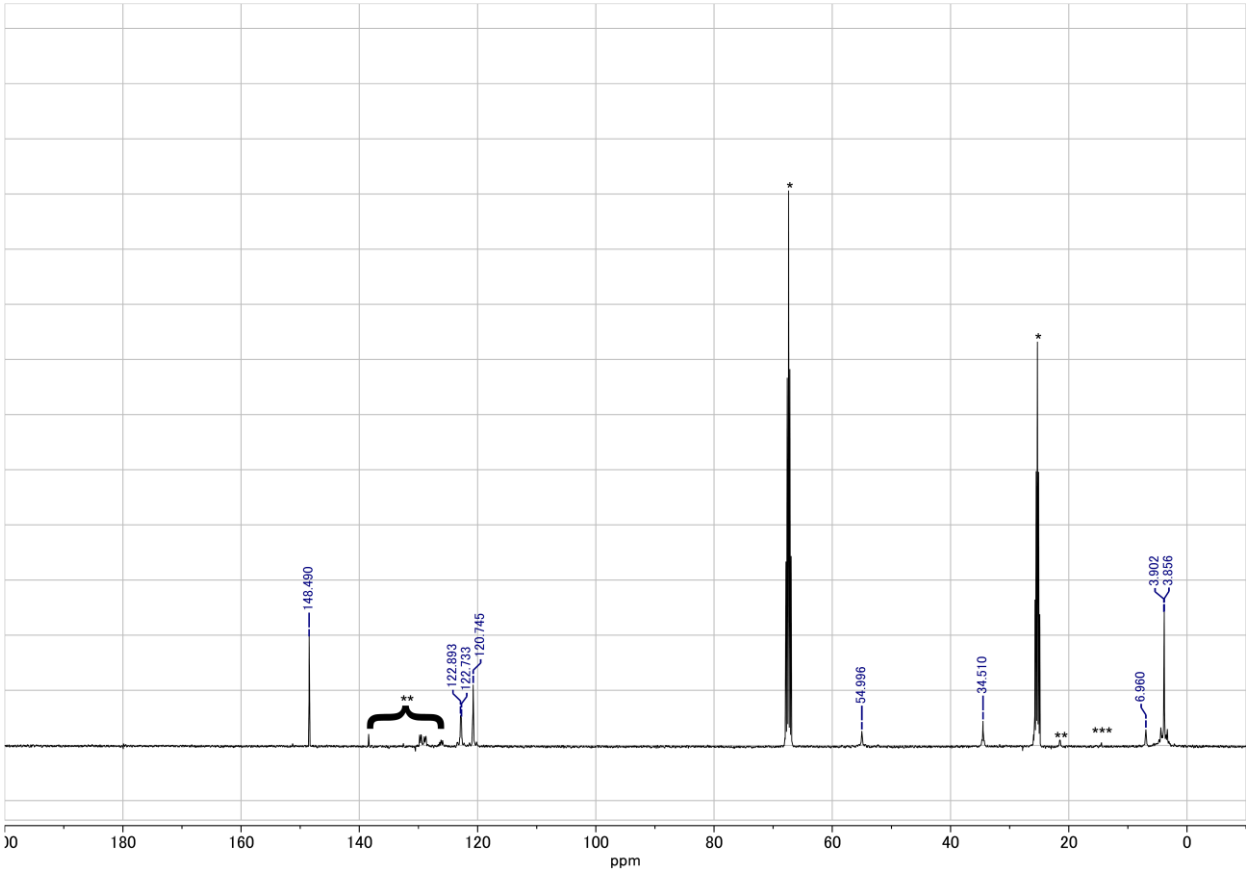

Figure 19. The ^{13}C NMR spectrum of **3** (*THF-d_8, **free toluene dissociated from **3**, ***hexane from glovebox atmosphere)

Synthesis of 5

In a glovebox, pre-cooled (–35 °C) crystalline tetraalkyldialumane **S1** (50.0 mg, 67.0 μmol) and potassium graphite (50.0 mg, 369 μmol) were placed in a 3 mL vial with a glass stirring bar, then pre-cooled toluene/THF (1.50 mL, v/v = 100/1) was added to the mixture and the resulting suspension was stirred at –35 °C for 2 days. After the filtration by using a pre-cooled (–35 °C) plastic syringe with glass fiber filter, a red solution of **1** was obtained. To a precooled (–35 °C) toluene (1.00 mL) solution of diphenylacetylene (71.6 mg, 402 μmol) in a 3 mL vial, the solution of **1** was added. The resulting orange solution was stirred for 3 h at room temperature and then volatiles were evaporated under reduced pressure. To the residue, hexane was added and volatiles were removed in vacuo. This addition/evaporation cycle was repeated for three times. The obtained crude material was washed with hexane to afford **5** as yellow solids (67.2 mg, 91.1 μmol, 68%). Single crystals suitable for X-ray analysis were obtained by recrystallization from Et_2O with slow evaporation to silica gel in a sealed vial. ^{1}H NMR (Figure 5, 399 MHz, THF-d_8, 304 K) δ 0.07 (s, 36H, Si(CH_3)$_3$), 1.85 (s, 4H, CH_2), 6.57 (t, J = 7 Hz, 2H, *p*-C*H*), 6.84 (t, J = 8 Hz, 4H, *m*-C*H*), 6.94 (d, J = 8 Hz, 4H, *o*-C*H*); ^{13}C NMR (Figure 20, 100 MHz, THF-d_8, 304 K) δ 0.65 (4°), 4.03 (Si(*C*H$_3$)$_3$), 33.2 (*C*H$_2$), 120.8 (*p*-*C*H), 127.1 (*m*- and *o*-*C*H, overlapped, confirmed by HMQC), 151.0 (*ipso C*), 183.8 (*C*=*C*); mp 107-121 °C (decomp.);

Anal. Calcd for $C_{30}H_{50}AlKSi_4 \cdot 0.10(Et_2O)$ [estimated by ^1H NMR spectrum after evacuation]: C, 61.20; H, 8.61; found: C, 61.52; H, 8.97.

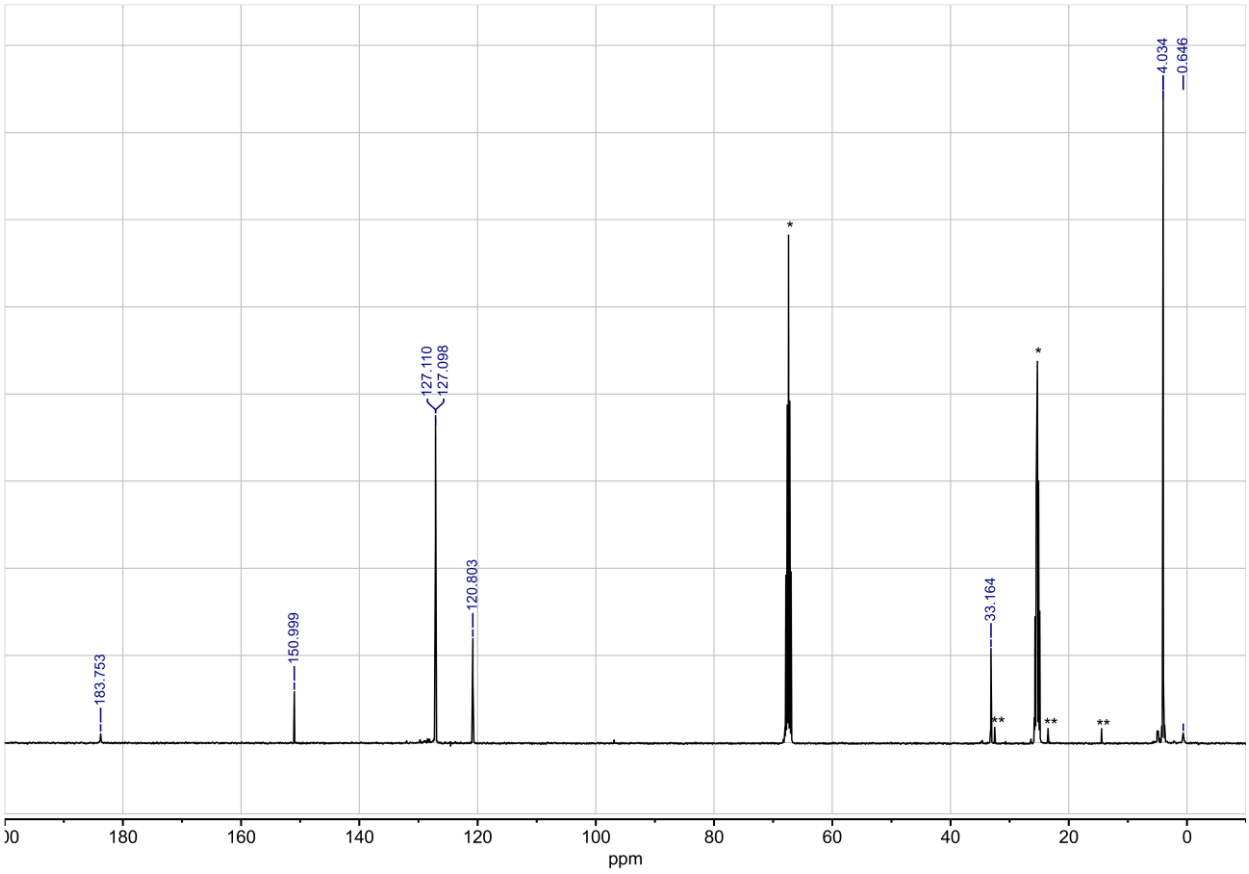

Figure 20. The ^{13}C NMR spectrum of **5** (*THF-d_8, ** hexane from glovebox atmosphere)

Synthesis of 6

Pre-cooled (–35 °C) **S1** (50.0 mg, 67.0 μmol) and potassium graphite (50.0 mg, 369 μmol) were placed in a 3 mL vial with a glass stirring bar, then pre-cooled toluene/THF (1.50 mL, v/v = 100:1) was added to the mixture and the resulting suspension was stirred at –35 °C for 2 days. After the filtration by using a pre-cooled (–35 °C) plastic syringe with glass fiber filter, a red solution of **1** was obtained. To a precooled (–35 °C) toluene (1.00 mL) solution of 1,2-bis(4',4',5',5'-tetramethyl[1',3',2'-dioxaborolan-2'-yl] ethyne (40.0 mg, 147 μmol) in a 15 mL vial, the solution of **1** was added. The resulting orange solution was stirred for 2 h at room temperature and then volatiles were evaporated under reduced pressure. To the residue, hexane was added and volatiles were removed in vacuo. This addition/evaporation cycle was repeated for three times. The obtained crude material was washed with hexane to afford yellow solids. To a benzene (10.0 mL) solution of the residue, the benzene (2.00 mL) solution of [2.2.2]-Cryptand (43.0 mg, 116 μmol) was added. After stirring the resulting solution for 1 h at room temperature, the yellow solution was evaporated under reduced pressure. The residue was washed by hexane afford **6** as yellow solids (99.2 mg, 93.1 μmol, 69%). Single crystals suitable for X-ray analysis were obtained by recrystallization from benzene at room temperature. ^1H NMR (Figure 6, 399 MHz, THF-d_8, 304 K) δ 0.02 (s, 36H, Si(CH_3)$_3$), 1.16 (s, 24H, CH_3), 1.74 (s, CH_2), 2.58 (t, J = 5 Hz, 12 H, NCH_2CH$_2$O, 3.57 (t, J = 5 Hz, 12 H, OCH_2CH$_2$N), 3.62 (s, 12 H, OCH_2-CH_2O); ^{11}B NMR

(Figure 21, 128 Hz, 304 K) δ –4.50 (THF coordination to Bpin), 31.3 ^{13}C NMR (Figure 22, 100 MHz, THF-d_8, 304 K) δ -2.24 (4°), 4.07 (Si(*C*H$_3$)$_3$), 33.2 (*C*H$_2$), 54.8 (N*C*H$_2$CH$_2$O), 68.5 (NCH$_2$*C*H$_2$O), 71.4 (OCH$_2$-*C*H$_2$O), 80.6 (*C*Me$_2$); (Al–*C*=*C*-B was not detected from ^{13}C NMR and HMBC), mp 122-155 °C (decomp.); Anal. Calcd for $C_{48}H_{100}AlB2N2KO10Si4$: C, 54.12; H, 9.46: N 2.63 found; C, 54.42; H, 9.44; N, 2.54.

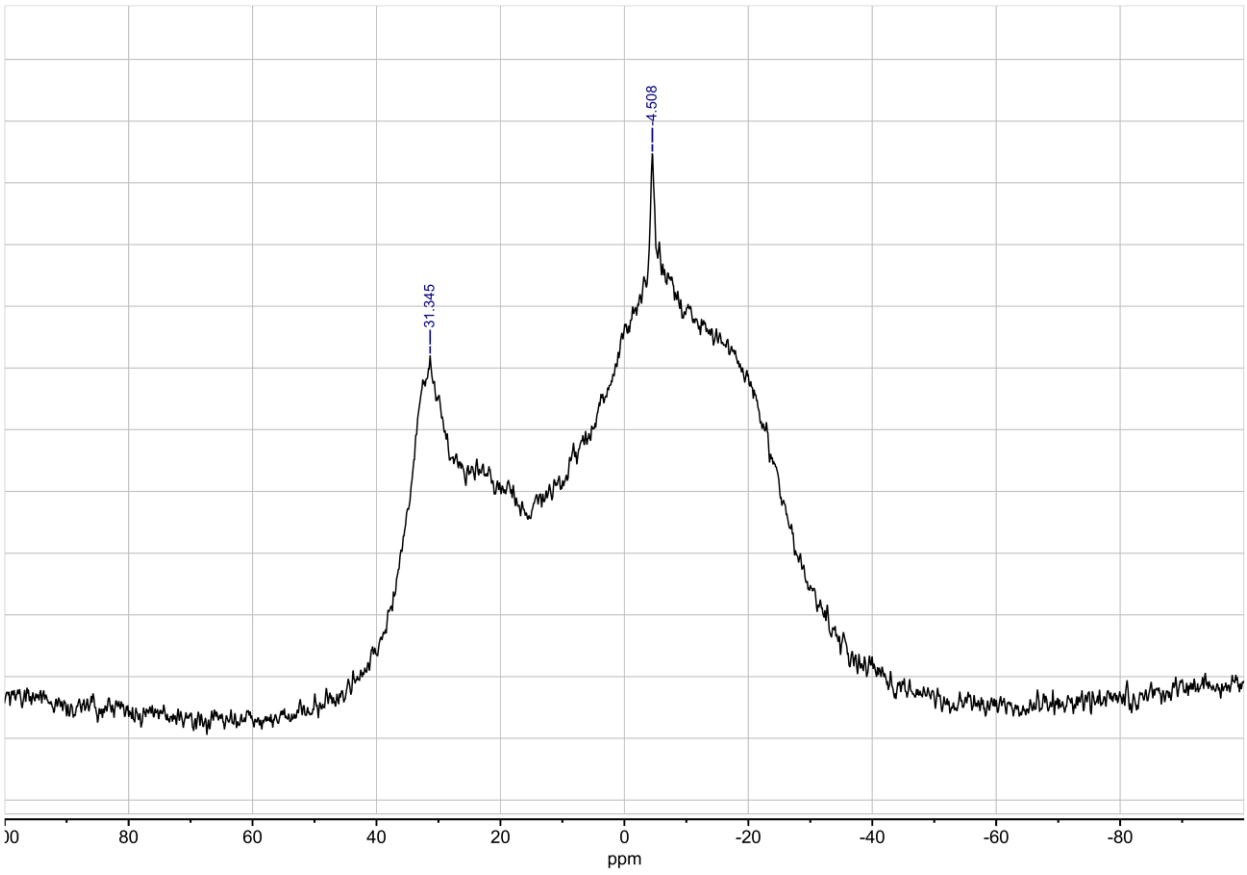

Figure 21. The ^{11}B NMR spectrum of **6**

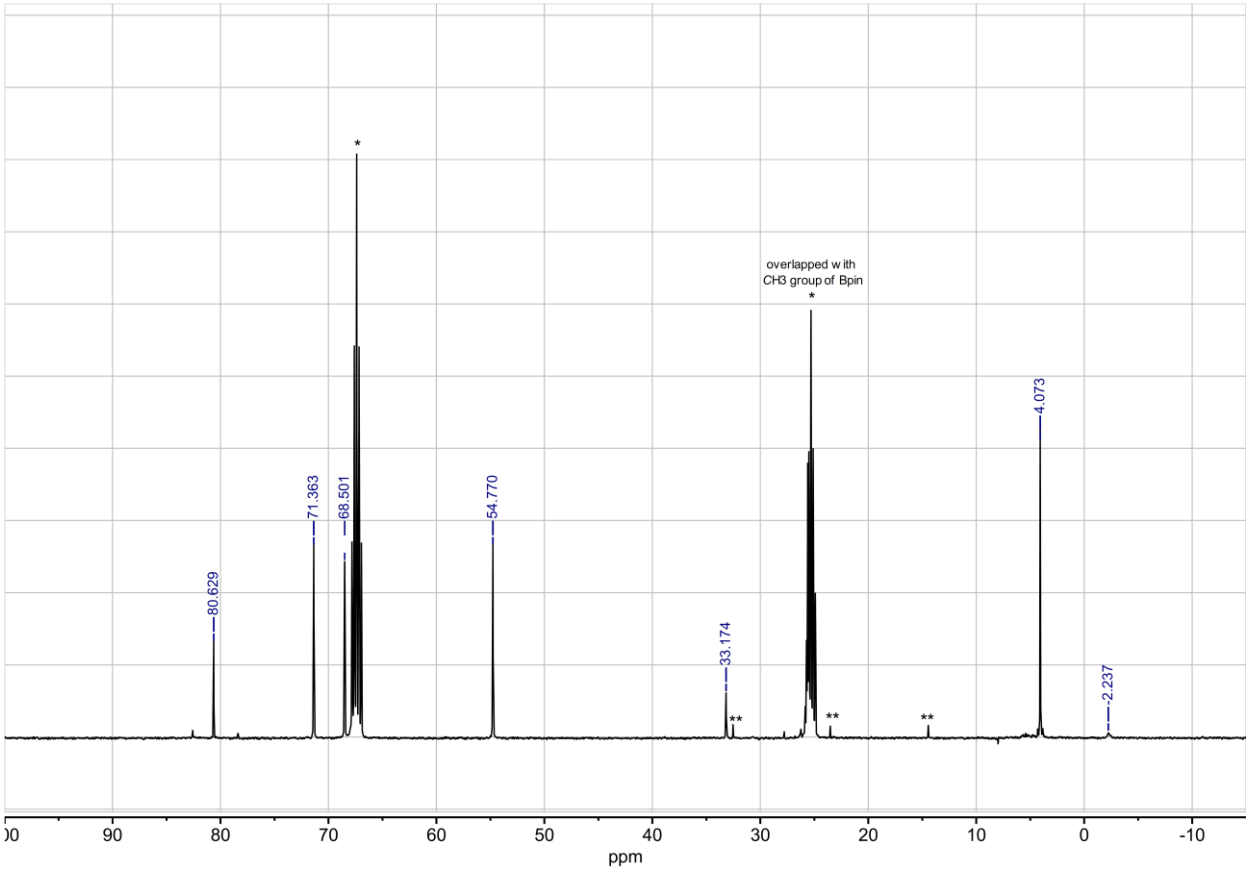

Figure 22. The ^{13}C NMR spectrum of **6** (*THF-d_8 **hexane from glovebox atmosphere)

Synthesis of *trans*-8

In a glovebox, pre-cooled (–35 °C) crystalline tetraalkyldialumane **S1** (50.0 mg, 67.0 μmol) and potassium graphite (50.0 mg, 369 μmol) were placed in a 3 mL vial with a glass stirring bar, then pre-cooled toluene/THF (1.50 mL, v/v = 100/1) was added to the mixture and the resulting suspension was stirred at –35 °C for 2 days. After the filtration by using a pre-cooled (–35 °C) plastic syringe with glass fiber filter, a red solution of **1** was obtained. To a precooled (–35 °C) toluene (1.00 mL) solution of (*E*)-stilbene (74.2 mg, 402 μmol) in a 3 mL vial, the solution of **1** was added. The resulting orange solution was stirred for 2 h at room temperature and then volatiles were evaporated under reduced pressure. To the residue, hexane was added and volatiles were removed in vacuo. This addition/evaporation cycle was repeated for three times. The obtained crude material was washed with hexane to afford yellow solids. To a benzene (3.00 mL) solution of the residue, the benzene (2.00 mL) solution of [2.2.2]-Cryptand (41.0 mg, 114 μmol) was added. After stirring the resulting solution for 1 h at room temperature, the yellow-green solution was evaporated under reduced pressure. The residue was washed by hexane afford *trans*-**5** as yellow solids (111 mg, 114 mmol, 85%). Single crystals suitable for X-ray analysis were obtained by recrystallization from benzene at room temperature. ^{1}H NMR (Figure 23, 399 MHz, THF-d_8, 304 K) δ –0.24 (s, 18H, Si(CH_3)$_3$), 0.17 (s, 18H, Si(CH_3)$_3$, 1.82 (m, 4H, CH_2), 2.50 (t, J = 5 Hz, 12 H, NCH_2CH$_2$O), 2.57 (s, 2H, *CH*Ph), 3.48 (t, J = 5 Hz, 12 H, OCH_2CH$_2$N), 3.53 (s, 12 H, OCH_2-CH_2O), 6.29 (t, J = 7 Hz, 2H, *p*-C*H*); 6.76 (t, J = 8 Hz, 4H, *m*-CH), 6.96 (d, J = 8 Hz, 4 H, *o*-C*H*); ^{13}C NMR (Figure 24, 100 MHz, THF-d_8, 304 K) δ 0.94 (4°), 3.63 (Si(*C*H$_3$)$_3$), 4.42 (Si(*C*H$_3$)$_3$), 33.9 (*C*H$_2$), 34.8 (*C*H), 54.7 (N*C*H$_2$CH$_2$O), 68.4 (NCH$_2$*C*H$_2$O), 71.3 (OCH$_2$-*C*H$_2$O) 116.5 (*para*-*C*H), 124.3 (*ortho*-*C*H),

127.4 (*meta*-*C*H), 157.1 (*ipso C*); mp 137-151 °C (decomp.); Anal. Calcd for $C_{48}H_{88}AlKN_2O_6Si_4 \cdot 0.09(C_6H_6)$ [estimated by ^{1}H NMR spectrum after evacuation]: C, 59.82; H, 9.16: N 2.87 found; C, 59.79; H, 9.33; N, 2.77.

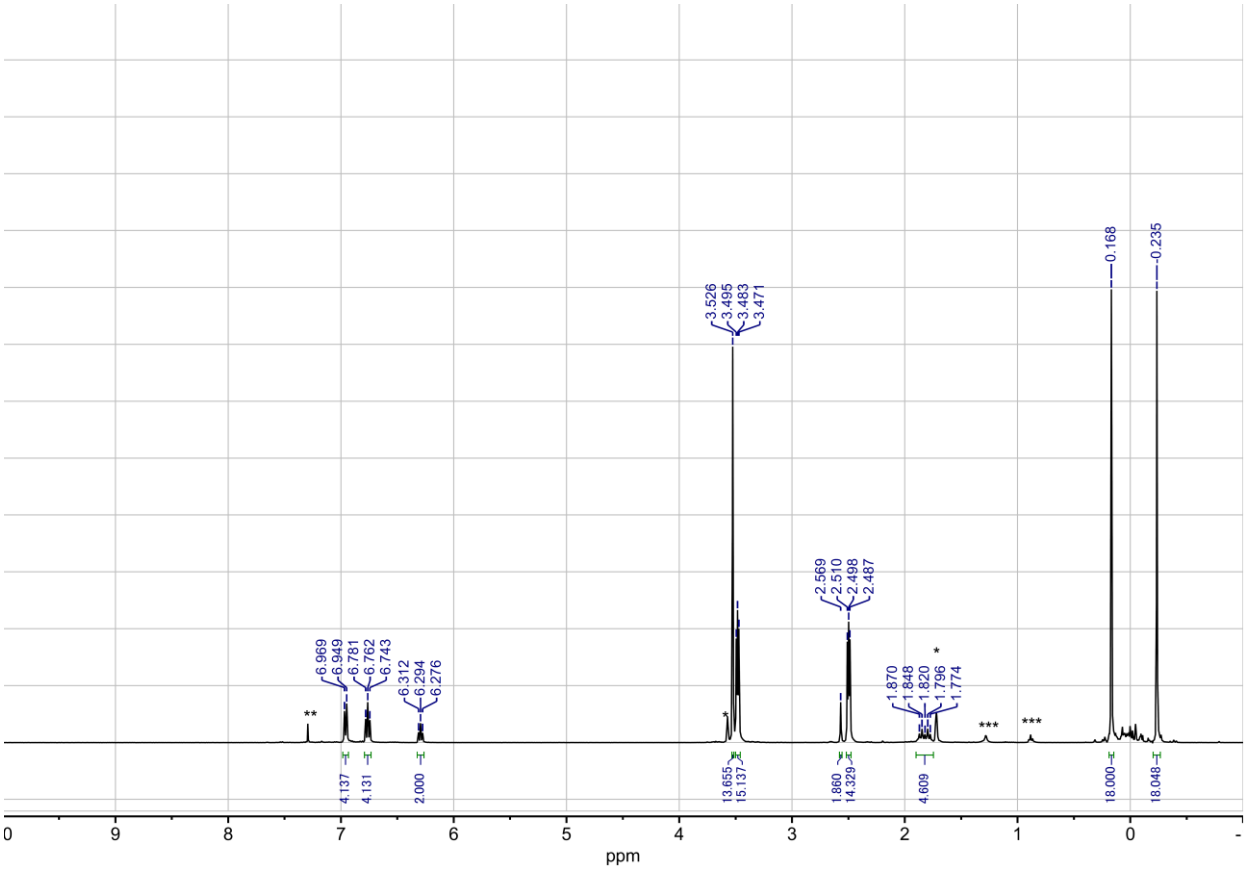

Figure 23. The ^{1}H NMR spectrum of *trans*-**5** (*THF-d_7, **free benzene dissociated from recrystallized *trans*-**5**, ***hexane from glovebox atmosphere)

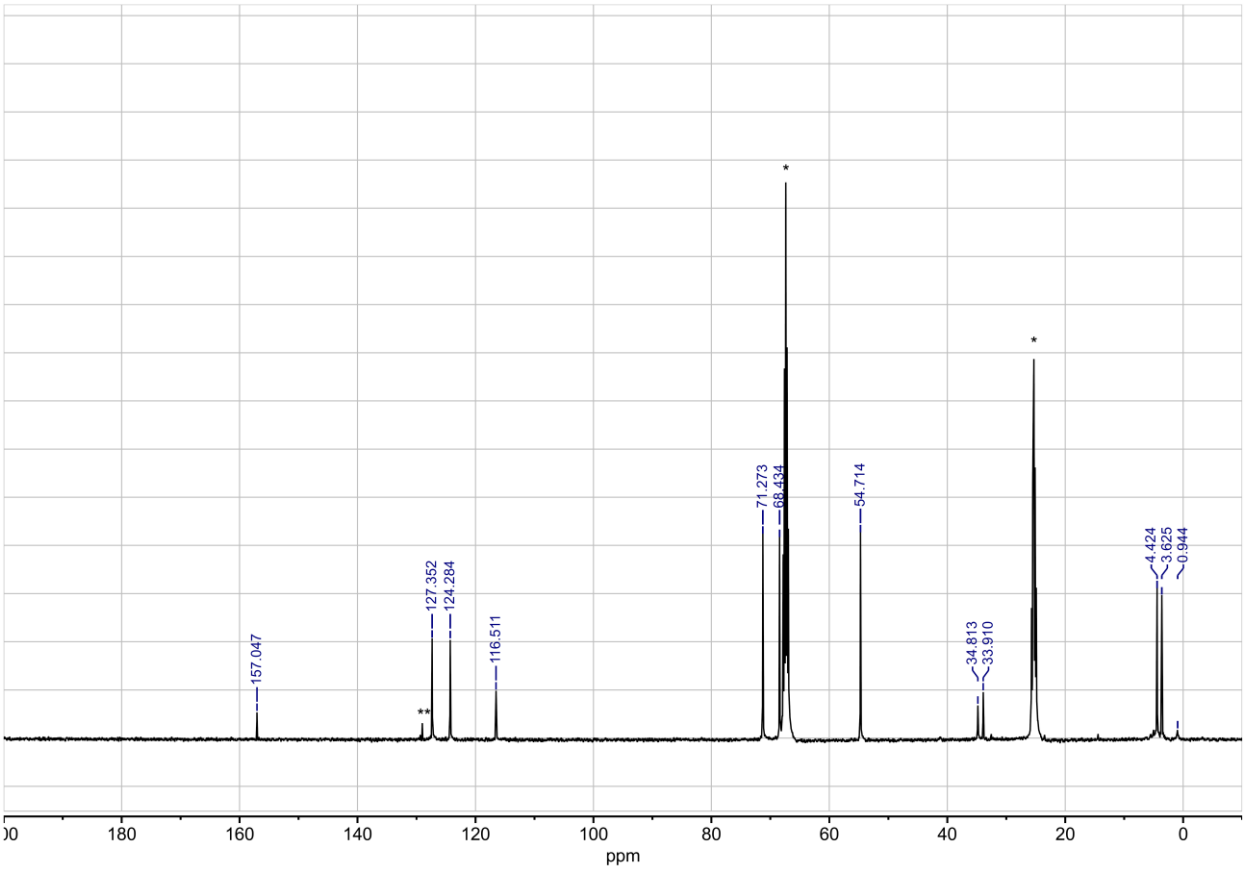

Figure 24. The ^{13}C NMR spectrum of *trans*-**5** (*THF-d_8, **free benzene dissociated from recrystallized *trans*-**5**, ***hexane from glovebox atmosphere)

Comparison of NMR spectra for the reactions of 1 with (*E*)- and (*Z*)-stilbene

In a glovebox, crystalline **1** (20 mg, 34 μmol) and (*E*)- or (*Z*)-stilbenes (6.0 mg, 34 μmol) were placed in a 3 mL vial, then the mixture was cooled to –35 °C, then pre-cooled Et_2O (1.00 mL) was added to the mixture. After stirring at room temperature for 2 h, the volatiles were evaporated under reduced pressure. To both of the crude products, C_6D_6 (600 μL) was added. The ^1H NMR spectra of the crude products for the reaction of (*E*)- or (*Z*)-stilbenes exhibited identical signals (Figure 8).

The reaction of 1 with (*E*)-stilbene under dark condition

In a glovebox, pre-cooled (–35 °C) crystalline tetraalkyldialumane **S1** (11.5 mg, 15.4 μmol) and potassium graphite (16.0 mg, 118 μmol) were placed in a 3 mL vial with a glass stirring bar, then pre-cooled toluene/THF (1.00 mL, v/v = 100/1) was added to the mixture and the resulting suspension was stirred at –35 °C for 2 days. After the filtration by using a pre-cooled (–35 °C) plastic syringe with glass fiber filter, a red solution of **1** was obtained. To a precooled (–35 °C) toluene (1.00 mL) solution of (*E*)-stilbene (16.6 mg, 92.0 μmol) in a 15 mL vial covered by an aluminum foil, the solution of **1** was added under dark condition with turning off the room light. The resulting solution was stirred for 2 h at room temperature and then volatiles were evaporated under reduced pressure. To the residue, hexane was added and volatiles were removed in vacuo. This addition/evaporation cycle was repeated for three times. The obtained crude product was washed

with hexane to afford yellow solids. To the crude product, C_6D_6 (600 μL) was added. The ^{1}H NMR spectrum of the crude product indicated the quantitative formation of *trans*-**5** (Figure 25).

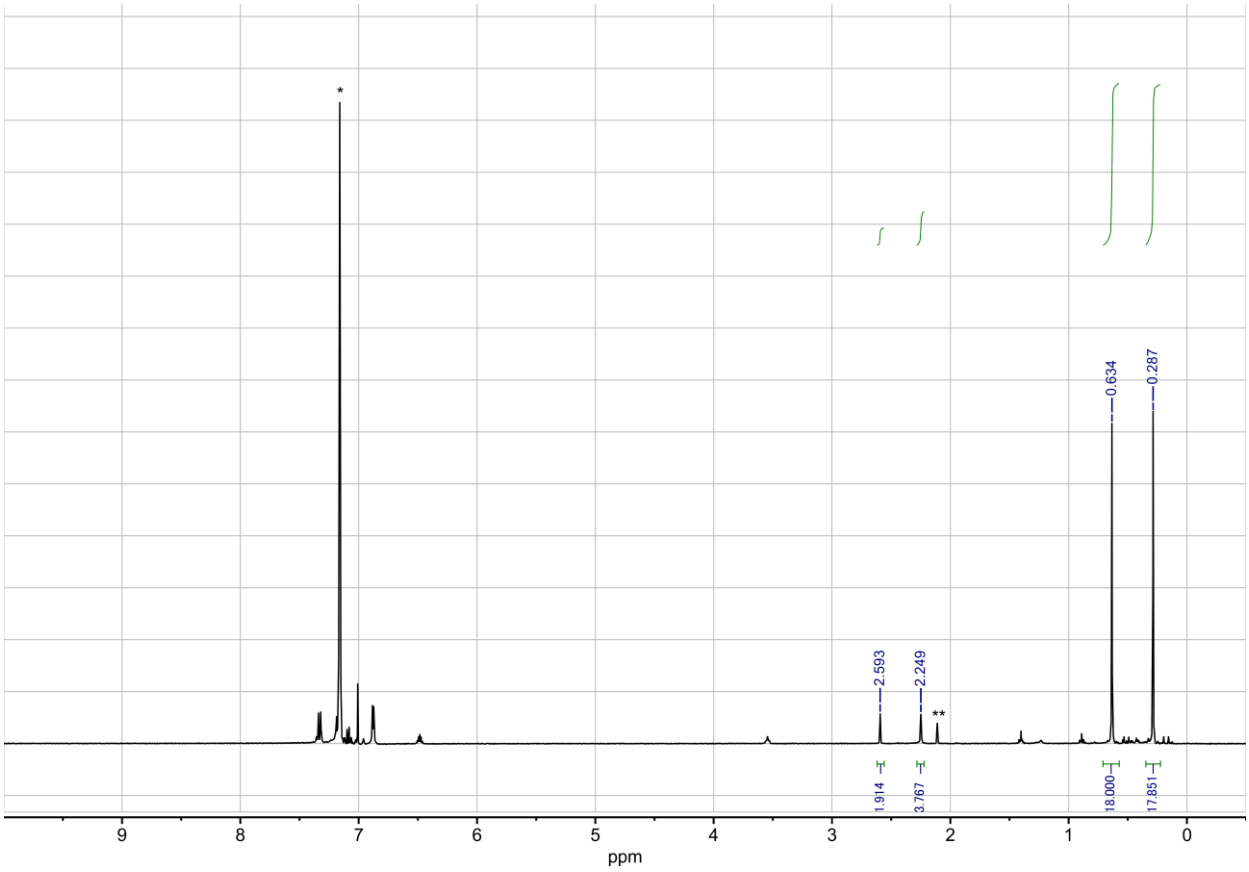

Figure 25. The ^{1}H NMR spectrum of the crude product for the reaction of **1** with (*E*)-stilbene in the dark condition (*C_6D_5H, **toluene)

Hydrolysis of 3

In a glovebox, **3** (8.0 mg, 12 μmol) and C_6D_6 (0.50 mL) were added to a J-young NMR tube. After bringing out the NMR tube from the glovebox, a drop of distilled H_2O was added to the solution. After 5 min, C_6D_6 (0.10 mL) solution of 1,3,5-trimethoxybenzene (internal standard, 5.2 mg, 30 μmol) was added to the resulted white suspension. The ^{1}H NMR spectrum of the crude product revealed that *cis*-stilbene (12 μmol) formed quantitatively (Figure 26).

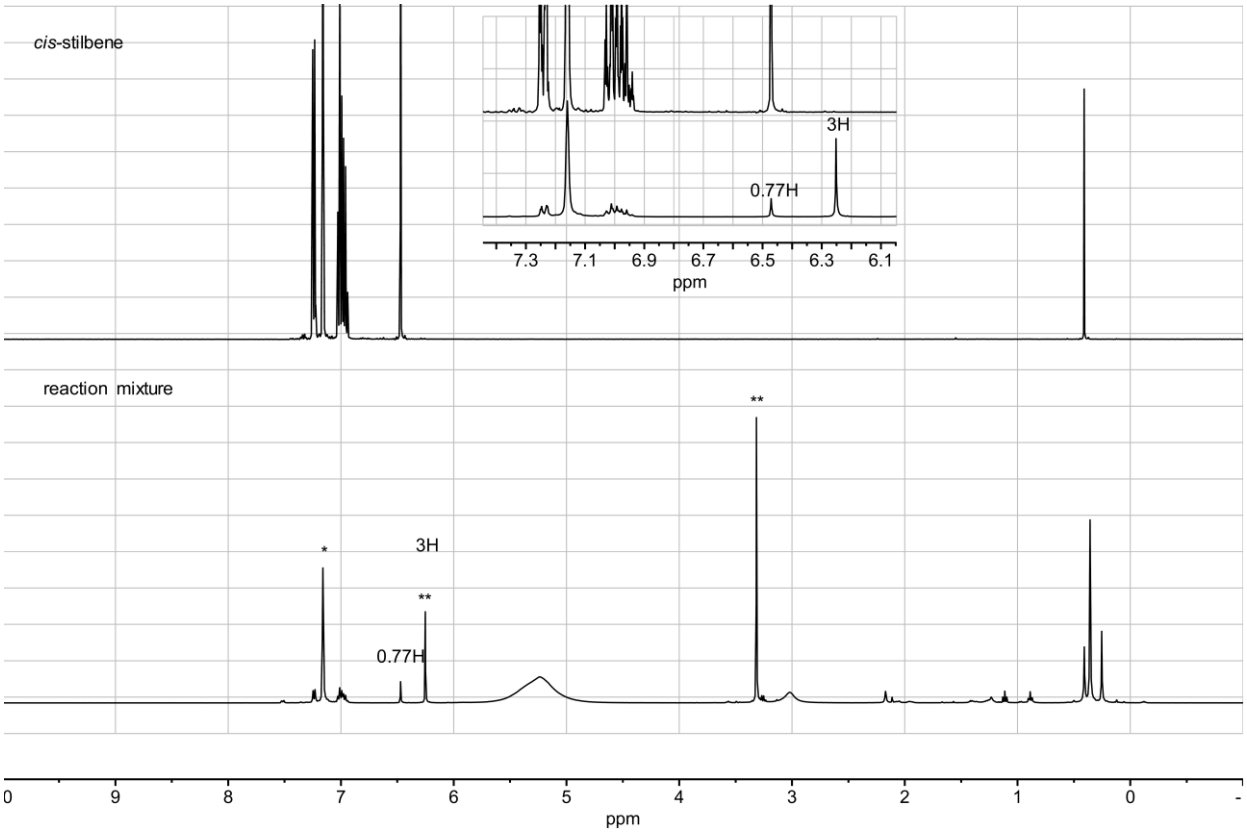

Figure 26. The NMR yield estimation of hydrolysis of **4** (*C_6D_5H **1,3,5-trimethoxybenzene)

Synthesis of 10

In a glovebox, pre-cooled (–35 °C) crystalline tetraalkyldialumane **S1** (16 mg, 22 μmol) and potassium graphite (20.0 mg, 369 μmol) were placed in a 3 mL vial with a glass stirring bar, then pre-cooled toluene/THF (1.50 mL, v/v = 100/1) was added to the mixture and the resulting suspension was stirred at –35 °C for 1 days. After the filtration by using a pre-cooled (–35 °C) plastic syringe with glass fiber filter, a red solution of **1** was obtained. To a precooled (–35 °C) toluene (1.0 mL) solution of diboryldiyne (7.7 mg, 22 μmol) in a 15 mL vial, the solution of **1** was added. The resulting orange solution was stirred for 2 h at room temperature and then volatiles were evaporated under reduced pressure. To the residue, THF was added and volatiles were removed in vacuo. Single crystals suitable for preliminary X-ray analysis were obtained by recrystallization from thf at –35 °C. ^{1}H NMR (Figure 27, 399 MHz, C_6D_6, 304 K) δ 0.39 (s, 72H, Si(CH_3)$_3$), 1.14 (s, 24H, CH_3, 2.22 (s, 4H, CH_2).

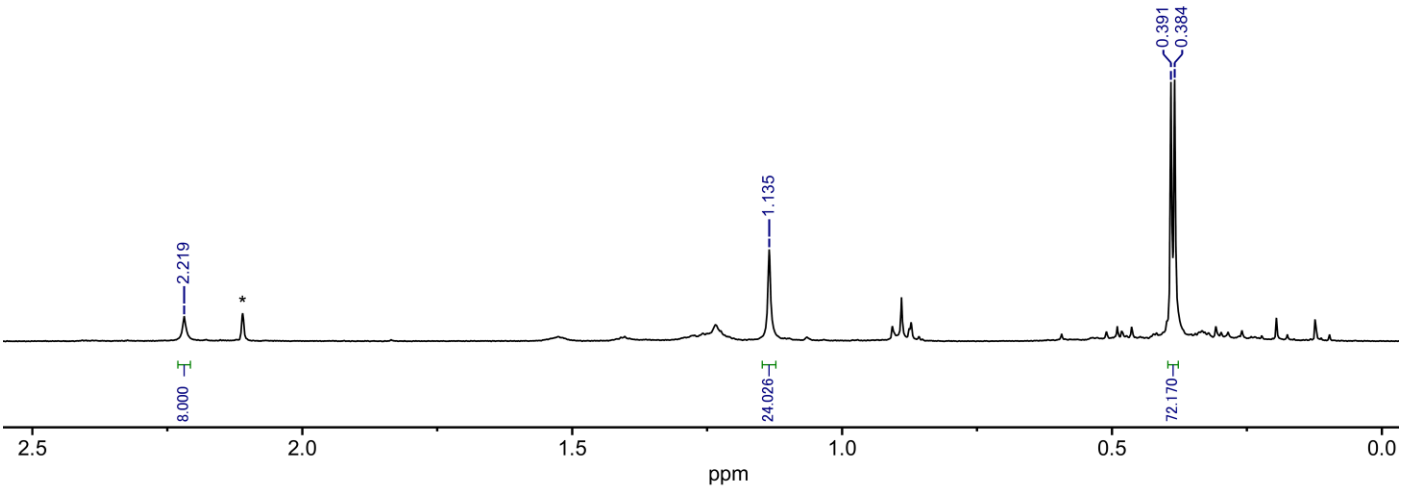

Figure 27. The ^{1}H NMR spectrum of **12** (*toluene)

Details for X-ray Crystallography

Crystallographic data for **2**, **3**, **5**, **6**, *trans*-**8** are summarized in Table 3. The crystals were coated with immersion oil and put on a MicroMountTM (MiTeGen, LLC), and then mounted on diffractometer. Diffraction data were collected on a Rigaku Saturn CCD or a Bruker Photon detectors using MoKα radiation. The Bragg spots were integrated using CrysAlisPro program package.[29] Absorption corrections were applied. All the following procedure for analysis, Yadokari-XG 2009[30] was used as a graphical interface. The structure was solved by a direct method with programs of SIR2014[31] and refined by a full-matrix least squares method with the program of SHELXL-2018.[32] Anisotropic temperature factors were applied to all non-hydrogen atoms. The hydrogen atoms were put at calculated positions, and refined applying riding models. The detailed crystallographic data have been deposited with the Cambridge Crystallographic Data Centre (except compound **6**.) A copy of the data can be obtained with free of charge via http://www.ccdc.cam.ac.uk/products/csd/request.

Table 3. Crystallographic data and structure refinement details for **2**, **3**, **5**, **6**, and *trans*-**8**

Compound #	**2**	**3**	**5**	**6**	*trans*-**8**·(0.5 C_6H_6)
CCDC deposit #	1918148	1963697	1918149	####	1951008
Empirical formula	$C_{33}H_{56}AlKSi_4$	$C_{44}H_{66}AlKSi_4$	$C_{38}H_{70}AlKO_2Si_4$	$C_{48}H_{100}AlB_2KN_2O_{10}Si_4$ ·0.5(C_6H_{14})	$C_{30}H_{52}AlKN_2O_6Si_4$ ·0.5(C6H6)
Formula weight	631.21	773.4	737.38	1108.44	1006.69
T (K)	93(2)	93(2)	93(2)	93(2)	93(2)
λ (Å)	0.71073	0.71073	0.71073	0.71073	0.71073
Crystal system	*Monoclinic*	*Triclinic*	*Orthorhombic*	*Triclinic*	*Triclinic*
Space group	$P2_1/c$	$P\text{-}1$	$Pca2_1$	$P\text{-}1$	$P\text{-}1$
a (Å)	11.7213(4)	9.2307(2)	20.4759(12)	13.9313(5)	13.5205(3)
b (Å)	11.3399(3)	13.9014(3)	10.9548(4)	16.0719(6)	15.8685(4)
c (Å)	27.9013(8)	18.7277(4)	20.1946(8)	17.0606(6)	15.8725(4)
α (Å)	90	94.114(2)	90	71.048(3)	64.768(3)
β (Å)	98.684(3)	98.480(2)	90	70.154(3)	71.897(2)
γ (Å)	90	107.380(2)	90	68.238(3)	89.584(2)
V (Å^3)	3666.08(19)	2251.21(9)	4529.8(4)	3249.3	2896.84(14)
Z	4	2	4	2	2
$D_{calc,}$ (g/m^3)	1.144	1.141	1.081	1.133	1.154
μ (mm^{-1})	0.32	0.272	0.271	0.218	0.234
F(000)	1368	836	1608	1210	1094
Crystal size (mm)	0.16×0.12×0.05	0.22×0.16×0.06	0.19×0.11×0.01	0.11×0.07×0.04	0.11×0.10×0.04
2θ range (°)	1.758-30.870	1.789-27.499	1.859-30.623	1.625-30.669	1.550-30.738
Reflns collected	39748	32950	24702	53295	50498
Indep reflns/R_{int}	9388/0.0463	10050/0.0385	9573/0.0587	16014/0.0514	14301/0.0673
Param	405	465	431	687	598
GOF on F^2	1.055	1.024	0.927	1.032	1.029
R_1, wR_2 [$I>2\sigma(I)$]	0.0386, 0.0946	0.0373, 0.0899	0.0420, 0.0858	0.0468, 0.1031	0.0474, 0.0999
R_1, wR_2 (all data)	0.0582, 0.1013	0.0507, 0.0952	0.0646, 0.0914	0.0752, 0.1119	0.0796, 0.1110

Computational details

Part of the computations were performed using workstation at Research Center for Computational Science, National Institutes of Natural Sciences, Okazaki, Japan. The theoretical approach is based on the framework of density functional theory (DFT). The artificial force induced reaction (AFIR) method implemented in the GRRM17 program was used for searching the reaction pathways initially.[33] The calculations were performed by using Gaussian 16 (revision B.01[34] or C.01[34]) program, with the B3LYP functional[35] using def2-SVP basis set[36] with empirical dispersion correction (DFT-D3BJ)[37] for structure optimization and vibrational frequency calculation. All local minima and saddle points were confirmed by their vibrational frequency calculations (with zero and one imaginary frequencies, respectively). The saddle points found were confirmed to be the correct ones by IRC. To include solvent effect, single point PCM correction using SMD method[38] (toluene) was adopted. All the values of free-energy change are at 298.15 K.

2.5. References

1. Nikonov, I. G.; Chu, T. *Chem.Rev.* **2018,** *118,* 3608-3680.

2. Roesky, H. W.; Kumar, S. S. *Chem. Commun.* **2005**, 4027-4038; (b) Woodward, S.; Dagorne, S., *Modern Organoaluminum Reagents: Preparation, Structure, Reactivity and Use*. Springer Berlin Heidelberg: 2012; (c) Wehmschulte, R. J., The Chemistry of Low-Valent Organoaluminum Species. In *PATAI'S Chemistry of Functional Groups*, Rappoport, Z., Ed. John Wiley & Sons: 2016; pp 223-252; (d) Jones, C.; Stasch, A., The Chemistry of the Group 13 Metals in the +1 Oxidation State. In *The Group 13 Metals Aluminium, Gallium, Indium and Thallium: Chemical Patterns and Peculiarities*, Aldridge, S.; Downs, A. J., Eds. Wiley: 2011; pp 285-341; (e) Uhl, W.; Layh, M., Formal Oxidation State +2: Metal–Metal Bonded Versus Mononuclear Derivatives. In *The Group 13 Metals Aluminium, Gallium, Indium and Thallium: Chemical Patterns and Peculiarities*, Aldridge, S.; Downs, A. J., Eds. Wiley: 2011; pp 246-284.

3. (a) Uhl, W. *Z. Naturforsch., B: Chem. Sci.* **1988,** *43*, 1113-1118; (b) Fedushkin, I. L.; Moskalev, M. V.; Lukoyanov, A. N.; Tishkina, A. N.; Baranov, E. V.; Abakumov, G. A. *Chem. Eur. J.* **2012,** *18*, 11264-11276; (c) Mocker, M.; Robl, C.; Schnöckel, H. *Angew. Chem. Int. Ed. Engl.* **1994,** *33*, 862-863; (d) Ecker, A.; Baum, E.; Friesen, M. A.; Junker, M. A.; Üffing, C.; Köppe, R.; Schnöckel, H. *Z. Anorg. Allg. Chem.* **1998,** *624*, 513-516; (e) Wiberg, N.; Amelunxen, K.; Blank, T.; Nöth, H.; Knizek, J. *Organometallics* **1998,** *17*, 5431-5433; (f) Klimek, K. S.; Cui, C.; Roesky, H. W.; Noltemeyer, M.; Schmidt, H.-G. *Organometallics* **2000,** *19*, 3085-3090; (g) Minasian, S. G.; Arnold, J. *Chem. Commun.* **2008**, 4043-4045; (h) Bonyhady, S. J.; Collis, D.; Frenking, G.; Holzmann, N.; Jones, C.; Stasch, A. *Nat. Chem.* **2010,** *2*, 865-869; (i) Zhao, Y.; Liu, Y.; Yang, L.; Yu, J. G.; Li, S.; Wu, B.; Yang, X. J. *Chem. Eur. J.* **2012,** *18*, 6022-6030; (j) Li, B.; Kundu, S.; Zhu, H.; Keil, H.; Herbst-Irmer, R.; Stalke, D.; Frenking, G.; Andrada, D. M.; Roesky, H. W. *Chem. Commun.* **2017,** *53*, 2543-2546; (k) Bonyhady, S. J.; Holzmann, N.; Frenking, G.; Stasch, A.; Jones, C. *Angew. Chem. Int. Ed.* **2017,** *56*, 8527-8531; (l) Bicho, B. A. C.; Bruhn, C.; Guthardt, R.; Weyer, N.; Siemeling, U. *Z. Anorg. Allg. Chem.* **2018,** *644*, 1329-1336; (m) Hofmann, A.; Lamprecht, A.; González-Belman, O. F.; Dewhurst, R. D.; Jiménez-Halla, J. O. C.; Kachel, S.; Braunschweig, H. *Chem. Commun.* **2018,** *54*, 1639-1642; (n) Kazarina, O. V.; Gourlaouen, C.; Karmazin, L.; Morozov, A. G.; Fedushkin, I. L.; Dagorne, S. *Dalton Trans.* **2018,** *47*, 13800-13808; (o) Wehmschulte, R. J.; Ruhlandt-Senge, K.; Olmstead, M. M.; Hope, H.; Sturgeon, B. E.; Power, P. P. *Inorg. Chem* **1993,** *32*, 2983-2984; (p) Wright, R. J.; Phillips, A. D.; Power, P. P. *J. Am. Chem. Soc.* **2003,** *125*, 10784-10785; (q) Cui, C.; Li, X.; Wang, C.; Zhang, J.; Cheng, J.; Zhu, X. *Angew. Chem. Int. Ed.* **2006,** *45*, 2245-2247; (r) Agou, T.; Nagata, K.; Tokitoh, N. *Angew. Chem. Int. Ed.* **2013,** *52*, 10818-10821; (s) Nagata, K.; Agou, T.; Tokitoh, N. *Angew. Chem. Int. Ed.* **2014,** *53*, 3881-3884.

4. (a) Dohmeier, C.; Robl, C.; Tacke, M.; Schnöckel, H. *Angew. Chem. Int. Ed. Engl.* **1991,** *30*, 564-565; (b) Schulz, S.; Roesky, H. W.; Koch, H. J.; Sheldrick, G. M.; Stalke, D.; Kuhn, A. *Angew. Chem. Int. Ed. Engl.* **1993,** *32*, 1729-1731; (c) Purath, A.; Dohmeier, C.; Ecker, A.; Schnöckel, H.; Amelunxen, K.; Passler, T.; Wiberg, N. *Organometallics* **1998,** *17*, 1894-1896; (d) Schnitter, C.; Roesky, H. W.; Röpken, C.; Herbst-Irmer, R.; Schmidt, H. G.; Noltemeyer, M. *Angew. Chem. Int. Ed.* **1998,** *37*, 1952-1955; (e) Purath, A.; Schnöckel, H. *J. Organomet. Chem.* **1999,** *579*, 373-375; (f) Wiberg, N.; Blank, T.; Amelunxen, K.; Nöth, H.; Schnöckel, H.; Baum, E.; Purath, A.; Fenske, D. *Eur. J. Inorg. Chem.* **2002,** *2002*, 341-350; (g) Schiefer, M.; Reddy, N. D.; Roesky, H. W.; Vidovic, D. *Organometallics* **2003,** *22*, 3637-3638; (h) Dohmeier, C.; Baum, E.; Ecker, A.; Köppe, R.; Schnöckel, H. *Organometallics* **1996,** *15*, 4702-4706; (i) Huber, M.; Schnöckel, H. *Inorganica*

Chimica Acta **2008,** *361*, 457-461; (j) Tomlinson, W. W.; Mayo, D. H.; Wilson, R. M.; Hooper, J. P. *J. Phys. Chem. A* **2017,** *121*, 4678-4687; (k) Sitzmann, H.; Lappert, M. F.; Dohmeier, C.; Üffing, C.; Schnöckel, H. *J. Organomet. Chem.* **1998,** *561*, 203-208; (l) Schnöckel, H.; Schnepf, A., Aluminium and Gallium Clusters: Metalloid Clusters and their Relationship to the Bulk Phases, to Naked Clusters and to Nanoscaled Materials. In *The Group 13 Metals Aluminium, Gallium, Indium and Thallium: Chemical Patterns and Peculiarities*, Aldridge, S.; Downs, A. J., Eds. Wiley: 2011; pp 402-487.

5. (a) Pluta, C.; Pörschke, K. R.; Krüger, C.; Hildenbrand, K. *Angew. Chem. Int. Ed. Engl.* **1993,** *32*, 388-390; (b) Wright, R. J.; Brynda, M.; Power, P. P. *Angew. Chem. Int. Ed.* **2006,** *45*, 5953-5956; (c) Zhao, Y.; Lei, Y.; Dong, Q.; Wu, B.; Yang, X. J. *Chem. Eur. J.* **2013,** *19*, 12059-12066; (d) Agou, T.; Wasano, T.; Jin, P.; Nagase, S.; Tokitoh, N. *Angew. Chem. Int. Ed.* **2013,** *52*, 10031-10034; (e) Nagata, K.; Murosaki, T.; Agou, T.; Sasamori, T.; Matsuo, T.; Tokitoh, N. *Angew. Chem. Int. Ed.* **2016,** *55*, 12877-12880; (f) Bag, P.; Porzelt, A.; Altmann, P. J.; Inoue, S. *J. Am. Chem. Soc.* **2017,** *139*, 14384-14387.

6. (a) Schnockel, H. *Z. Naturforsch., B: Chem. Sci.* **1976,** *31*, 1291-1292; (b) Tacke, M.; Schnoeckel, H. *Inorg. Chem.* **1989,** *28*, 2895-2896.

7. Hofmann, A.; Tröster, T.; Kupfer, T.; Braunschweig, H. *Chem. Sci.* **2019,** *10*, 3421-3428.

8. Cui, C.; Roesky, H. W.; Schmidt, H. G.; Noltemeyer, M.; Hao, H.; Cimpoesu, F. *Angew. Chem. Int. Ed.* **2000,** *39*, 4274-4276.

9. Mellerup, S. K.; Cui, Y.; Fantuzzi, F.; Schmid, P.; Goettel, J. T.; Bélanger-Chabot, G.; Arrowsmith, M.; Krummenacher, I.; Ye, Q.; Engel, V.; Engels, B.; Braunschweig, H. *J. Am. Chem. Soc.* **2019,** *141*, 16954-16960.

10. (a) Schwamm, R. J.; Anker, M. D.; Lein, M.; Coles, M. P. *Angew. Chem. Int. Ed.* **2019,** *58*, 1489-1493; (b) Anker, M. D.; Coles, M. P. *Angew. Chem. Int. Ed.* **2019,** *58*, 13452-13455.

11. Schwamm, J. R.; Coles, P. M.; Hill, S. M.; Mahon, F. M.; McMullin, L. C.; Rajabi, A. N.; Wilson, S. S. A. *Angew. Chem. Int. Ed.* **2020,** in press. doi:10.1002/anie.201914986

12. (a) Hicks, J.; Vasko, P.; Goicoechea, J. M.; Aldridge, S. *Nature* **2018,** *557*, 92-95; (b) Hicks, J.; Mansikkamäki, A.; Vasko, P.; Goicoechea, J. M.; Aldridge, S. *Nat. Chem.* **2019,** *11*, 237-241.

13. Hicks, J.; Vasko, P.; Goicoechea, J. M.; Aldridge, S. *J. Am. Chem. Soc.* **2019,** *141*, 11000-11003.

14. Kurumada, S.; Takamori, S.; Yamashita, M. *Nat. Chem.* **2020,** *12*, 36-39.

15. (a) Zhu, H.; Chai, J.; Fan, H.; Roesky, H. W.; He, C.; Jancik, V.; Schmidt, H. G.; Noltemeyer, M.; Merrill, W. A.; Power, P. P. *Angew. Chem. Int. Ed.* **2005,** *44*, 5090-5093; (b) Zhu, H.; Oswald, R. B.; Fan, H.; Roesky, H. W.; Ma, Q.; Yang, Z.; Schmidt, H.-G.; Noltemeyer, M.; Starke, K.; Hosmane, N. S. *J. Am. Chem. Soc.* **2006,** *128*, 5100-5108; (c) Bakewell, C.; White, A. J. P.; Crimmin, M. R. *Angew. Chem. Int. Ed.* **2018,** *57*, 6638-6642; (d) Hooper, T. N.; Lau, S.; Chen, W.; Brown, R. K.; Garçon, M.; Luong, K.; Barrow, N. S.; Tatton, A. S.; Sackman, G. A.; Richardson, C.; White, A. J. P.; Cooper, R. I.; Edwards, A. J.; Casely, I. J.; Crimmin, M. R. *Chem. Sci.* **2019,** *10*, 8083-8093.

16. Brand, S.; Elsen, H.; Langer, J.; Donaubauer, W. A.; Hampel, F.; Harder, S. *Angew. Chem. Int. Ed.* **2018,** *57*, 14169-14173.

17. Kira, M.; Ishida, S.; Iwamoto, T.; Kabuto, C. *J. Am. Chem. Soc.* **1999,** *121*, 9722-9723.

18. Kira, M.; Ishida, S.; Iwamoto, T.; Kabuto, C. *J. Am. Chem. Soc.* **2002,** *124*, 3830-3831.

19. ‘‘Boronic Acids’’ Hall, G. D. Eds. Wiley: 2011.

20. (a) Kira, M.; Ishida, S.; Iwamoto, T.; Meijere, A. d.; Fujitsuka, M.; Ito, O. *Angew. Chem. Int. Ed.* **2004,** *43*, 4510-4512; (b) Ishida, S.; Iwamoto, T.; Kira, M. A *Heteroat. Chem.* **2011,** *22*, 432-437.
21. Lehmkuhl, H.; Shakoor, A.; Mehler, K.; Kruger, C.; Tsay, Y. H. *Z. Naturforsch., B: Chem. Sci.* **1985,** *40*, 1504-1510.
22. Uhl, W.; Spies, T.; Koch, R.; Saak, W. *Organometallics* **1998,** *18,* 4598-4602.
23. Kurumada, S.; Nakano, R.; Yamashita, M. *manuscript in preparation.*
24. (a) Neumann, C. N.; Hooker, J. M.; Ritter, T., *Nature* **2016,** *534*, 369-373. (b) Kwan, E. E.; Zeng, Y.; Besser, H. A.; Jacobsen, E. N., *Nat. Chem.* **2018,** *10*, 917-923.
25. He, G.; Kang, L.; Delgado, T. W.; Shynkaruk, O.; Ferguson, J. M.; McDonald, R.; Rivard, E. *J. Am. Chem. Soc.* **2013,** *135,* 5360-5363.
26. (a) Choi, C.; Elber, R. *J. Chem. Phys.* **1991,** *94*, 751-760; (b) Ayala, P. Y.; Schlegel, H. B. *J. Chem. Phys.* **1997,** *107*, 375-384.
27. Shynkaruk, O.; Qi, Y.; Cottrell-Callbeck, A.; Delgado, T. W.; McDonald, R.; Ferguson, J. M.; He, G.; Rivard, E. *Organometallics,* **2016,** *35,* 2232-2241.
28. Gandon, V.; Leca, D.; Aechtner, T.; Vollhardt, P. C. K.; Malacria, M.; Aubert, C. *Org. Lett.* **2004,** *6,* 3405-3407.
29. CrysAlisPRO *CrysAlisPRO*, Oxford Diffraction/Agilent Technologies UK Ltd: Yarnton, England, 2015.
30. Kabuto, C.; Akine, S.; Kwon, *J. Cryst. Soc. Jpn.* **2009,** *51*, 218-224.
31. Burla, M. C.; Caliandro, R.; Carrozzini, B.; Cascarano, G. L.; Cuocci, C.; Giacovazzo, C.; Mallamo, M.; Mazzone, A.; Polidori, G. *J. Appl. Crystallogr.* **2015,** *48*, 306-309.
32. Sheldrick, G. Crystal structure refinement with SHELXL. *Act. Cryst. Sec. C* **2015,** *71*, 3-8.
33. (a) Maeda, S.; Harabuchi, Y.; Sumiya, Y.; Takagi, M.; Suzuki, K.; Hatanaka, M.; Osada, Y.; Taketsugu, T.; Morokuma, K.; Ohno, K. *GRRM17*, see http://iqce.jp/GRRM/index_e.shtml (accessed date Nov. 30, 2019); (b) Maeda, S.; Ohno, K.; Morokuma, K. *Phys. Chem. Chem. Phys.* **2013,** *15*, 3683-3701; (c) Maeda, S.; Taketsugu, T.; Morokuma, K.; Ohno, K. *Bull. Chem. Soc. Jpn.* **2014,** *87*, 1315-1334; (d) Maeda, S.; Harabuchi, Y.; Takagi, M.; Saita, K.; Suzuki, K.; Ichino, T.; Sumiya, Y.; Sugiyama, K.; Ono, Y. *J. Comput. Chem.* **2018,** *39*, 233-251.
34. Frisch, M. J.; Trucks, G. W.; Schlegel, H. B.; Scuseria, G. E.; Robb, M. A.; Cheeseman, J. R.; Scalmani, G.; Barone, V.; Petersson, G. A.; Nakatsuji, H.; Li, X.; Caricato, M.; Marenich, A. V.; Bloino, J.; Janesko, B. G.; Gomperts, R.; Mennucci, B.; Hratchian, H. P.; Ortiz, J. V.; Izmaylov, A. F.; Sonnenberg, J. L.; Williams; Ding, F.; Lipparini, F.; Egidi, F.; Goings, J.; Peng, B.; Petrone, A.; Henderson, T.; Ranasinghe, D.; Zakrzewski, V. G.; Gao, J.; Rega, N.; Zheng, G.; Liang, W.; Hada, M.; Ehara, M.; Toyota, K.; Fukuda, R.; Hasegawa, J.; Ishida, M.; Nakajima, T.; Honda, Y.; Kitao, O.; Nakai, H.; Vreven, T.; Throssell, K.; Montgomery Jr., J. A.; Peralta, J. E.; Ogliaro, F.; Bearpark, M. J.; Heyd, J. J.; Brothers, E. N.; Kudin, K. N.; Staroverov, V. N.; Keith, T. A.; Kobayashi, R.; Normand, J.; Raghavachari, K.; Rendell, A. P.; Burant, J. C.; Iyengar, S. S.; Tomasi, J.; Cossi, M.; Millam, J. M.; Klene, M.; Adamo, C.; Cammi, R.; Ochterski, J. W.; Martin, R. L.; Morokuma, K.; Farkas, O.; Foresman, J. B.; Fox, D. J. *Gaussian 16, Revision B.01*, Wallingford, CT, 2016.
35. (a) Lee, C.; Yang, W.; Parr, R. G. *Phys. Rev. B* **1988,** *37*, 785-789; (b) Miehlich, B.; Savin, A.; Stoll, H.; Preuss, H. *Chem. Phys. Lett.* **1989,** *157*, 200-206; (c) Becke, A. D. D. *J. Chem. Phys.* **1993,** *98*, 5648-5652.

36. (a) Weigend, F.; Ahlrichs, R. *Phys. Chem. Chem. Phys.* **2005,** *7*, 3297-3305; (b) Weigend, F. *Phys. Chem. Chem. Phys.* **2006,** *8*, 1057-1065.
37. (a) Grimme, S.; Antony, J.; Ehrlich, S.; Krieg, H. *J. Chem. Phys.* **2010,** *132*, 154104; (b) Grimme, S.; Ehrlich, S.; Goerigk, L. *J. Comput. Chem.* **2011,** *32*, 1456-1465.
38. Marenich, A. V.; Cramer, C. J.; Truhlar, D. G. *J. Phys. Chem. B* **2009,** *113*, 6378-6396.

Chapter 3

Synthesis and Photophysical Properties of An Alumanylyttrium Complex

3.1. Introduction

Aluminum contains three valence electrons and is the most electropositive in the p-block[1].Accordingly, aluminum-ligated transition metal complexes generally exhibit a coordination number of at least four at the aluminum center in order to satisfy the electron deficiency of the aluminum atom. Such aluminum containing ligands are typically classified into (i) Z-type Al ligand,[2] (ii) L-type Al ligands containing Cp*Al ligands,[3] and base-stabilized alumylene ligands,[4] (iii) X-type Al ligands containing base-stabilized alumanyl ligands,[5] and (iv) bridging forms of (ii) and (iii)[6,7,8] (Figure 1)

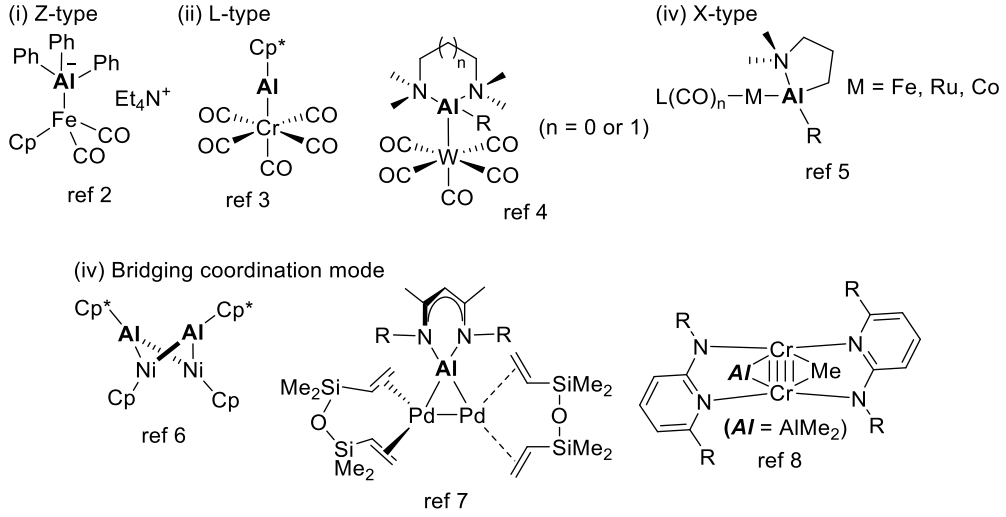

Figure 1. Transition metal complexes having aluminum ligand (coordination number > 3 on Al center)

In contrast, examples for the synthesis of transition metal complexes that possess a three-coordinated aluminum ligand remain limited. Such ligands can be synthesized by the following four methods as found in nice reports (Scheme 1): (A) A nucleophilic attack of anionic transition metal complexes to an aluminum electrophile,[9] (B) a simple coordination of a base-stabilized Al(I) species to a metal,[10] (C) an elimination of alkane through a metathesis reaction,[11] (D) an oxidative addition of an Al–H bond to a metal center in a low-oxidation state.[12]

Scheme 1. Synthetic methods for three-coordinated aluminum-transition metal complexes

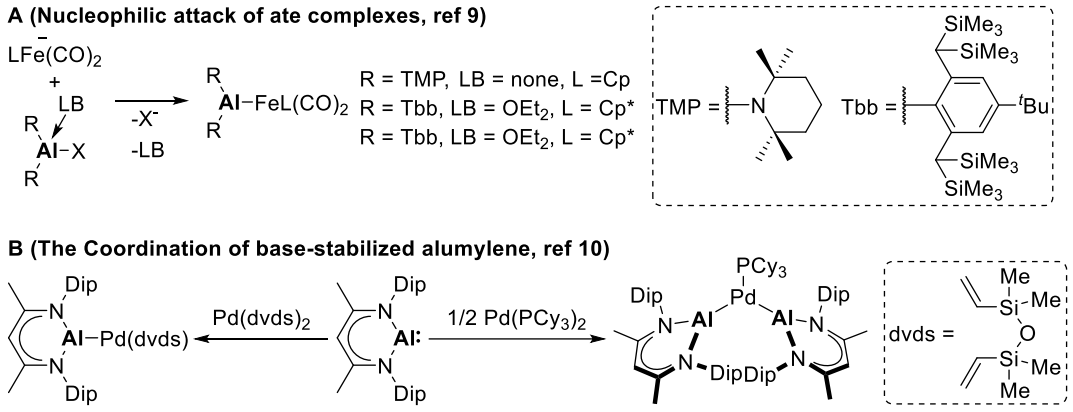

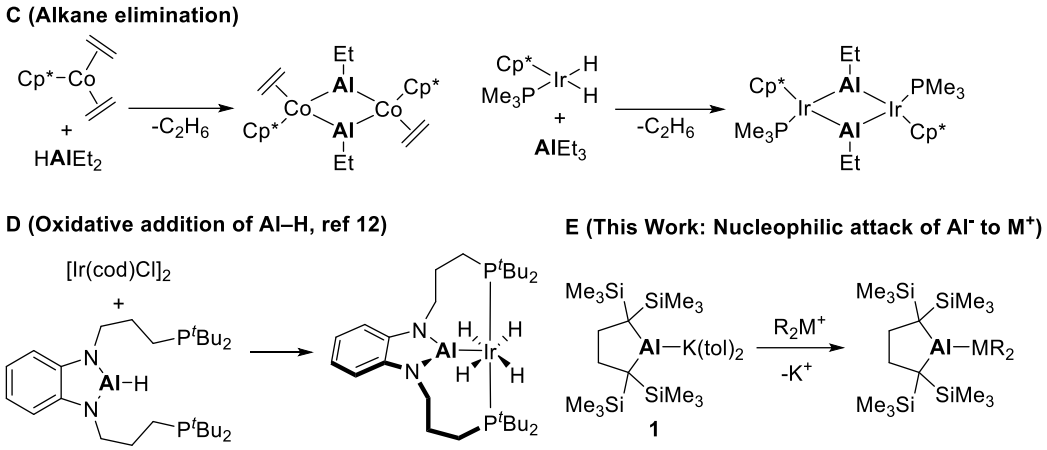

On the other hand, Four anionic and nucleophilic aluminum species[13]have been reported recently and were used as an Al(I) species in a low oxidation state.[13, 14] It should be noted here that the base-stabilized alumanyl anion was used for the synthesis of a base-stabilized alumanylgold complex.[5h] Herein, the reaction of dialkylalumanylpotassium **1** with a cationic yttrium complex is investigated for the synthesis of an alumanylyttrium **2**, which has three-coordinated alumanyl ligand and is the first example of Al–Y single bond compound.[15] Furthermore, Complex **2** has absorption in visible region, although **2** has no any π-electron substituents.

3.2. This Work

The reaction of a dialkylalumanylpotassium **1** with the cationic complex $[Y(CH_2SiMe_3)_2]^+[BPh_4]^-$[16] in diethyl ether at –35 °C furnished the corresponding alumanylyttrium complex **2** as a bright yellow crystalline solid (Scheme 2). The ^{1}H NMR spectrum of **2** in cyclohexane-d_{12} (Figure 2) exhibited two singlets which could be assigned to trimethylsilyl groups in 1:2 integral ratio. It also has a singlet signal of methylene groups in 5-membered ring, indicating that the complex **2** has a C_{2v} symmetrical structure in solution. Furthermore, a doublet ($^2J_{YH}$ = 2.6 Hz) was found for the yttrium-bonded methylene groups were found at δ = –0.65 ppm, that are coupled to the ^{89}Y nuclei (100% abundance; I = 1/2).[17] In the ^{13}C NMR spectrum of **2**, the two tetrasubstituted carbon atoms at the α position relative to the Al atom were also coupled the Y atom ($^2J_{YC}$ = 6 Hz) This value is smaller than the that for the directly bonded CH_2 groups to the Y atom ($^1J_{YC}$ = 36 Hz). This result clearly indicates that in solution, the Al atom is directly bonded to Al atom (Figure 3).

Scheme 2 Synthesis of a dialkykalumanyl yttrium complex **2**

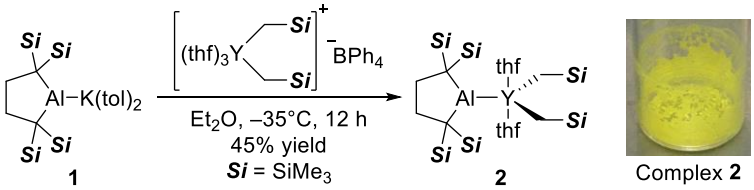

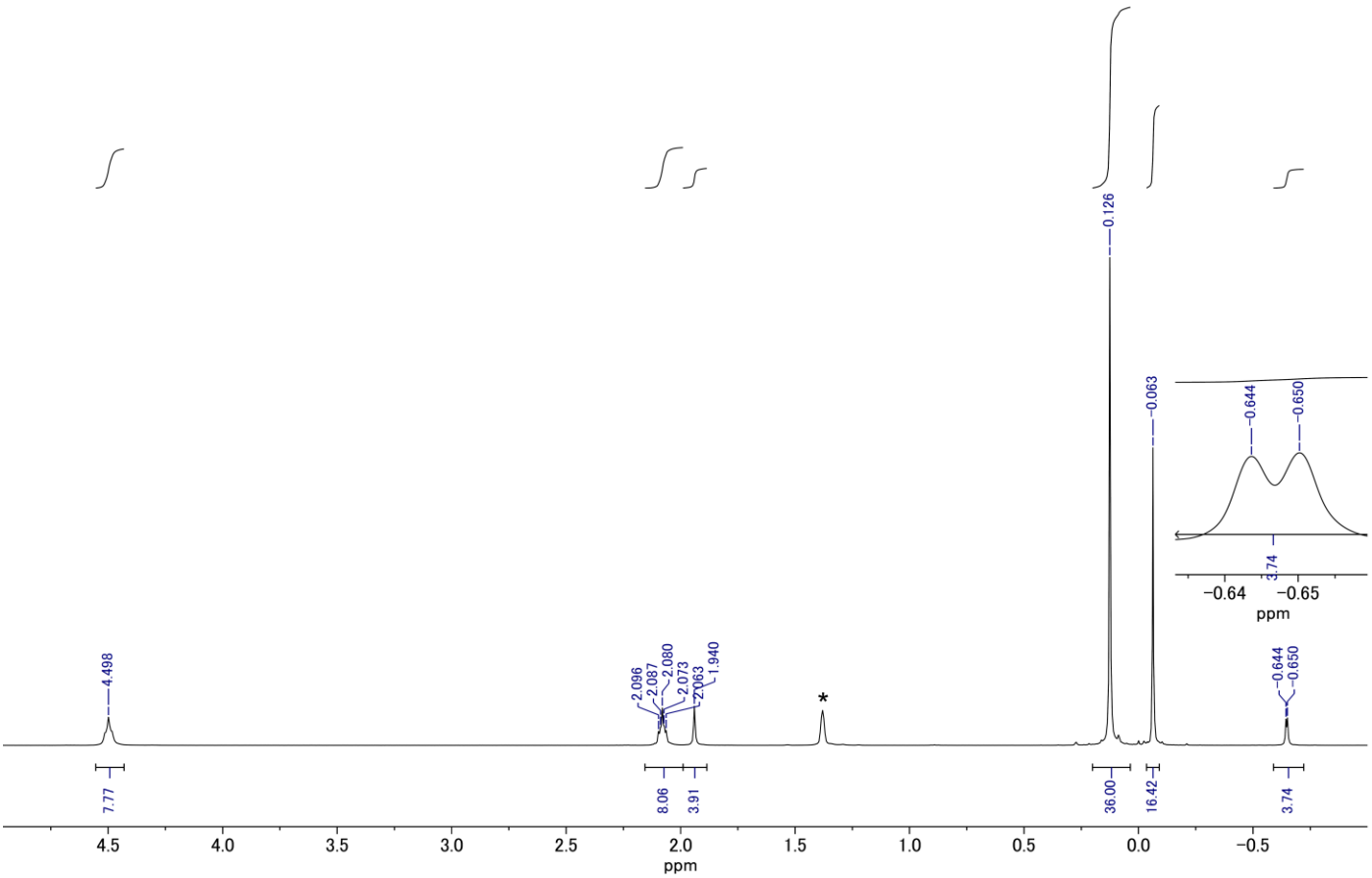

Figure 2. The ^{1}H NMR spectrum of **2** (*$C_6D_{11}H$)

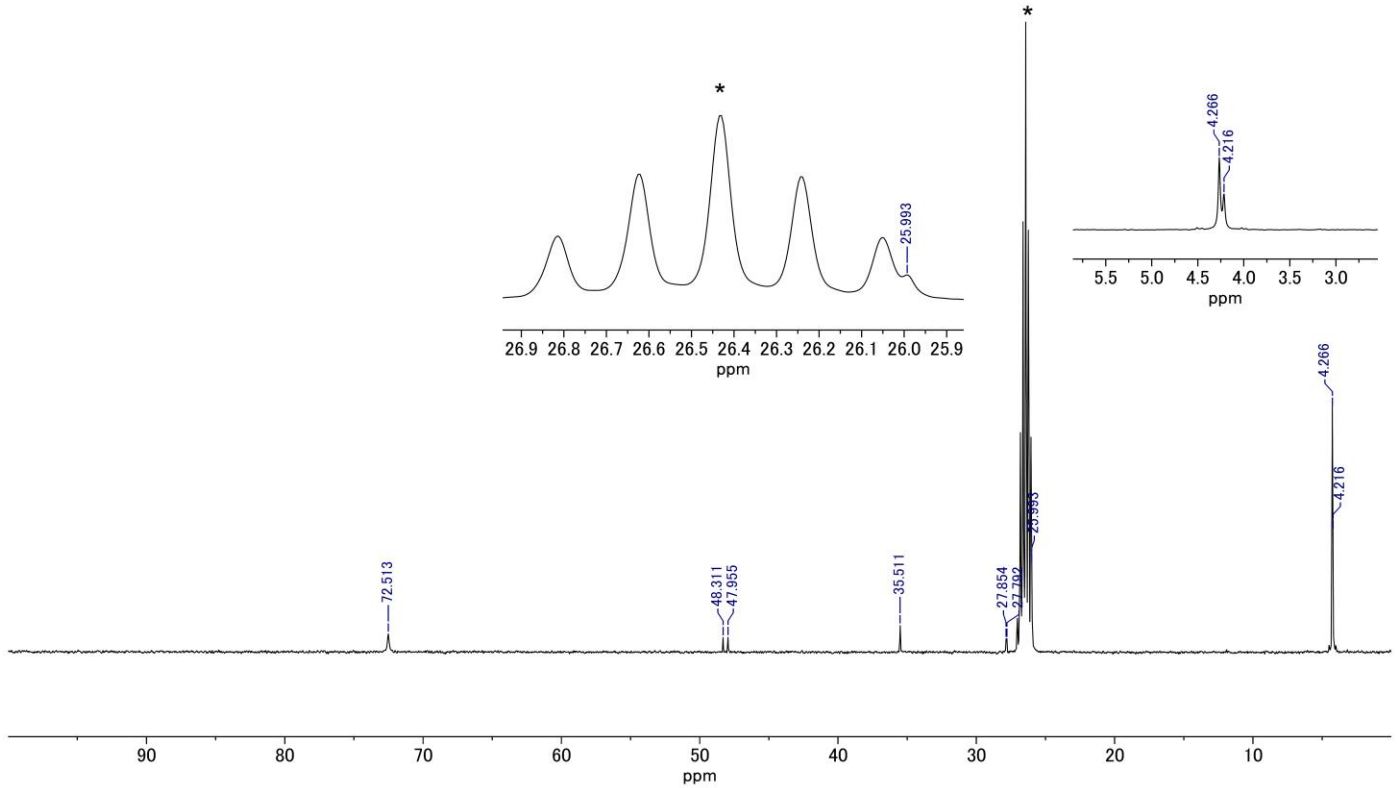

Figure 3. The ^{13}C NMR spectrum of **2** (*$C_6D_{11}H$)

It should be noted that the reaction of **1** with MCl_3 and $Cp^*_2MCl(thf)$[18] (M=Sc, Y) did not give any Al-M bonded compound under the same condition as the Scheme 3, instead, a toluene adduct **3**[19] was observed in ^1H NMR measurement (Scheme 4, See details in chapter 2). Reaction of **1** with $[Sc(CH_2SiMe_3)_2]^+[BPh_4]^-$ complex[16] also did not give alumanylscandium complex but gave **4** within an hour at –35 °C (Scheme 5). In contrast, **1** decomposed in toluene to furnish **3** for 5 h at room temperature. Comparing these two reactions, cationic scandium would accelerate the *meta*-selective C–H insertion of **1**. The rapid insertion of **1** and the formation of **4** through the loss of hydride would be explained by the following mechanism (Scheme 6). In the first step, nucleophilic attack to scandium center to give an alumanylscandium intermediate **1-Sc**. Subsequently, the scandium-bonded alumanyl anion underwent the nucleophilic attack toward *meta*-position of the coordinating toluene to afford (*m*-tolyl)(hydrido)aluminate **3-Sc** *via* a 3-membered ring transition state **A** in the same manner as the reaction of **1** with toluene (see details for chapter 2). Then the scandium atom would undergo an abstraction of hydride in **3-Sc** to give (*m*-tolyl) alumane **4** with a precipitation of dimeric scandium hydride. As a control experiment under the same condition, independently isolated (*m*-tolyl)(hydrido)aluminate **3** reacted with Cp_2ZrCl_2 to give **4** (Scheme 5, right), supporting that **4** formed through **3** as an intermediate. The reason for the formation of **4** instead of the corresponding alumanylscandium complex could be explained that smaller ionic radius of scandium than yttrium would lead to higher Lewis acidity of scandium, being capable to the stronger coordination of toluene to scandium metal.

Scheme 4. The reaction of **1** with group 3 metal halide

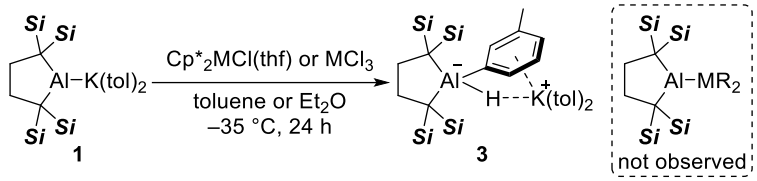

Scheme 5. The reaction of **1** with the cationic scandium complex

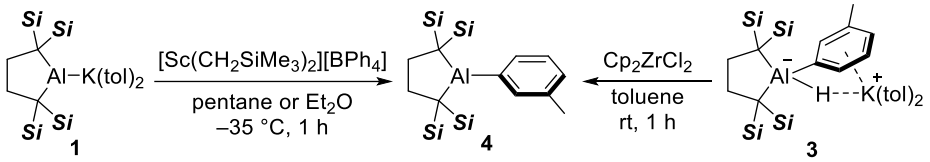

Scheme 6. Possible mechanism for the formation **4** from a cationic scandium complex (***Si*** = $SiMe_3$)

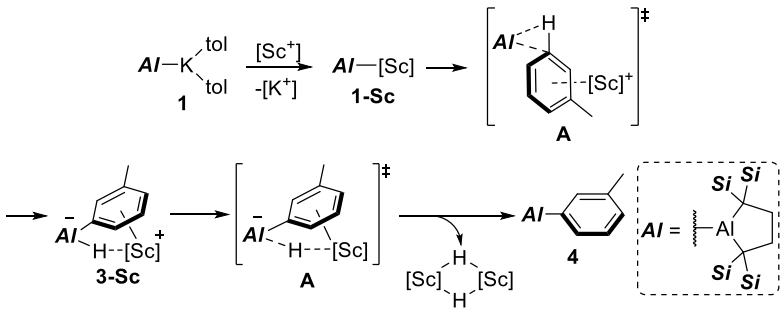

Single crystals of **2** were obtained from diethyl ether solution at –35 °C. The molecular structure of **2** was unambiguously determined by a single crystal X-ray diffraction analysis (Figure 3). In the crystalline state, the Al and Y atoms adopt a trigonal planar and trigonal bipyramidal coordination geometry, respectively. The Al–Y bond is the first example of a 2-center-2-electron (2c-2e) bond between Al and Y atoms. The Al–Y bond lengths [3.1870(8), 3.1942(8) Å] of the two crystallographically independent molecules of **2** per asymmetric unit are longer than the sum of the radii (2.87 Å) of the Al and Y atoms.[19]. A structural comparison with the previously reported dialkylalumanyl potassium **1** and its precursor tetraalkyldialane **5** summarized in Table 1. The Al–C bond lengths [2.028(3), 2.038(3), 2.033(3), 2.041(3) Å] in **2** are shorter than those in **1** [2.0846(9) Å] and longer than those in **5** [2.005(3), 2.011(3)]. The C–Al–C angles in **2** [93.81(11), 93.66 (11) °] are wider and narrower than **1** and **5** respectively. These results indicated that aluminum atom on **2** is sp^2-hybridized character which is similar to **5** rather than that to the s-rich Al–K bond in **1**, which is supported by a natural bond orbital (NBO) analysis (35.35% s-orbital character and 64.45% p-orbital character.). Table 2 shows the structural comparison of **2** with doubly thf-ligated dialkylyttrium complexes possessing an anionic ligand. The Y–O and Y–C bonds in **2** are similar to those of reference compounds, indicating that dialkylalumanyl ligand did not affect the structural parameters directly. Figure 5 shows the structural difference of **2** and (boryl)Y$(CH_2SiMe_3)_2(thf)_2$ **6** from the view along with Al–Y and B–Y bonds. The C–Al–Y–C torsion angles [7.4(1)°, 8.0(2)°] in **2** are closed to zero and stand in stark contrast to the C–Y–B–N torsion angle [–73.4(3)°] of the previously reported **6**.

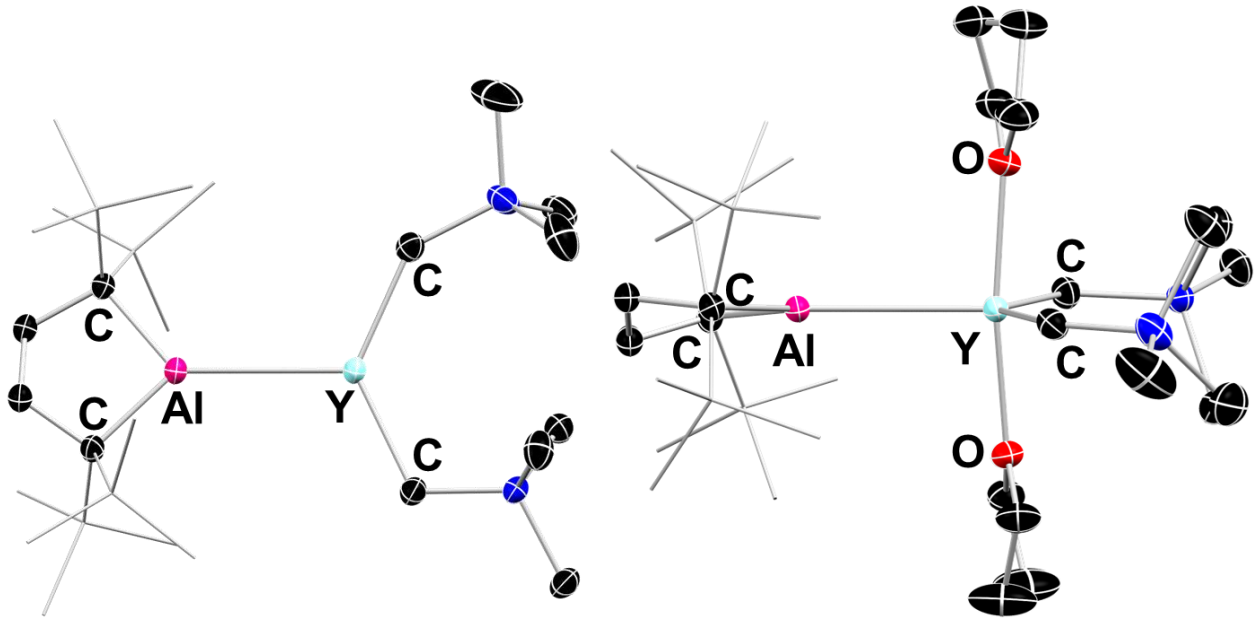

Figure 4. Molecular structure of **2** (left: top view right: side view, thermal ellipsoids set at 50% probability; one of two independent molecules and hydrogen atoms were omitted for clarity), thf ligands were omitted for clarity in top view. Selected bond lengths (Å) and angles (°): Al–Y 3.1870(8), 3.1942(8); Al–C 2.028(3), 2.038(3), 2.033(3), 2.041(3); Y–C 2.398(3), 2.401(3), 2.390(3), 2.405(3); Y–O 2.3651(18), 2.3651(18), 2.3637(19), 2.365(2); C–Al–C 93.81(11), 93.66(11); C–Y–C 129.70(9), 129.64(10); O–Y–O 171.64(7), 171.40(7).

Table 1. Structual comparison of aluminium-containing five-membered ring compounds

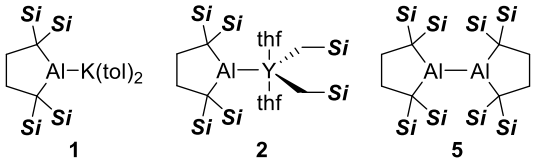

Compound	C-Al (Å)	C-Al-C (°)
1	2.0846(9)	90.40(5)
2	2.028(3), 2.038(3) 2.033(3), 2.041(3)	93.81(11) 93.66(11)
5	2.005(3), 2.011(3)	97.78(12)

Table 2. Structural comparison of **2** with $XY(CH_2\boldsymbol{Si})_2(thf)_2$ compounds[19] (X: anionic ligand, ***Si*** = $SiMe_3$).

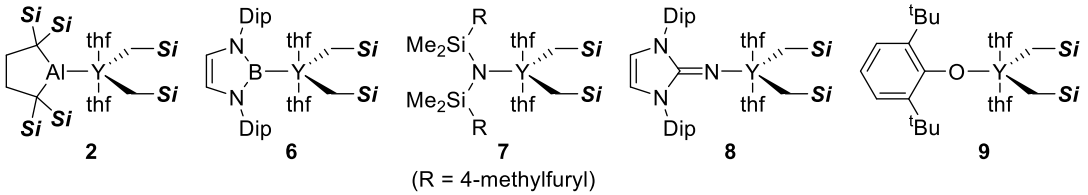

Compound	2	6	7	8	9
Y–C (Å)	2.398(3), 2.401(3) 2.390(3), 2.405(3)	2.424(4) 2.394(6)	2.403(3)	2.4469(15) 2.4334(17)	2.427(16) 2.411(13)
Y–O(thf) (Å)	2.3651(18), 2.3651(18) 2.3637(19), 2.365(2)	2.350(3) 2.370(3)	2.374(2)	2.3629(10) 2.3697(10)	2.343(9) 2.343(9)
C–Y–C (°)	129.70(9) 129.64(10)	136.3(1)	104.12(15)	135.84(6)	123.7(5)
O(thf)–Y–O(thf) (°)	171.64(7) 171.40(7)	159.54(8)	177.27(9)	160.50(4)	172.6(4)

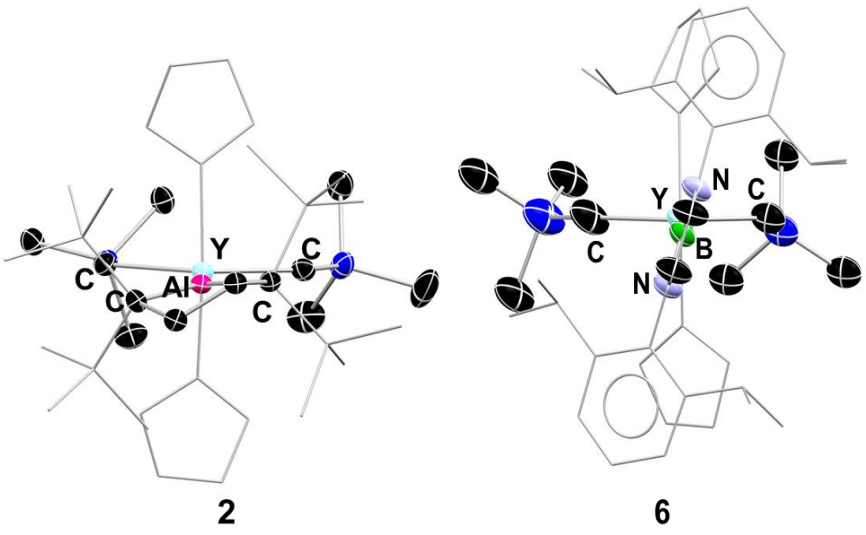

Figure 5. Crystal structures of **2** (left) and **6** (right) along with Al–Y and B–Y bonds (50% thermal ellipsoid, thf ligands, trimethylsilyl groups and Dip groups were illustrated as a wireframe form)

The electronic structure of **2** was examined by DFT calculation using B3LYP/LANL2DZ (for Y)/ 6-31+g(d) (all other atoms) level of theory. The theoretically optimized structure of **2** was in good agreement with the experimentally obtained structure (e.g. calculated Al–Y bond 3.281 Å; experimental: 3.187(8) Å, 3.1942(8) Å). The HOMO and LUMO are illustrated in (Figure 6, left). The HOMO represents the 2c-2e bond between Al and Y atoms, which exhibit Al^- and Y^+ character (**2'** in Figure 7). With reflection of their electronegativity [Pauling, Al: 1.61, Y: 1.22; Allen, Al: 1.613, Y: 1.12][1]. In contrast, the LUMO consists of significantly overlapping vacant 3p- and 4d-orbitals of the Al and Y atoms, respectively due to the strong electron affinity of the Al atoms. The HOMO level of **2** (–4.62 eV) is higher than that of **6**[19d, e] (–5.02 eV) at the same level of theory (Figure 6, right) due to the stronger σ-donor ability of the aluminum atom relative to that of the B atom, which is based on the difference in electronegativity of these atoms.[1] The LUMO level (–1.18 eV) of **2** is lower than that of **6** (–0.46 eV) because of effective overlapping of the vacant orbital between Al and Y atoms in **2** and π-bonding interaction between N and B atoms in **6** (Figure 7).

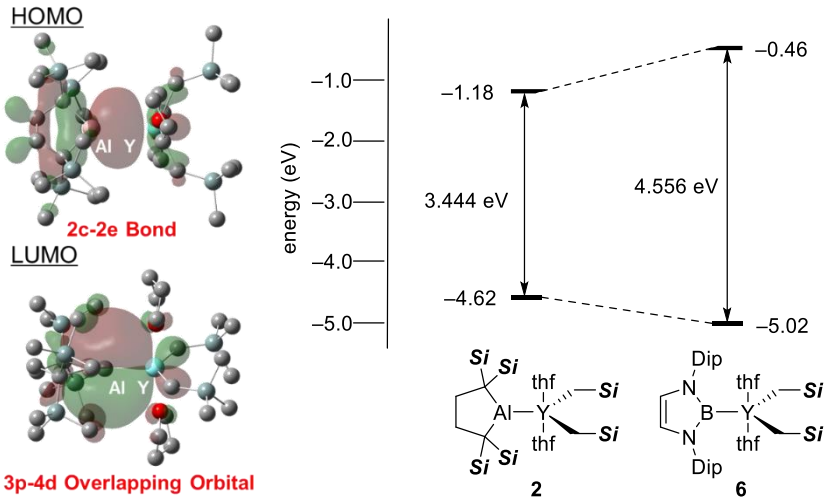

Figure 6. HOMO and LUMO of **2** (left), HOMO-LUMO gap comparison between **2** and **6**

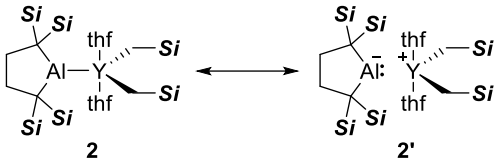

Figure 6. Resonance structure of **2**

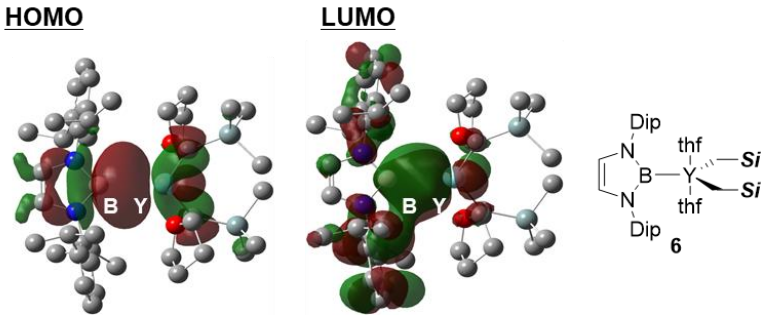

Figure 7. The HOMO and LUMO of **6**

An atoms in molecule (AIM) analysis[20] of **2** afforded insight into the properties of this unprecedented Al–Y bond (Figure 8). The $\Delta\rho(r)$ value (0.028237 e/a_0^3) and at the bond critical point (BCP) between the Al–Y atoms in **2** indicate that the Al–Y bond in **2** is stronger than the previously reported Al–K bond in **1** [$\Delta\rho(r)$: (0.01173 e/a_0^3)]. Considering the $\nabla^2\rho(r)$ value (0.009537 e/a_0^5) at the BCP for Al–Y bond in **2** is smaller than that in **1** [$\nabla^2\rho(r)$: (0.020826 e/a_0^5)], the Al–Y bond in **2** should be less polarized than that in **1**, but is apparently ionic because the value is positive.

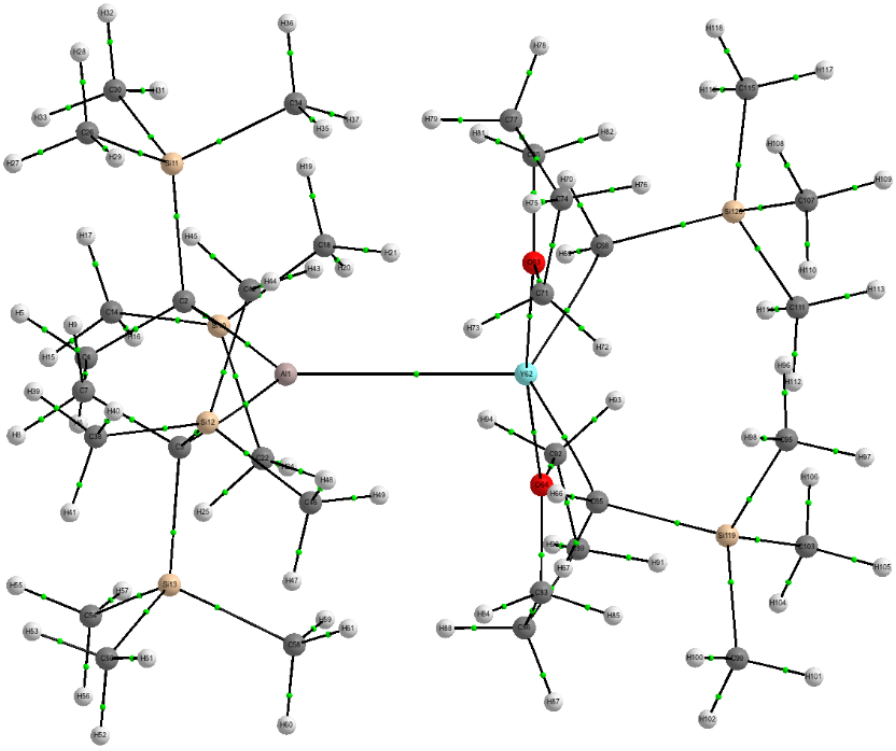

Figure 8. Molecular graph of **2** with bond critical points (green sphere) and bond paths (solid and dotted lines) calculated by AIM analysis

The UV-Vis absorption and emission spectra of **2** were measured in cyclohexane (Figure 9a). The UV-Vis spectrum exhibited two absorption maxima at 351 (ε = 3700) and 432 (ε = 2400) nm, while the emission spectrum (λ_{ex} = 440 nm) showed an emission maximum at 536 nm. The fluorescent quantum yield of **2** was low (ϕ = 0.0016), probably due to the high degree of freedom for all the aliphatic substituents. It should be noted that the emission became weaker upon repetitive measurements, probably due to the decomposition of **2** to an unidentified non-emissive product (Figure 10). Based on TD-DFT calculations, the absorption at 432

nm was assigned to the HOMO–LUMO transition (421 nm; f = 0.0316, Figure 9b). To reveal the substituent effect of the dialkylalumanyl ligand in **2**, the UV-Vis spectrum of independently synthesized $Y(CH_2SiMe_3)_3(thf)_3$ was measured in cyclohexane, albeit that an absorption beyond 300 nm was not observed. Additionally, the HOMO-LUMO transition of the previously reported[16d, e] "a pale yellow microcrystalline powder" of **6** was estimated to be at 304 nm based on TD-DFT calculations (Figure 9c). Thus, the introduction of the dialkylalumanyl ligand to the yttrium atom narrows the HOMO-LUMO gap of the d^0 complex without π-electrons and results in a visible absorption.

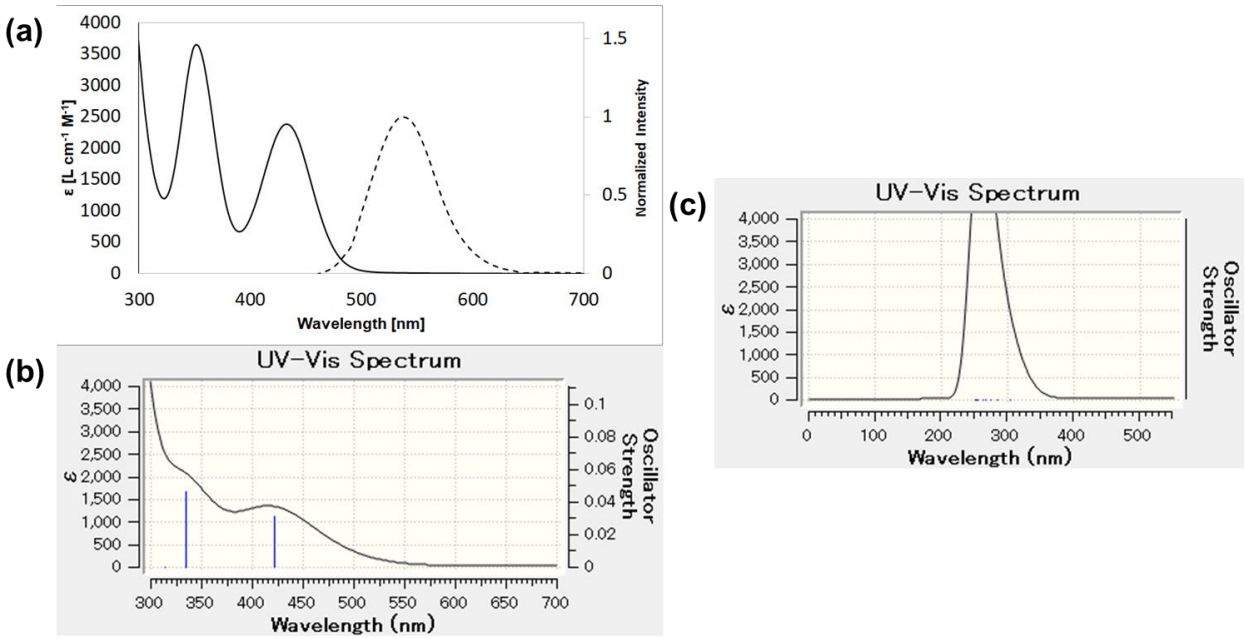

Figure 9. (a) Experimental UV-Vis absorption (solid line; λ_{max} = 351, 432 nm, e = 3700, 2400) and emission (dashed line; λ_{em} =536 nm λ_{ex} = 440 nm) spectra of **2** in 5.13×10^{-4} M cyclohexane solution.) A simulated UV-Vis spectrum for (b) **2** (b) **6** at CAM-B3LYP level of the theory using LANL2DZ (for Y) and 6-31+g(d) (for other elements) basis set.

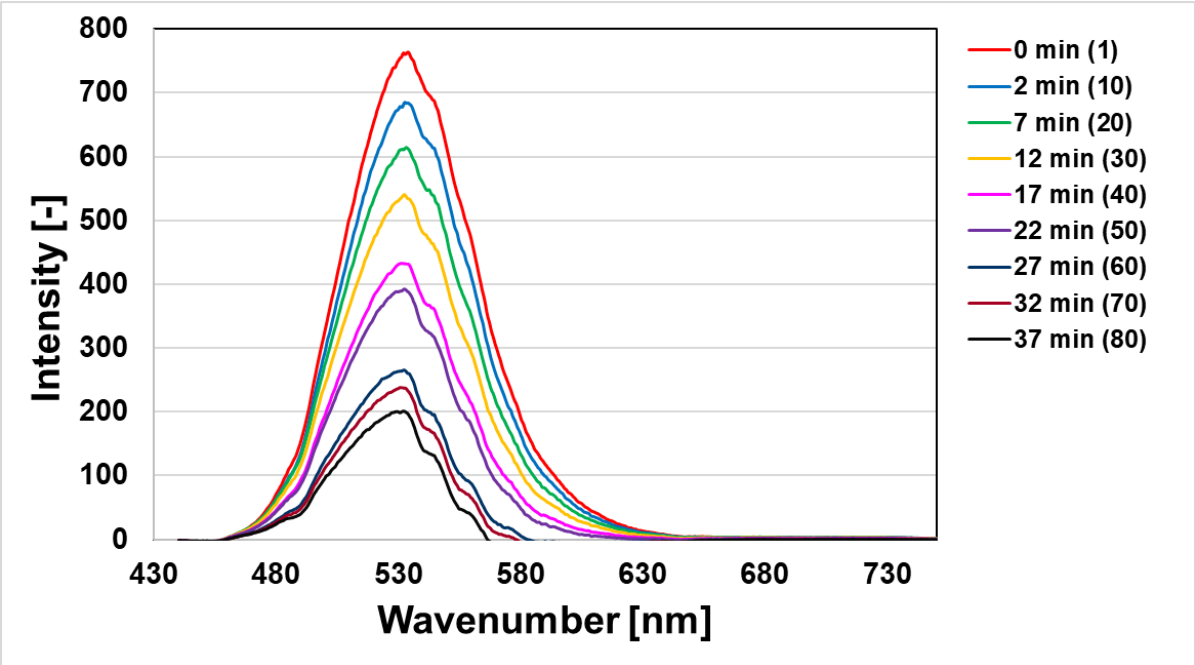

Figure 10. Repetitive measurement of fluorescent spectra of **2** (cyclohexane, numbers in parentheses of notes describe number of measurements).

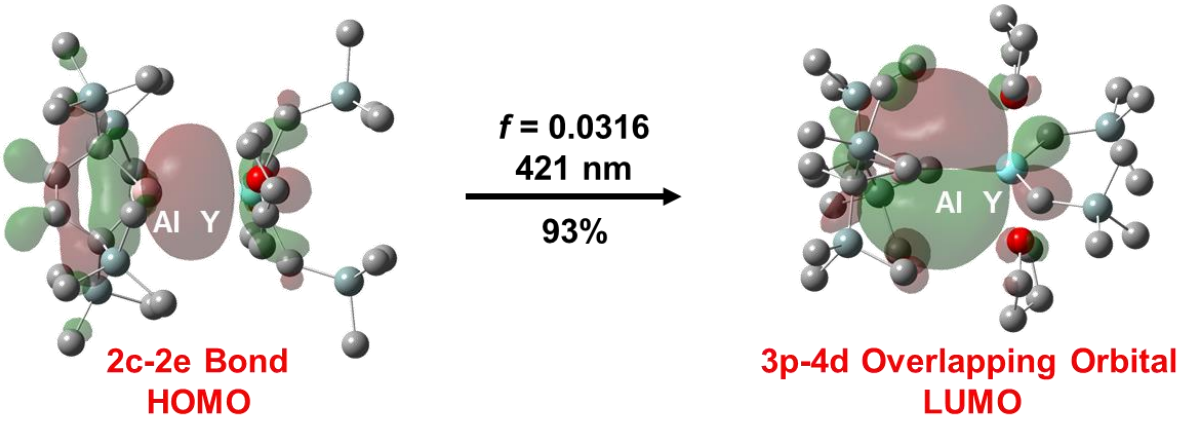

Figure 11. Transition mode at 421 nm on TD-DFT calculation

3.3. Conclusion

The reaction of a dialkylalumanyl potassium **1** with a cationic yttrium complex furnished the first example of an alumanylyttrium complex (**2**). A spectral and structural analysis of **2** in combination with DFT calculations revealed its electronic properties. The UV-Vis spectrum of **2** showed an absorption in visible region due to a narrow HOMO-LUMO gap, which stems from the strong σ-donor ability of the dialkylalumanyl substituent and the overlapping vacant 3p- and 4d-orbitals of the Al and Y atoms, respectively.

3.4. Experimental Section

All manipulations involving the air- and moisture-sensitive compounds were carried out under an argon atmosphere using glovebox (Korea KIYON) technique. All glasswares were dried for 20 min in the 250 °C oven before use. Toluene and Et_2O were purified by passing through a solvent purification system (Grass Contour). C_6D_{12} and pentane were dried over sodium/potassium alloy, followed by filtering through pad of activated neutral alumina. The nuclear magnetic resonance (NMR) spectra were recorded on JEOL ECS-400 (399 MHz for ^1H, 100 MHz for ^{13}C). Chemical shifts are reported in δ ppm relative to the residual protiated solvent for ^1H, deuterated solvent for ^{13}C used as references. The absolute values of the coupling constants are given in Hertz (Hz). Multiplicities are abbreviated as singlet (s), doublet (d), triplet (t), quartet (q), multiplet (m), and broad (br). Melting points were determined on Optimelt (SRS) and were uncorrected. Elemental analyses were performed on a Perkin Elmer 2400 series II CHN analyzer. Alumanylpotassium **1**[12c] and $[Y(CH_2SiMe_3)_2(thf)_3][BPh_4]$[15], and $Y(CH_2SiMe_3)_3(thf)_3$[20] $Cp^*_2MCl(thf)$[16] were prepared by according to procedures. UV-Vis absorption spectra were recorded on a Shimazu UV-3600 spectrometer using a 10 mm square quartz cell. Emission spectra were measured on a JASCO FP-8200 spectrometer. Quantum yield was estimated on a JASCO FP-6500. For solution samples, dry cyclohexane was used.

Synthesis of 2

In glove box, pre-cooled (–35 °C) a crystalline **1** (60.0 mg, 101 μmol) and $[Y(CH_2SiMe_3)_2(thf)_3][BPh_4]$ (87.0 mg, 101 μmol) were placed in a 3 mL vial, then pre-cooled (–35 °C) Et_2O was added to the mixed

powder. The resulting bright yellow suspension was stirred for 12 hours at –35 °C and then volatiles were evaporated under reduced pressure. Generated $KBPh_4$ was removed by filtration through a plastic syringe with a glass fiber filter by using pre-cooled (–35 °C) pentane, then the yellow solution was evaporated under reduce pressure. The residue was recrystallized from pentane at –35 °C to afford a yellow crystal of **2** (35.8 mg, 45.9 μmol, 45% yield). Single crystals suitable for X-ray analysis were obtained by recrystallization from Et_2O at –35 °C. ^{1}H NMR (Figure S1, 399 MHz, C_6D_{12}, 292 K) δ –0.65 (d, 2H, J_{YH} = 2.6 Hz, $YC\underline{H}_2$), –0.06 (s, 18H, $YCH_2Si(C\underline{H}_3)_3$), 0.13 (s, 36H, $Si(C\underline{H}_3)_3$ on the five-membered ring), 1.94 (s, 4H, $\underline{C}H_2$ of the five-membered ring), 2.08 (t, 8H, $O(CH_2C\underline{H}_2)_2$), 4.50 (br, 8H, $O(C\underline{H}_2CH_2)_2$); ^{13}C NMR (Figure S2, 100 MHz, C_6D_{12}, 292 K) δ 4.22 ($YCH_2Si(\underline{C}H_3)_3$), 4.27 ($Si(\underline{C}H_3)_3$ on the five-membered ring), 26.0 ($O(CH_2\underline{C}H_2)_2$), 27.8 (d, $^2J_{YC}$ = 6 Hz, 4° next to Al), 35.1 ($\underline{C}H_2$ of the five-membered ring), 48.1 (d, $^1J_{YC}$ = 36 Hz, $Y\underline{C}H_2$), 72.5 ($O(\underline{C}H_2CH_2)_2$); mp 63.4-72.4 °C (decomp.); Anal. Calcd for $C_{32}H_{78}AlO_2Si_6Y$: C, 49.32; H, 10.09; Found; C, 49.18; H, 10.38.

Details for crystallography

Crystallographic data for **2** are summarized in Table S1. The crystal was coated with Paratone-N (Hampton Research) and put on a MicroMount™ (MiTeGen, LLC), and then mounted on diffractometer. Diffraction data were collected on a Rigaku HyPix-6000 detector using Mo*K*α radiation (λ = 0.7103 Å). The Bragg spots were integrated using the CrysAlis^{Pro} program package. [21] Absorption corrections were applied. All structures were solved by the *SHELXT* program. Refinement on F^2 was carried out by full-matrix least-squares using the *SHELXL* in the *SHELX* software package[22] and expanded using Fourier techniques. All non-hydrogen atoms were refined using anisotropic thermal parameters. The hydrogen atoms were assigned to idealized geometric positions and included in the refinement with isotropic thermal parameters. The *SHELXL* was interfaced with Yadokari-XG 2009[23] for most of the refinement steps. The pictures of molecules were prepared using ORTEP-III for Windows.[24] The detailed crystallographic data have been deposited with the Cambridge Crystallographic Data Centre: Deposition code CCDC-1918147 (**2**). These data can be obtained free of charge from the Cambridge Crystallographic Data Centre via http://www.ccdc.cam.ac.uk/products/csd/request

Table 3. Crystallographic data for **2**.

	2
CCDC #	1918147
Empirical formula	$C_{32}H_{78}AlO_2Si_6Y$
Formula weight	779.37
Crystal system	*Triclinic*
Space group	*P*-1
T (K)	93(2)
Color	yellow
Habit	plate
a (Å)	13.2335(3)
b (Å)	19.1383(4)
c (Å)	21.2465(6)
α (°)	116.434(2)
β (°)	101.976(2)
γ (°)	90.0842(19)
V (Å^3)	4686.4(2)
Z	4
D_{calc} (g cm^{-3})	1.105
Abs. coeff (mm^{-1})	1.440
F(000)	1688
Crystal size (mm)	0.29×0.14×0.05
θ range (°)	1.704–30.764
Reflns collected	44523
Indep reflns/R_{int}	21290/0.0392
Parameters	793
GOF on F^2	1.032
R_1, wR_2 [I>2σ(I)]	0.0449, 0.1056
R_1, wR_2 (all data)	0.0645, 0.1116

Computational Details

Gaussian 16 (rev. A.03) software package[25] was employed to perform all of the calculations. The full model of **2** and **6**[15d, 15e] were optimized from the crystallographically obtained structure at the B3LYP[26] level of theory using LanL2DZ[27] (for Y) and 6-31+g(d)[28] (for others) basis sets. The TD-DFT calculations[29] were performed to estimate UV-vis spectra of **2** and **6** with CAM-B3LYP[30] level of theory using LanL2DZ[27] (for Y) and 6-31+g(d) [28] (for others) basis sets. AIM analysis[30] was performed by using AIMAll program package [31] with wavefunction file generated by Gaussian program.[32]

TD-DFT calculations

Table 4. Excitation energies and oscillator strengths for **2** obtained from TD-DFT calculations

Excited State	1:	Singlet-A	2.9436 eV 421.19 nm f = 0.0316	<S**2>=0.000
197 ->198		0.68284	HOMO to LUMO	
197 ->200		0.12989	HOMO to LUMO+2	

This state for optimization and/or second-order correction.

Total Energy, E(TD-HF/TD-DFT) = -3433.32618059

Copying the excited state density for this state as the 1-particle RhoCI density.

Excited State	2:	Singlet-A	3.7120 eV 334.01 nm f=0.0463	<S**2>=0.000
197 ->201		-0.24330	HOMO to LUMO+3	
197 ->203		0.55402	HOMO to LUMO+5	
197 ->206		0.12483	HOMO to LUMO+8	
197 ->207		0.29996	HOMO to LUMO+9	

Table 5. Excitation energies and oscillator strengths for **4** obtained from TD-DFT calculations

Excited State	1:	Singlet-A	4.0829 eV 303.66 nm f=0.0235	<S**2>=0.000
199 -> 202		0.28653		
199 -> 203		-0.18254		
199 -> 205		0.39280		
199 -> 207		0.14730		
199 -> 212		0.14213		
199 -> 213		0.11071		
199 -> 214		-0.31373		
199 -> 217		-0.12316		

This state for optimization and/or second-order correction.

Total Energy, E(TD-HF/TD-DFT) = -2545.61577578

Copying the excited state density for this state as the 1-particle RhoCI density.

Table 6. Cartesian coordinates of **2**

Atom	X	Y	Z	Atom	X	Y	Z
Al	1.7528	0	0.0001	H	0.8757	-3.0607	2.0129
C	3.164	1.5076	-0.0976	Y	1.5078	0.0001	-0.0001
C	3.1639	-1.5078	0.0982	O	1.6655	-0.6063	-2.354
C	4.4807	0.7264	0.2678	O	1.6662	0.6066	2.3536
H	5.3865	1.2371	-0.0988	C	2.5067	-2.1324	0.5653
H	4.6059	0.6806	1.3578	H	1.9802	-2.8344	-0.1103
C	4.4808	-0.7267	-0.2666	H	2.0354	-2.3153	1.5509
H	5.3863	-1.2375	0.1003	C	2.5064	2.1327	-0.5659
H	4.6064	-0.681	-1.3566	H	1.9797	2.8348	0.1095
Si	2.7386	2.7544	1.269	H	2.0352	2.3153	-1.5516
Si	3.3147	2.3746	-1.786	C	1.8194	-1.9728	-2.8702
Si	2.7388	-2.7544	-1.2687	H	2.6289	-2.4465	-2.3164
Si	3.3138	-2.3749	1.7866	H	0.8821	-2.5027	-2.6777
C	4.2263	3.8047	1.8314	C	2.1015	-1.8191	-4.3648
H	5.0755	3.1718	2.1195	H	1.7248	-2.6719	-4.9378
H	3.9516	4.4023	2.7118	H	3.1795	-1.7365	-4.5462
H	4.5774	4.4963	1.0584	C	1.3937	-0.4997	-4.7102
C	1.323	3.942	0.8029	H	1.7841	-0.0262	-5.6164
H	1.5754	4.6119	-0.0265	H	0.3174	-0.659	-4.8411
H	1.0789	4.5768	1.6661	C	1.6637	0.3432	-3.4689
H	0.4102	3.4044	0.5185	H	0.9004	1.0951	-3.2646
C	2.1562	1.8954	2.8786	H	2.6473	0.8227	-3.5021
H	1.3034	1.2214	2.7242	C	1.6651	-0.343	3.4684
H	1.8447	2.6614	3.6031	H	0.9019	-1.0951	3.2645
H	2.9558	1.3166	3.3536	H	2.6488	-0.8222	3.5012
C	4.4254	1.4428	-3.025	C	1.3955	0.4998	4.71
H	5.4359	1.2724	-2.6336	H	1.7861	0.0262	5.616
H	4.5282	2.0578	-3.9297	H	0.3192	0.6593	4.841
H	4.02	0.4746	-3.3351	C	2.1033	1.8191	4.3643
C	4.1273	4.1039	-1.726	H	1.7271	2.672	4.9376
H	3.5592	4.848	-1.1574	H	3.1814	1.7364	4.545
H	4.2275	4.4841	-2.7521	C	1.8201	1.9731	2.87
H	5.1366	4.0586	-1.2973	H	2.629	2.4471	2.3155
C	1.6302	2.5846	-2.6513	H	0.8825	2.5027	2.6783
H	1.2384	1.6073	-2.9619	C	5.1191	-2.8081	-1.0077
H	1.7379	3.198	-3.5562	H	5.0718	-1.857	-1.5534
H	0.8765	3.0597	-2.0133	H	6.1802	-3.072	-0.9046
C	4.2264	-3.8048	-1.8307	H	4.6582	-3.5815	-1.6377
H	5.0762	-3.1719	-2.1176	C	4.4397	-4.443	1.4831
H	3.9522	-4.4015	-2.7118	H	3.8936	-5.1936	0.8961
H	4.5767	-4.4971	-1.058	H	5.487	-4.7695	1.549
C	2.1569	-1.8951	-2.8784	H	4.0232	-4.4613	2.4995
H	1.3044	-1.2207	-2.7241	C	5.3152	-1.5303	1.7858
H	1.8452	-2.661	-3.6028	H	4.9127	-1.4616	2.806
H	2.9569	-1.3167	-3.3533	H	6.3516	-1.8832	1.873
C	1.3229	-3.9419	-0.8033	H	5.3478	-0.5141	1.3737
H	1.575	-4.6121	0.026	C	5.3144	1.5304	-1.7868
H	1.079	-4.5765	-1.6667	H	4.9117	1.4622	-2.8069
H	0.4101	-3.4044	-0.5189	H	6.3509	1.8828	-1.8741
C	4.1266	-4.1041	1.7268	H	5.3466	0.514	-1.375
H	3.5586	-4.8483	1.1581	C	5.1192	2.8076	1.0071
H	4.2267	-4.4843	2.7529	H	5.072	1.8564	1.5525
H	5.136	-4.0588	1.2981	H	6.1802	3.0716	0.9037
C	4.424	-1.4431	3.0261	H	4.6584	3.5809	1.6374
H	5.4346	-1.2725	2.6351	C	4.4396	4.4433	-1.4832
H	4.5266	-2.0583	3.9307	H	3.8941	5.1938	-0.8955
H	4.0184	-0.4751	3.3362	H	5.487	4.7695	-1.5495
C	1.629	-2.5851	2.651	H	4.0224	4.4621	-2.4992
H	1.2367	-1.6078	2.9611	Si	4.2816	-2.7094	0.7028
H	1.7364	-3.1981	3.5562	Si	4.2813	2.7095	-0.7033

Table 7. Cartesian coordinates of **6**

Atom	X	Y	Z	Atom	X	Y	Z
Y	1.0112	-0.0305	0.0356	H	1.8816	1.4036	2.3994
B	1.7194	0.0996	-0.0535	H	1.1184	2.1736	4.5738
N	2.6128	1.2744	0.0269	H	1.3443	3.8703	4.1512
N	2.7231	-0.9768	-0.2121	H	0.0805	2.9154	3.3477
O	1.1566	-2.1495	1.2591	H	3.5982	1.8432	4.1526
O	1.5321	2.0801	-1.1171	H	4.275	2.0721	2.5295
C	3.9573	0.8925	-0.0781	H	3.8406	3.4828	3.5161
C	4.0229	-0.4513	-0.218	H	2.9921	-5.1514	1.7216
C	2.3176	2.6727	0.1142	H	2.3226	-6.2804	-0.3748
C	2.0525	3.2607	1.3773	H	1.8568	-4.9519	-2.4002
C	1.8097	4.641	1.4288	H	1.6183	-1.2722	-2.4891
C	1.8471	5.428	0.2774	H	0.889	-2.2036	-4.5997
C	2.1342	4.8401	-0.9528	H	1.5194	-3.8067	-4.2213
C	2.3742	3.4622	-1.0607	H	0.1255	-3.1649	-3.3275
C	2.7292	2.8642	-2.4214	H	3.2737	-1.3894	-4.3517
C	4.09	3.3893	-2.925	H	3.8923	-2.9257	-3.7127
C	1.6346	3.1063	-3.4779	H	4.0838	-1.4293	-2.7754
C	2.1133	2.44	2.6645	H	3.2669	-1.4193	2.0758
C	1.1032	2.8831	3.7374	H	5.1375	-2.3239	3.4178
C	3.5447	2.4605	3.2465	H	4.9263	-3.9283	2.6922
C	2.5766	-2.4015	-0.2552	H	5.4603	-2.5682	1.6914
C	2.8661	-3.1574	0.9076	H	2.7754	-2.3411	4.3095
C	2.7671	-4.5556	0.8401	H	2.4474	-3.9392	3.6247
C	2.3944	-5.1957	-0.3395	H	1.3933	-2.5686	3.2246
C	2.1292	-4.4402	-1.4822	H	0.8083	-1.7056	3.2634
C	2.2259	-3.0413	-1.4721	H	2.5163	-1.865	2.7934
C	2.0414	-2.2442	-2.7636	H	2.2334	-4.0696	3.7159
C	1.0882	-2.9006	-3.7771	H	0.4961	-4.0796	3.3656
C	3.408	-1.98	-3.4361	H	1.3304	-5.4501	1.5293
C	3.3281	-2.5022	2.209	H	2.7843	-4.4449	1.355
C	4.7994	-2.8522	2.5176	H	0.1005	-3.6899	0.6361
C	2.4315	-2.8636	3.4081	H	1.3714	-3.4408	-0.3424
C	1.5182	-2.2886	2.6716	H	0.3257	3.4784	-0.1676
C	1.4775	-3.7891	2.9756	H	2.0377	3.4713	0.3406
C	1.7162	-4.4281	1.5986	H	2.0827	5.347	-1.1872
C	0.9708	-3.4776	0.6695	H	3.0652	1.4526	-2.366
C	1.3567	3.4041	-0.5116	H	1.5867	2.0014	-3.1922
C	1.7218	4.4023	-1.606	H	3.7677	3.711	-1.8927
C	2.2796	2.2061	-2.3685	H	2.919	4.01	-3.422
C	2.7975	3.6431	-2.3977	H	1.5782	0.4894	2.8481
C	2.0578	1.0007	1.9922	H	1.5771	1.998	1.976
C	1.9965	-1.1545	-1.8999	H	1.3103	-2.0216	-1.9677
C	4.2577	-3.1501	-1.0932	H	1.6684	-0.5013	-2.7322
C	5.0451	-0.4398	-2.2683	H	5.2815	-3.4778	-1.3181
C	3.8089	-2.5735	-4.0577	H	4.2467	-2.7956	-0.0546
C	4.7074	2.4285	1.162	H	3.6155	-4.0391	-1.1519
C	4.8653	-0.3387	2.4631	H	6.0372	-0.8867	-2.4197
C	4.1043	2.0939	4.1352	H	5.0706	0.0917	-1.3085
Si	3.8544	1.28	2.4252	H	4.9109	0.3064	-3.0633
H	0.8519	4.6179	-2.2353	H	4.8186	-2.9463	-4.2808
H	4.7628	1.614	-0.0523	H	3.1134	-3.4175	-4.1596
H	4.896	-1.082	-0.3175	H	3.5466	-1.8428	-4.835
H	1.601	5.1129	2.3844	H	5.7738	2.5402	1.3997
H	1.6638	6.498	0.3428	H	4.2696	3.4359	1.1698
H	2.1794	5.4629	-1.8432	H	4.6385	2.0408	0.1378
H	2.8196	1.7826	-2.2936	H	5.9316	-0.1201	2.6115
H	4.3611	2.9031	-3.8705	H	4.5593	-0.9951	3.2892
H	4.8879	3.1888	-2.2014	H	4.7752	-0.9097	1.5302
H	4.0622	4.4723	-3.1008	H	5.1677	2.2489	4.3659
H	1.9079	2.6232	-4.4244	H	3.6787	1.4735	4.9357
H	0.676	2.6896	-3.1515	H	3.6073	3.0722	4.1854
H	1.4911	4.1749	-3.683	Si	3.7032	-1.7958	-2.3164

3.5. References

1. (a) Pauling, L. THE NATURE OF THE CHEMICAL BOND. IV. THE ENERGY OF SINGLE BONDS AND THE RELATIVE ELECTRONEGATIVITY OF ATOMS. *J. Am. Chem. Soc.* **1932,** *54*, 3570-3582; (b) Pauling, L., *The Nature of The Chemical Bond*. 3 ed.; Cornell University Press: Ithaca, 1960; (c) Allen, L. C. Electronegativity is the average one-electron energy of the valence-shell electrons in ground-state free atoms. *J. Am. Chem. Soc.* **1989,** *111*, 9003-9014.

2. (Cp*Al ligand) (a) Yu, Q.; Purath, A.; Donchev, A.; Schnöckel, H. *J. Organomet. Chem.* **1999,** *584*, 94-97; (b) Weiss, D.; Steinke, T.; Winter, M.; Fischer, R. A.; Fröhlich, N.; Uddin, J.; Frenking, G. *Organometallics* **2000,** *19*, 4583-4588; (c) Steinke, T.; Gemel, C.; Cokoja, M.; Winter, M.; Fischer, R. A. *Angew. Chem. Int. Ed.* **2004,** *43*, 2299-2302; (d) Steinke, T.; Gemel, C.; Winter, M.; Fischer, R. *Chem. Eur. J.* **2005,** *11*, 1636-1646; (e) Steinke, T.; Cokoja, M.; Gemel, C.; Kempter, A.; Krapp, A.; Frenking, G.; Zenneck, U.; Fischer, R. A. *Angew. Chem. Int. Ed.* **2005,** *44*, 2943-2946; (f) Buchin, B.; Steinke, T.; Gemel, C.; Cadenbach, T.; Fischer, R. A. *Z. Anorg. Allg. Chem.* **2005,** *631*, 2756-2762; (g) Gamer, M. T.; Roesky, P. W.; Konchenko, S. N.; Nava, P.; Ahlrichs, R. *Angew. Chem. Int. Ed.* **2006,** *45*, 4447-4451; (h) Cadenbach, T.; Gemel, C.; Bollermann, T.; Fischer, R. A. *Inorg.Chem.* **2009,** *48*, 5021-5026; (i) Molon, M.; Bollermann, T.; Gemel, C.; Schaumann, J.; Fischer, R. A. *Dalton Trans.* **2011,** *40*, 10769-10774; (j) Molon, M.; Gemel, C.; Fischer, R. A. *J. Organomet. Chem.* **2014,** *751*, 573-578; (k) Weßing, J.; Göbel, C.; Weber, B.; Gemel, C.; Fischer, R. A. *Inorg. Chem.* **2017,** *56*, 3517-3525; (m) Hornung, J.; Weßing, J.; Jerabek, P.; Gemel, C.; Pöthig, A.; Frenking, G.; Fischer, R. A. *Inorg. Chem.* **2018,** *57*, 12657-12664.

3. (Z-type ligand) (a) Burlitch, J. M.; Leonowicz, M. E.; Petersen, R. B.; Hughes, *Inorg. Chem.* **1979,** *18*, 1097-1105; (b) Mayer, J. M.; Calabrese, J. C. *Organometallics* **1984,** *3*, 1292-1298; (c) Buchin, B.; Gemel, C.; Kempter, A.; Cadenbach, T.; Fischer, R. A. *Inorg. Chim. Acta* **2006,** *359*, 4833-4839; (d) Braunschweig, H.; Gruss, K.; Radacki, K. *Angew. Chem. Int. Ed.* **2007,** *46*, 7782-7784; (e) Bauer, J.; Braunschweig, H.; Brenner, P.; Kraft, K.; Radacki, K.; Schwab, K. *Chem.Eur. J.* **2010,** *16*, 11985-11992; (f) Rudd, P. A.; Liu, S.; Gagliardi, L.; Young, V. G.; Lu, C. C. *J. Am. Chem. Soc.* **2011,** *133*, 20724-20727; (g) Bauer, J.; Bertermann, R.; Braunschweig, H.; Gruss, K.; Hupp, F.; Kramer, T. *Inorg. Chem.* **2012,** *51*, 5617-5626; (h) Bauer, J.; Braunschweig, H.; Radacki, K. *Chem. Commun.* **2012,** *48*, 10407-10409; (i) Rudd, P. A.; Planas, N.; Bill, E.; Gagliardi, L.; Lu, C. C. *Eur. J. Inorg. Chem.* **2013,** *2013*, 3898-3906; (j) Oishi, M.; Oshima, M.; Suzuki, H. *Inorg. Chem.* **2014,** *53*, 6634-6654; (k) Devillard, M.; Nicolas, E.; Ehlers, A. W.; Backs, J.; Mallet-Ladeira, S.; Bouhadir, G.; Slootweg, J. C.; Uhl, W.; Bourissou , D. *Chem. Eur. J.* **2015,** *21*, 74-79; (l) Cowie, B. E.; Tsao, F. A.; Emslie, D. J. H. *Angew. Chem. Int. Ed.* **2015,** *54*, 2165-2169; (m) Devillard, M.; Declercq, R.; Nicolas, E.; Ehlers, A. W.; Backs, J.; Saffon-Merceron, N.; Bouhadir, G.; Slootweg, J. C.; Uhl, W.; Bourissou, D. *J. Am. Chem.Soc.* **2016,** *138*, 4917-4926; (n) Thompson, A. B.; Pahls, D. R.; Bernales, V.; Gallington, L. C.; Malonzo, C. D.; Webber, T.; Tereniak, S. J.; Wang, T. C.; Desai, S. P.; Li, Z.; Kim, I. S.; Gagliardi, L.; Penn, R. L.; Chapman, K. W.; Stein, A.; Farha, O. K.; Hupp, J. T.; Martinson, A. B. F.; Lu, C. C. *Chem. Mater.* **2016,** *28*, 6753-6762; (o) Saito, T.; Hara, N.; Nakao, Y. *Chem. Lett.* **2017,** *46*, 1247-1249; (p) Moore, J. T.; Smith, N. E.; Lu, C. C. *Dalton Trans.* **2017,** *46*, 5689-5701; (q) Hara, N.; Saito, T.; Semba, K.; Kuriakose, N.; Zheng, H.; Sakaki, S.; Nakao, Y. *J. Am. Chem. Soc.* **2018,** *140*, 7070-7073; (r) Hofmann, A.; Lamprecht, A.; Jiménez - Halla, J. O. C.; Tröster, T.; Dewhurst, R. D.; Lenczyk, C.; Braunschweig, H. *Chem. Eur. J.* **2018,** *24*, 11795-11802.

4. (base-stabilized alumylene ligand) (a) Fischer, R. A.; Schulte, M. M.; Weiss, J.; Zsolnai, L.; Jacobi, A.; Huttner, G.; Frenking, G.; Boehme, C.; Vyboishchikov, S. F. *J. Am. Chem. Soc.***1998,** *120*, 1237-1248; (b) Fölsing, H.; Segnitz, O.; Bossek, U.; Merz, K.; Winter, M.; Fischer, R. A. *J. Organomet. Chem.* **2000,** *606*, 132-140; (c) Tan, G.; Szilvási, T.; Inoue, S.; Blom, B.; Driess, M. *J. Am. Chem. Soc.* **2014,** *136*, 9732-9742; (d) Dange, D.; Sindlinger, C. P.; Aldridge, S.; Jones, C. B. *Chem. Commun.* **2017,** *53*, 149-152.
5. (base-stabilized alumanyl ligand) (a) Fryzuk, M. D.; McManus, N. T.; Rettig, S. J.; White, G. S. *Angew. Chem. Int. Ed. Engl.* **1990,** *29*, 73-75; (b) Fischer, R. A.; Priermeier, T. *Organometallics* **1994,** *13*, 4306-4314; (c) Braunschweig, H.; Müller, J.; Ganter, B. *Inorg. Chem.* **1996,** *35*, 7443-7444; (d) Jones, C.; Aldridge, S.; Gans-Eichler, T.; Stasch, A. *Dalton Trans.* **2006**, 5357-5361; (e) Riddlestone, I. M.; Urbano, J.; Phillips, N.; Kelly, M. J.; Vidovic, D.; Bates, J. I.; Taylor, R.; Aldridge, S. *Dalton Trans.* **2013,** *42*, 249-258; (f) Takaya, J.; Iwasawa, N. *J. Am. Chem. Soc.* **2017,** *139*, 6074-6077; (g) Agnew, D. W.; Moore, C. E.; Rheingold, A. L.; Figueroa, J. S. *Dalton Trans.* **2017,** *46*, 6700-6707; (h) Hicks, J.; Mansikkamäki, A.; Vasko, P.; Goicoechea, J. M.; Aldridge, S. *Nat. Chem.* **2019,** *11*, 237-241.; (i) Semba, K.; Fujii, I.; Nakao, Y. *Inorganics,* **2019,** *7,* 140-149.
6. (bridged Cp*Al) (a) Dohmeier, C.; Krautscheid, H.; Schnöckel, H. *Angew. Chem. Int. Ed. Engl.* **1995,** *33*, 2482-2483; (b) Üffing, C.; Ecker, A.; Köppe, R.; Schnöckel, H. *Organometallics* **1998,** *17*, 2373-2375.
7. (bridged base-stabilized alumylene) Kempter, A.; Gemel, C.; Fischer, R. A. *Chem. Commun.* **2006**, 1551-1553;
8. (bridged alane) Noor, A.; Glatz, G.; Müller, R.; Kaupp, M.; Demeshko, S.; Kempe, R. *Nat. Chem.* **2009,** *1*, 322-325.
9. (ate complex) Anand, B. N.; Krossing, I.; Nöth, H. *Inorg. Chem.* **1997,** *36*, 1979-1981.; (b) Agou, T.; Yanagisawa, T.; Sasamori, T.; Tokitoh, N. *Bull. Chem. Soc. Jpn.* **2016,** *89*, 1184-1186; (c) Yanagisawa, T.; Mizuhata, Y.; Tokitoh, N. *Heteroat. Chem.* **2018,** *29*, e21465.
10. (alumylene ligand) Kempter, A.; Gemel, C.; Fischer, R. A. *Chem. Eur. J.* **2007,** *13*, 2990-3000; (b) Nagata, K.; Agou, T.; Tokitoh, N. *Angew. Chem. Int. Ed.* **2014,** *53*, 3881-3884; (c) Hooper, T. N.; Garcon, M.; White, A. J. P.; Crimmin, M. R. *Chem. Sci.* **2018,** *9*, 5435-5440.
11. (alkane elimination) (a) Schneider, J. J.; Krüger, C.; Nolte, M.; Abraham, I.; Ertel, T. S.; Bertagnolli, H. *Angew. Chem. Int. Ed. Engl.* **1995,** *33*, 2435-2437; (b) Golden, J. T.; Peterson, T. H.; Holland, P. L.; Bergman, R. G.; Andersen, R. A. *J. Am. Chem. Soc.* **1998,** *120*, 223-224.
12. (PAlP) Morisako, S.; Watanabe, S.; Ikemoto, S.; Muratsugu, S.; Tada, M.; Yamashita, M. *Angew. Chem. Int. Ed.* **2019,** *58*, 15031-15035.
13. (Al anion) (a) Hicks, J.; Vasko, P.; Goicoechea, J. M.; Aldridge, S. *Nature* **2018,** *557*, 92-95; (b) Schwamm, R. J.; Anker, M. D.; Lein, M.; Coles, M. P. *Angew. Chem. Int. Ed.* **2019,** *58*, 1489-1493; (c) Kurumada, S.; Takamori, S.; Yamashita, M. *Nat. Chem.* **2020,** *12*, 36-39. (d) Schwamm, J. R.; Coles, P. M.; Hill, S. M.; Mahon, F. M.; McMullin, L. C.; Rajabi, A. N.; Wilson, S. S. A. *Angew. Chem. Int. Ed.* **2020,** in press. doi:10.1002/anie.201914986.
14. (a) Anker, M. D.; Coles, M. P. *Angew. Chem. Int. Ed.* **2019,** *58*, 13452-13455; (b) Anker, M. D.; Coles, M. P. *Angew. Chem. Int. Ed.* **2019,** *58*, 18261-18265; (c) Hicks, J.; Heilmann, A.; Vasko, P.; Goicoechea, J. M.; Aldridge, S. *Angew. Chem. Int. Ed.* **2019,** *58*, 17265-17268; (d) Hicks, J.; Vasko, P.; Goicoechea, J. M.;

Aldridge, S. *J. Am. Chem. Soc.* **2019,** *141*, 11000-11003; (e) Sugita, K.; Nakano, R.; Yamashita, M. *Chem. Eur. J.* **2020,** *25*, 2174-2177.
15. (Y+) Elvidge, B. R.; Arndt, S.; Zeimentz, P. M.; Spaniol, T. P.; Okuda, J. *Inorg. Chem.* **2005,** *44*, 6777-6788.
16. $Cp^*_2YCl(thf)$; Evans, J. W.; Peterson, T. T.; Rausch, D. M.; Hunter, E. W.; Zhang, H.; Atwood, J. L. *Organometallics* **1985,** *4,* 554-559. $Cp^*_2ScCl(thf)$; Thompson, E. M.; Baxter, M. S.; Ray Bulls, A.; Burger, J. B.; Nolan, C. M.; Santarsiero, D. B.; Schaefer, P. W.; Bercaw, E. J. *J. Am. Chem. Soc.* **1987,** *109,* 203-219.
17. Kurumada, S.; Nakano, R.; Yamashita, M. *manuscript in preparation.*
18. Emsley, J., *The Elements*. 3rd ed.; Oxford University Press: New York, 1998.
19. (a) Evans, L. T. J.; Coles, M. P.; Cloke, F. G. N.; Hitchcock, P. B. *Inorg. Chim. Acta* **2010,** *363*, 1114-1125; (b) Trambitas, A. G.; Panda, T. K.; Jenter, J.; Roesky, P. W.; Daniliuc, C.; Hrib, C. G.; Jones, P. G.; Tamm, M. *Inorg. Chem.* **2010,** *49*, 2435-2446; (c) Evans, W. J.; Broomhall-Dillard, R. N. R.; Ziller, J. W. S. *Organometallics* **1996,** *15*, 1351-1355; (d) Saleh, L. M. A.; Birjkumar, K. H.; Protchenko, A. V.; Schwarz, A. D.; Aldridge, S.; Jones, C.; Kaltsoyannis, N.; Mountford, P. *J. Am. Chem. Soc.* **2011,** *133*, 3836-3839; (e) Li, S.; Cheng, J.; Chen, Y.; Nishiura, M.; Hou, Z. *Angew. Chem. Int. Ed.* **2011,** *50*, 6360-6363.
20. (a) Bader, R. F. W., *Atoms In Molecules - A Quantum Theory*. Oxford University Press: New York, 1990; (b) Bader, R. F. W. A *Chem. Rev.* **1991,** *91,* 893-928.
21. Hultzsch, K. C.; Voth, P.; Beckerle, K.; Spaniol, T. P.; Okuda, J. *Organometallics* **2000,** *19,* 228-243.
22. CrysAlisPRO *CrysAlisPRO*, Oxford Diffraction/Agilent Technologies UK Ltd: Yarnton, England, 2015.
23. Sheldrick, G. *Act. Cryst. Sec. C* **2015,** *71*, 3-8.
24. Kabuto, C.; Akine, S.; Kwon, E. *J. Cryst. Soc. Jpn.* **2009,** *51*, 218-224.
25. Farrugi, L. J. *J. Appl. Crystallogr.* **1997,** *30*, 565-565.
26. Frisch, M. J.; Trucks, G. W.; Schlegel, H. B.; Scuseria, G. E.; Robb, M. A.; Cheeseman, J. R.; Scalmani, G.; Barone, V.; Petersson, G. A.; Nakatsuji, H.; Li, X.; Caricato, M.; Marenich, A. V.; Bloino, J.; Janesko, B. G.; Gomperts, R.; Mennucci, B.; Hratchian, H. P.; Ortiz, J. V.; Izmaylov, A. F.; Sonnenberg, J. L.; Williams; Ding, F.; Lipparini, F.; Egidi, F.; Goings, J.; Peng, B.; Petrone, A.; Henderson, T.; Ranasinghe, D.; Zakrzewski, V. G.; Gao, J.; Rega, N.; Zheng, G.; Liang, W.; Hada, M.; Ehara, M.; Toyota, K.; Fukuda, R.; Hasegawa, J.; Ishida, M.; Nakajima, T.; Honda, Y.; Kitao, O.; Nakai, H.; Vreven, T.; Throssell, K.; Montgomery Jr., J. A.; Peralta, J. E.; Ogliaro, F.; Bearpark, M. J.; Heyd, J. J.; Brothers, E. N.; Kudin, K. N.; Staroverov, V. N.; Keith, T. A.; Kobayashi, R.; Normand, J.; Raghavachari, K.; Rendell, A. P.; Burant, J. C.; Iyengar, S. S.; Tomasi, J.; Cossi, M.; Millam, J. M.; Klene, M.; Adamo, C.; Cammi, R.; Ochterski, J. W.; Martin, R. L.; Morokuma, K.; Farkas, O.; Foresman, J. B.; Fox, D. J. *Gaussian 16*, Wallingford, CT, 2016.
27. (a) Lee, C.; Yang, W.; Parr, R. G. *Phys. Rev. B* **1988,** *37*, 785-789; (b) Becke, A. D. *Phys. Rev. A* **1988,** *38*, 3098-3100; (c) Miehlich, B.; Savin, A.; Stoll, H.; Preuss, H. *Chem. Phys. Lett.* **1989,** *157*, 200-206.
28. (a) Hay, P. J.; Wadt, W. R. *J. Chem. Phys.* **1985,** *82*, 270-283; (b) Wadt, W. R.; Hay, P. J. *J. Chem. Phys.* ***1985,*** *82, 284-298; (c) Hay, P. J.; Wadt, W. R. J. Chem. Phys.* ***1985,*** *82, 299-310.*
29. Huzinaga, S.; Andzelm, J.; Klobukowski, M.; Radzio-Andzelm, E.; Sakai, Y.; Tatewaki, H., *Gaussian basis sets for molecular calculations*. Elsevier: 1984.
30. (a) Adamo, C.; Jacquemin, D. *Chemical Society Reviews* **2013,** *42*, 845-856; (b) Laurent, A. D.; Adamo, C.; Jacquemin, D. *Phys. Chem. Chem. Phys.* **2014,** *16*, 14334-14356.

31. Yanai, T.; Tew, D. P.; Handy, N. C. *Chem. Phys. Lett.* **2004,** *393*, 51-57.
32. Keith, T. A. *AIMALL*, (version 14.04.17); TK Gristmill Software, Overland Park KS, USA: 2014.

Chapter 4

One-electron Reduction of Group 4 Metal Complexes by Dialkylaluminum(I) Anion

4.1. Introduction

Titanium complexes in low-oxidation state, such as (III) and (II), are widely used for catalytic and stoichiometric reactions in synthetic organic chemistry and polymer chemistry,[1] such as olefin polymerization,[2] exo-olefination of carbonyl compounds,[3] Mcmurry coupling,[4] and cycloaddition of unsaturated compounds.[5] Although titanium(III) complexes should have an unpaired electron in their d-orbital to lead difficulty of characterization,[6] aluminum-containing titanium(III) complexes have been studied in detail because of their importance as an intermediate for Ziegler-Natta catalysts[2] and Tebbe reagent.[3] These aluminum-containing titanium(III) complexes have been synthesized by the following three methods (Scheme 1): (i) reaction of titanium(IV) dichloride with trialkylaluminum[7] or aluminum hydride,[8] (ii) one-electron reduction of titanocene difluoride by elemental aluminum,[9] and (iii) oxidation of chloride-bridged titanium(II) complex by using cyclopentadiene derivatives.[10]

Scheme 1. Synthesis of Al-containing titanium(III) complex

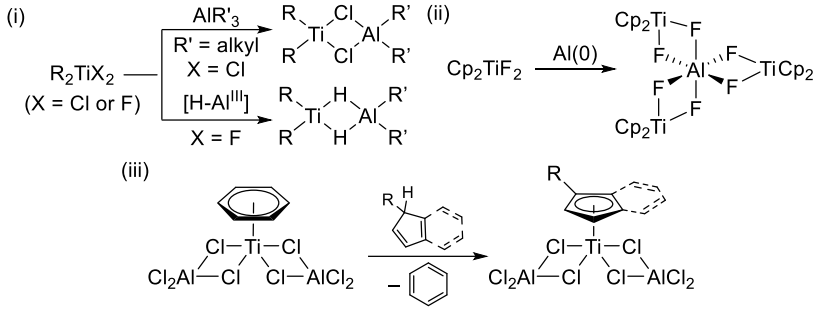

On the other hand, anionic aluminum(I) species **I-IV** and **1** have emerged in last three years (Figure 1).[11] Confirmed reactivity of these anionic aluminum(I) species can be classified into five types. Based on the lone pair electrons on the Al atom, these species can act as a nucleophile toward electrophiles (Scheme 2A).[11a, 11g, 11i] Nucleophilic transmetallation of alumanyl anion moiety to the other metals afforded the corresponding alumanylmetal species (Scheme 2B).[11a, 11b, 11g, 11k] Because of the low-oxidation state of anionic aluminum(I) species, these anionic alumanyl species can be easily oxidized to form Al–heteroatom bond (Scheme 2C).[11d, 11f, 11h, 11l] They also can undergo (1+2) or (1+4) cycloaddition reaction at the Al center (Scheme 2D).[11c, 11e, 11h, 11j] Oxidative addition with C–H bond at the Al center was also possible to give (hydrido)(carbyl) species (Scheme 2E).[11a, 11c, 11i] The strongly nucleophilic Al center due to electropositive character of aluminum in these alumanyl anion species would be expected to behave as one-electron reductant. Herein, we report the reaction of dialkylalumanylpotassium 1 with titanium tetraisopropoxide furnishing Ti(III) complex **2** through one-electron transfer reaction (Scheme 2F). The resulting open-shell Ti(III) species was characterized by a single-crystal X-ray diffraction analysis, ESR spectroscopy, and UV-Vis absorption spectroscopy. The unique electronic structure of **2** was also evaluated by DFT calculations.

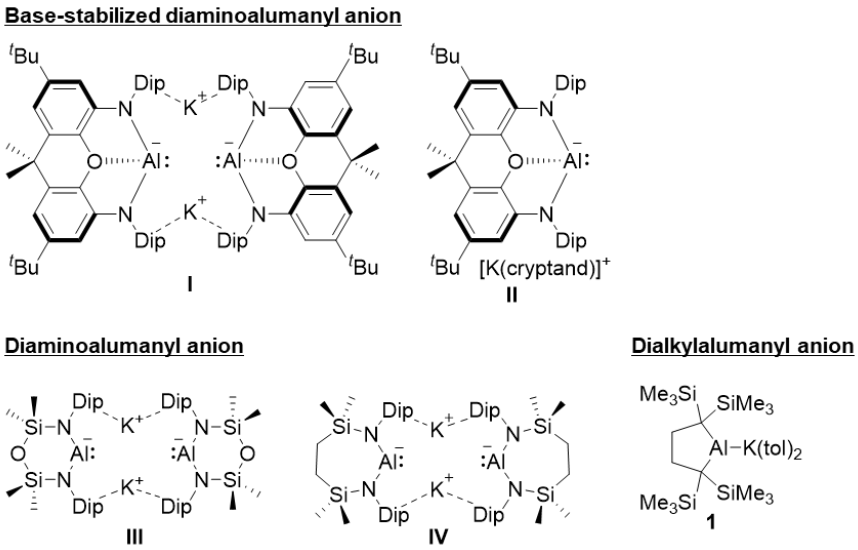

Figure 1. Examples of anionic aluminum(I) species **I**-**IV** and **1** (Dip = 2,6-diisopropylphenyl)

Scheme 2. Reactivity of **I**-**IV** and **1**

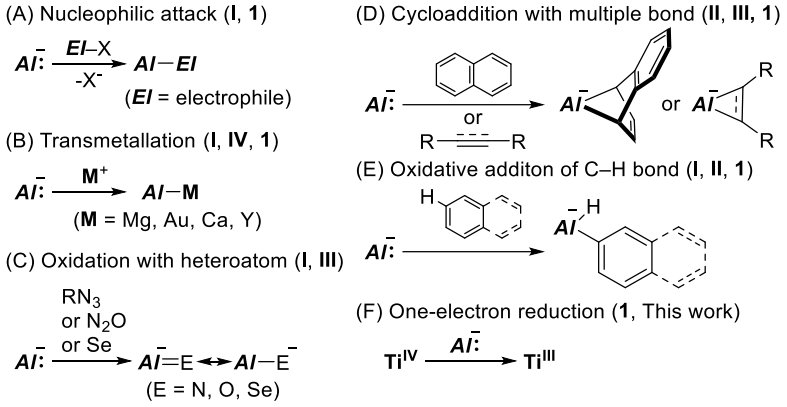

4.2. This work

The reaction of dialkylalumanylpotassium **1** with 1.5 equivalent of $Ti(O^iPr)_4$ furnished (dialkoxy)(dialkyl)aluminate-stabilized cationic titanium(III) diisopropoxide **2** as a blue crystalline solid (Scheme 3). It should be noted that the reaction with 2 equivalent of $Ti(O^iPr)_4$ led to a lower yield probably due to the subsequent reaction giving byproducts. Since **2** is NMR-silent, the structure of **2** was unambiguously confirmed as a contact ion pair between Ti(III) and aluminate anion by a single-crystal X-ray diffraction analysis (*vide infra*, Figure 3). Considering the stoichiometry of the reaction, potassium isopropoxide and titanium(III) isopropoxide would be eliminated from the reaction mixture. Thus, the present reaction proceeded via an unprecedented single electron transfer from anionic aluminum(I) species.

Scheme 3. The reaction of **1** with $Ti(O^iPr)_4$ (***Si*** = $SiMe_3$)

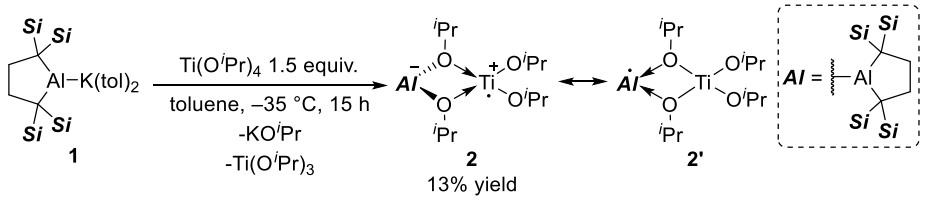

One electron reduction also proceeded by using Cp_2ZrCl_2 to afford zirconium(III) dimer **3** as a red crystalline solid (Scheme 4). In this reaction, one of C–H bond in Cp group was cleaved by the aluminum atom, two chloride anion were removed from Zr center, and ipso carbon atom of the resulting Al–Cp moiety coordinated to the Zr center of other molecule to form a dimeric structure. The structure of **3** was confirmed by single X-ray structure analysis. In the reaction of **1** with $Cp^*_2ZrCl_2$, dichloroaluminate **4** and (*m*-tolyl)(hydride)aluminate **5** were obtained (Scheme 5), as judged by the ^1H NMR spectrum of the crude product (Figure 2). These results also support the intermolecular electron transfer reaction from **1** to Lewis acidic zirconium center.

Scheme 4. The reaction of **1** with Cp_2ZrCl_2 (***Si*** = $SiMe_3$)

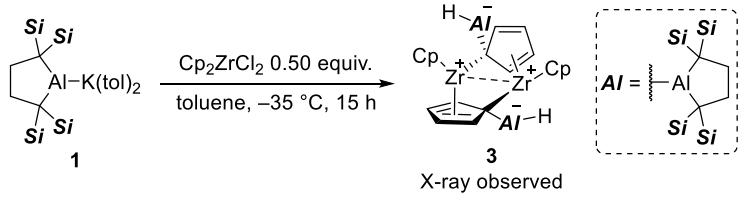

Scheme 5. The reaction of **1** with $Cp^*_2ZrCl_2$

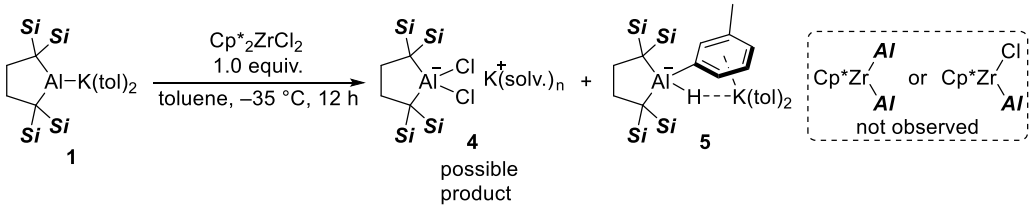

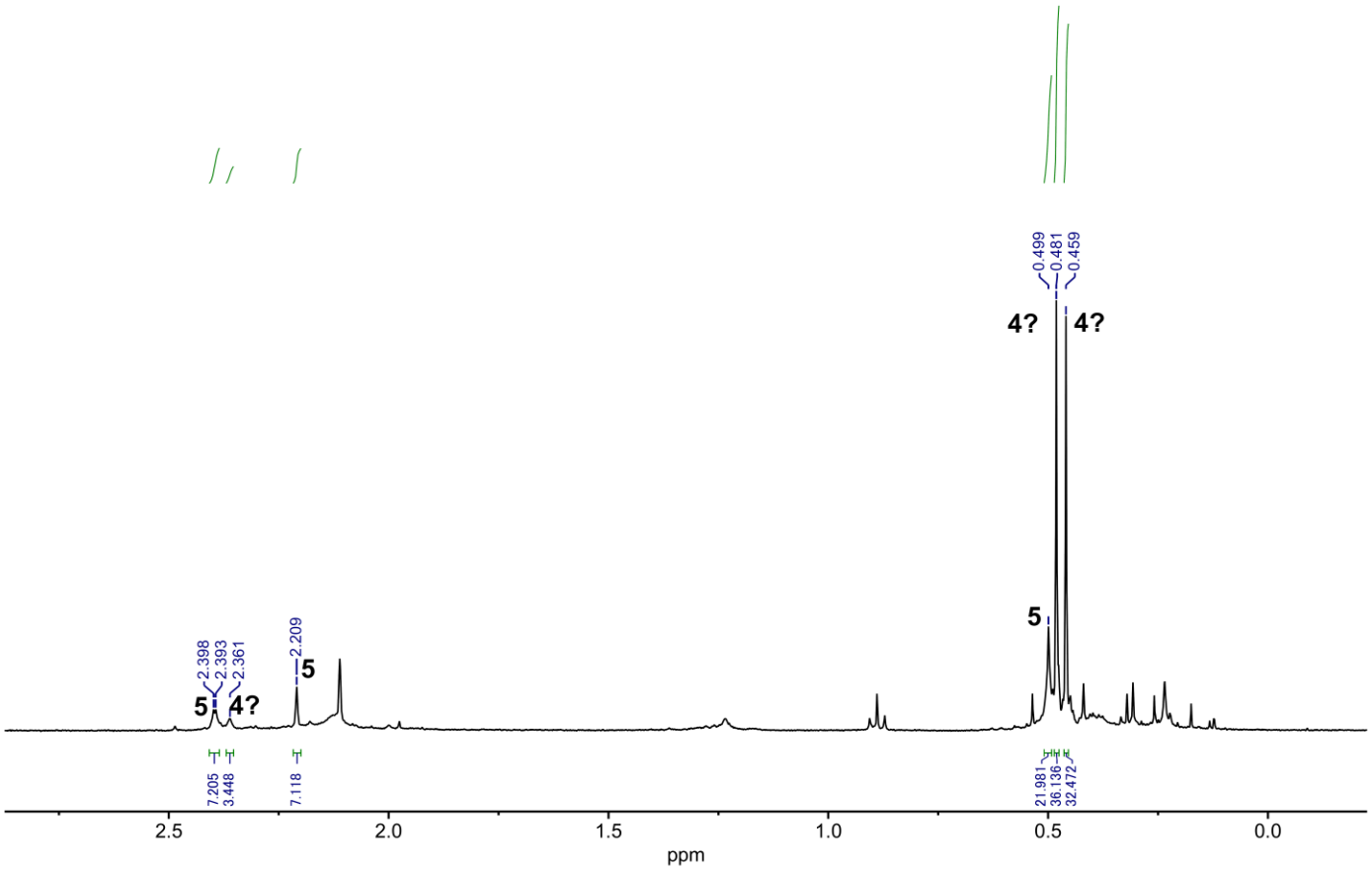

Figure 2. ^{1}H NMR of the crude product

The reaction of **1** with other group 4 metal chlorides at –35 °C gave tetraalkyldialumane **6** (Scheme 6). The formation of **5** can be explained by one-electron transfer to the metal(IV) chloride to give an Al-centered radical, potassium chloride, and metal(III) chloride, followed by a bimolecular coupling of the Al-centered radical (Scheme 7).

Scheme 6. The reaction of **1** with group 4 metal halide

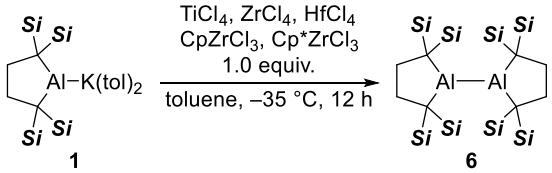

The proposed reaction mechanism of dialkylalumanylanion **1** and metal halides is shown in Scheme 7. Anion **1** abstracted chloride group on group 4 metal complexes, then the formation of chloroalumaneas an intermediate, and then the anion **1** attack alumanylchloride gave dialumane **6**.

Scheme 7. Possible mechanism for the formation of dialumane **6**

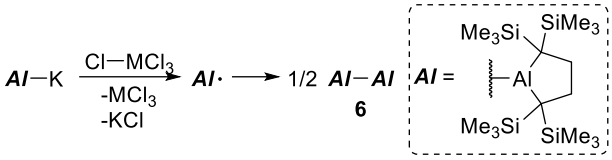

In the crystal structure of **2** (Figure 3), the sum of the internal angles in the Al–O–Ti–O four-membered ring is 359.99°, indicating its planarity. Table 1 shows the structural comparison of **2** with known titanium(IV) tetraadamantoxide **7**,[12] six-coordinate titanium(IV) dialkoxide complex **8** coordinated by two four-coordinate aluminum alkoxides,[13] and titanium(IV) tetraisopropoxide-aluminum complex **9**.[14] In the complex **2**, two terminal Ti–O bonds [1.786(2), 1.794(2)] are slightly longer than those of reported complexes **7-9** [1.739(2)~1.766(2) Å]. Two Ti–O bonds for the bridging alkoxide [2.0436(18), 2.0434(17) Å] are longer than the terminal Ti–O bond in **2**. These Ti–O bonds for bridging alkoxide in **2** are in the range for those of **8** and an Al–O coordinating bond in **9**. Two O–Al bonds [1.8395(18), 1.8506(18) Å] in **2** are longer than the O–Al bonds for bridging alkoxide in **8** and the O–Al coordination bond in **9**. Probably due to the conformational rigidity of the Al-containing five-membered ring in **2**, the O–Ti–O angle for terminal alkoxide are larger than those of **7-9** and the O–Ti–O angle for bridging alkoxide are smaller than that of **8**.

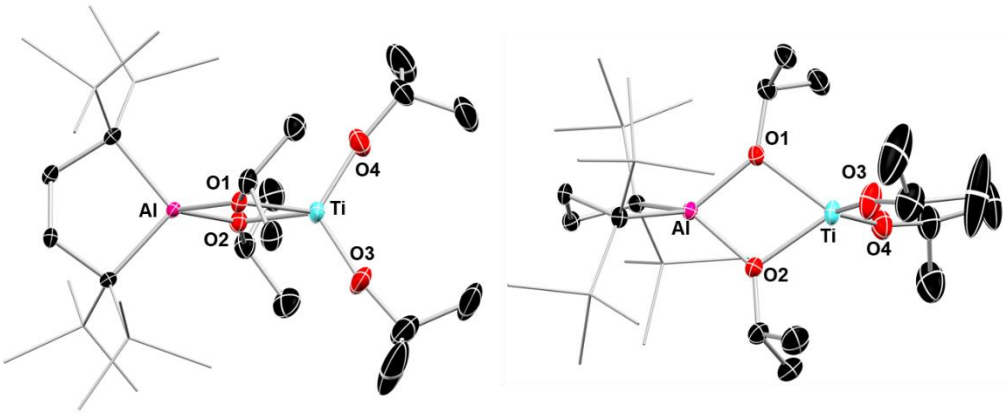

Figure 3. Molecular structure of **2** (thermal ellipsoids set at 50% probability; all hydrogen atoms are omitted and trimethylsilyl groups are displayed in a wireframe view for clarity).

Table 1. Selected bond distances (Å) and angles (°) of **2** and Ti-containing reference compounds **6-8**.

cpd	**2**	**7**	**8**	**9**
Ti–O	1.786(2) 1.789(2)	1.737(2) 1.766(2)	1.766(1)	1.739(2) 1.741(2)
Ti–O	2.0436(18) 2.0434(17)	-	2.130(1) 2.039(1)	1.979(2)
O–Al	1.8395(18) 1.8506(18)	-	1.814(1) 1.786(1)	1.834(2)
O–Ti–O	117.31(10)	92.0(7)[a]~ 117.1(7)[a]	99.39(10)	109.9(1)~ 110.9(1)
O–Ti–O	72.00(7)	-	84.38(6)	-

[a] Positional disorder of oxygen atom prevents accurate comparison.

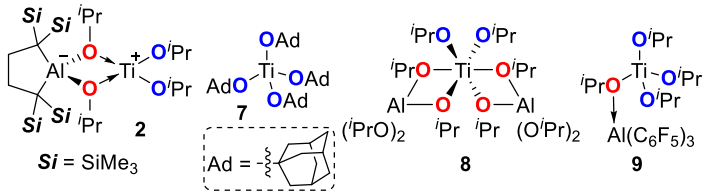

Molecular structure of 3 is shown in Figure 4. Zr(III)-Zr(III) length is shorter than reported Zr(III) dimer **10**[15a] and **11**[15b] (Figure 5) probably because of stronger Zr(III)-Zr(III) interaction enabled by electron donation from hydride atoms on Al to Zr(III) center.

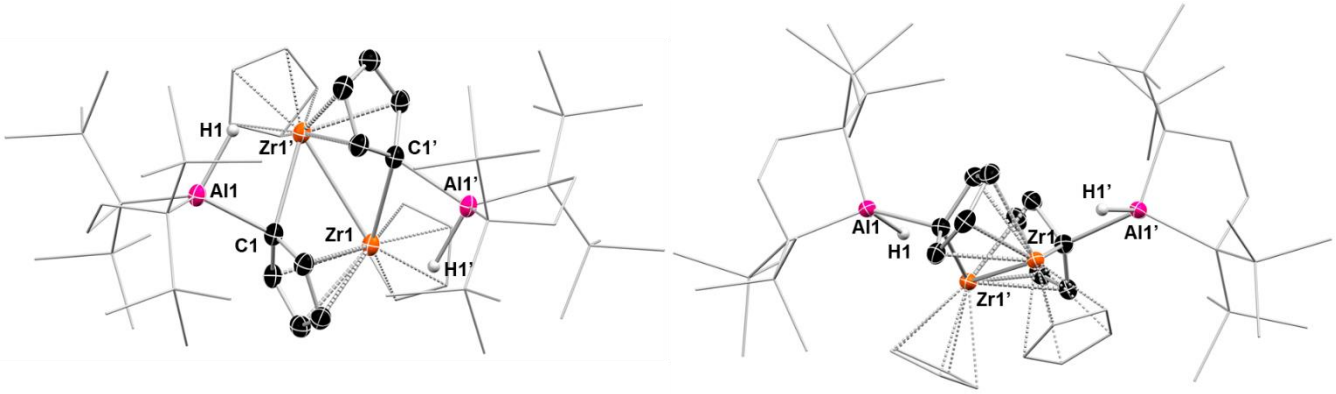

Figure 4. Molecular structure of **3** (thermal ellipsoids set at 50% probability; all hydrogen atoms are omitted aluminum-containing five-membered rings are displayed in a wireframe view for clarity).

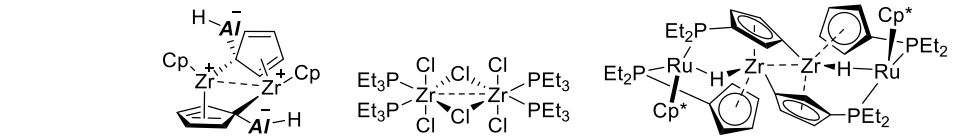

Figure 5. Bond length comparison of Zr(III)-Zr(III) dimer

To reveal the property of the unpaired electron in **2**, ESR spectrum was recorded in hexane solution at room temperature (Figure 4). A sextet-like signal was observed at g = 1.9635. A simulated spectrum with a hyperfine splitting by Ti and Al atoms (A[^{47}Ti] = 0.54 mT, A[^{49}Ti] = 0.54 mT, A[^{27}Al] = 0.38 mT) showed a good agreement with experimental data. The result indicates that the unpaired electron mainly exists on the Ti atom (Ti: 87%, Al: 13%). The hyperfine coupling with ^{27}Al nucleus in **2** is close to the lower end of the range of the previously reported values (0.23-2.25 mT) for chloride- or hydride-bridging Ti-Al systems.[8a, 10, 16](Table 2). Strong bridging between Ti and Al nuclei with chloride (two 2c-2e bonds) or hydride (two 2c-3e bonds with a short Ti-Al distance) would contribute to the electron-nuclear spin coupling. In contrast, a similar titanium(III) complex, $Cp_2Ti(Cl_2AlMe_2)$, having dichlorodimethylaluminate anion did not show hyperfine splitting to the ^{27}Al nucleus in the ESR spectrum.

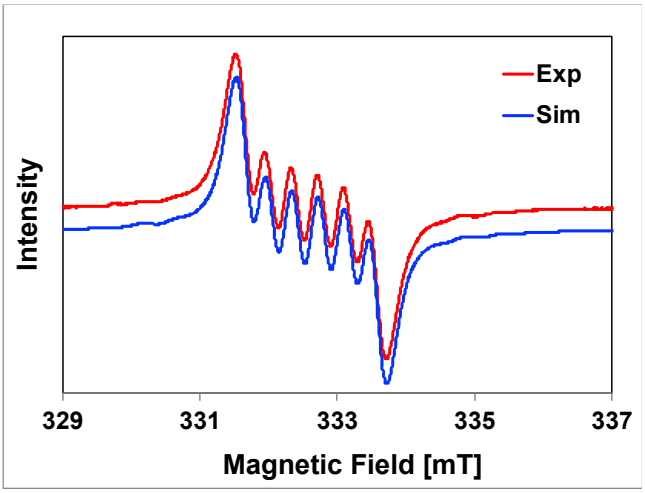

Figure 6. Observed ESR spectrum of **2** in hexane at room temperature (red line) and simulated ESR spectrum (blue) using g = 1.9635, $A[^{27}\mathrm{Al}]$ = 0.38 mT, $A[^{47}\mathrm{Ti}]$ = 0.54 mT, $A[^{47}\mathrm{Ti}]$ = 0.54 mT, Line width = 0.33 mT (left).

The electronic structure of **2** was also confirmed by DFT calculations. The SOMO is mainly located on the Ti atom with a small contribution of the Al atom (Figure 5). The ratio (Ti: 91%, Al 9%) of the calculated spin density on the Ti (1.12) and the Al (0.11) atoms in **2** is in good agreement with the ratio of the spin density derived from the experimental ESR data (*vide supra*). To clarify the character of SOMO, the UV-Vis absorption spectrum of **2** in hexane was measured (Figure 6). The characteristic absorption at 621 nm (λ = 29) and 903 nm (λ = 11) with a low intensity were observed to reflect the intense blue color of **2**. The TD-DFT calculations (Figure 7) provided an assignment of the absorption at 621 nm as transitions from SOMO to LUMO+1, LUMO+4, and LUMO+6 (624 nm, f = 0.0014, Table 3, Figure 8). Although the absorption at 903 nm could not be clearly assigned, one weak absorption (721 nm, f = 0.0006) and one forbidden absorption (1068 nm, f = 0.0000) were simulated. One can expect the flexibility of alkyl groups in **2** would break a symmetry of molecular orbitals to lead the weak absorption according to the transition from SOMO to LUMO.

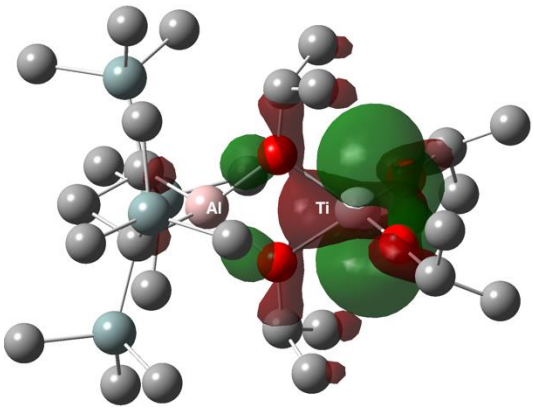

Figure 7. SOMO of **2** at the UB3LYP level of theory using LANL2DZ (for Ti) and 6-31+g(d) (all other atoms) basis sets. (right).

Table 2. Structural and ESR spectroscopic comparison of **2** with isolated Al-containing Ti(III) complexes showing hyperfine coupling to a ^{27}Al nucleus ($A[^{27}Al]$)

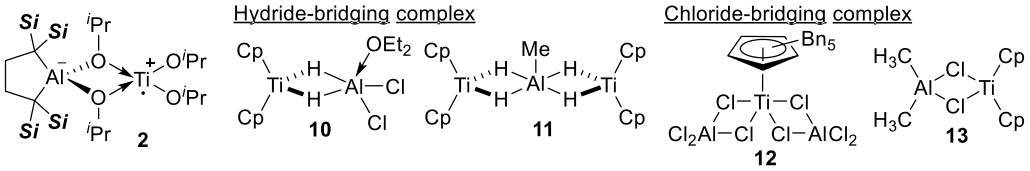

Cpd	2	10	11	12	13
Ti---Al (Å)	3.0534(9)	2.745(5) 2.755(5)	2.771(4) 2.770(4)	3.48(1) 3.48(1)	3.1815(8)[a]
A[^{27}Al] (mT)	0.38	1.04	0.38	0.54	0.23
multiplicity	Sextet	-[b]	octet[c]		-[b,c]

[a] disordered with CH_3,Cl-bridging complex, [c]not reported, [b]unresolved

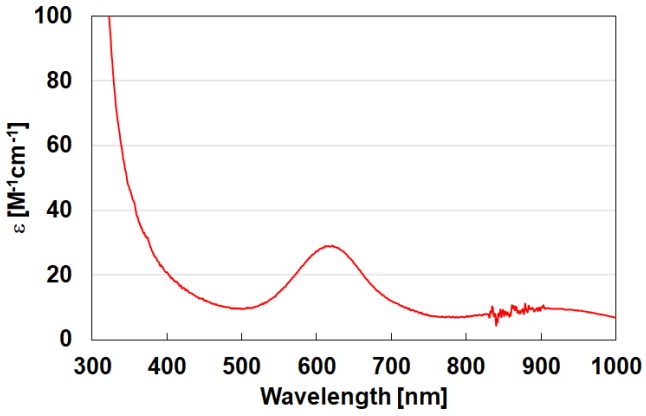

Figure 8. The UV-Vis absorption spectra of **2** in hexane [λ_{max} (ε) = 621 (29), 903 (11) nm].

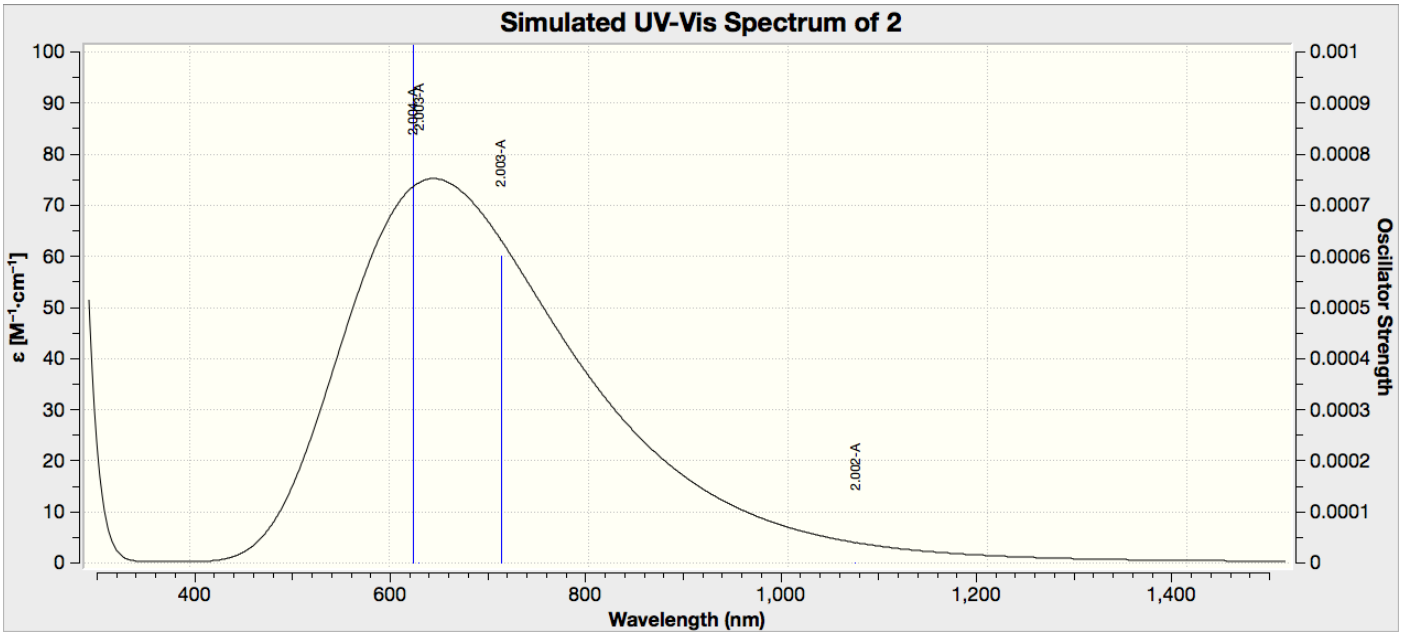

Figure 9. A simulated UV-Vis spectrum for **2** at UPBEh1PBE level of theory.

Table 3. Excitation energies and oscillator strength for **2** obtained from TD-DFT calculations

Excited State 1: 2.002-A 1.1606 eV 1068.23 nm f=0.0000 <S**2>=0.752
175A ->176A 0.97844
175A ->178A -0.14512
This state for optimization and/or second-order correction.
Total Energy, E(TD-HF/TD-DFT) = -2865.54084671
Copying the excited state density for this state as the 1-particle RhoCI density.

Excited State 2: 2.003-A 1.7395 eV 712.74 nm f=0.0006 <S**2>=0.753
175A ->177A 0.53515
175A ->180A -0.15332
175A ->183A 0.74701
175A ->184A 0.11480
175A ->189A 0.12938
175A ->196A 0.14791

Excited State 3: 2.003-A 1.9653 eV 630.87 nm f=0.0000 <S**2>=0.753
175A ->178A -0.56322
175A ->179A 0.78595

Excited State 4: 2.004-A 1.9856 eV 624.41 nm f=0.0014 <S**2>=0.754
175A ->177A 0.59280
175A ->180A 0.62548
175A ->182A 0.33856

175A ->183A -0.30360

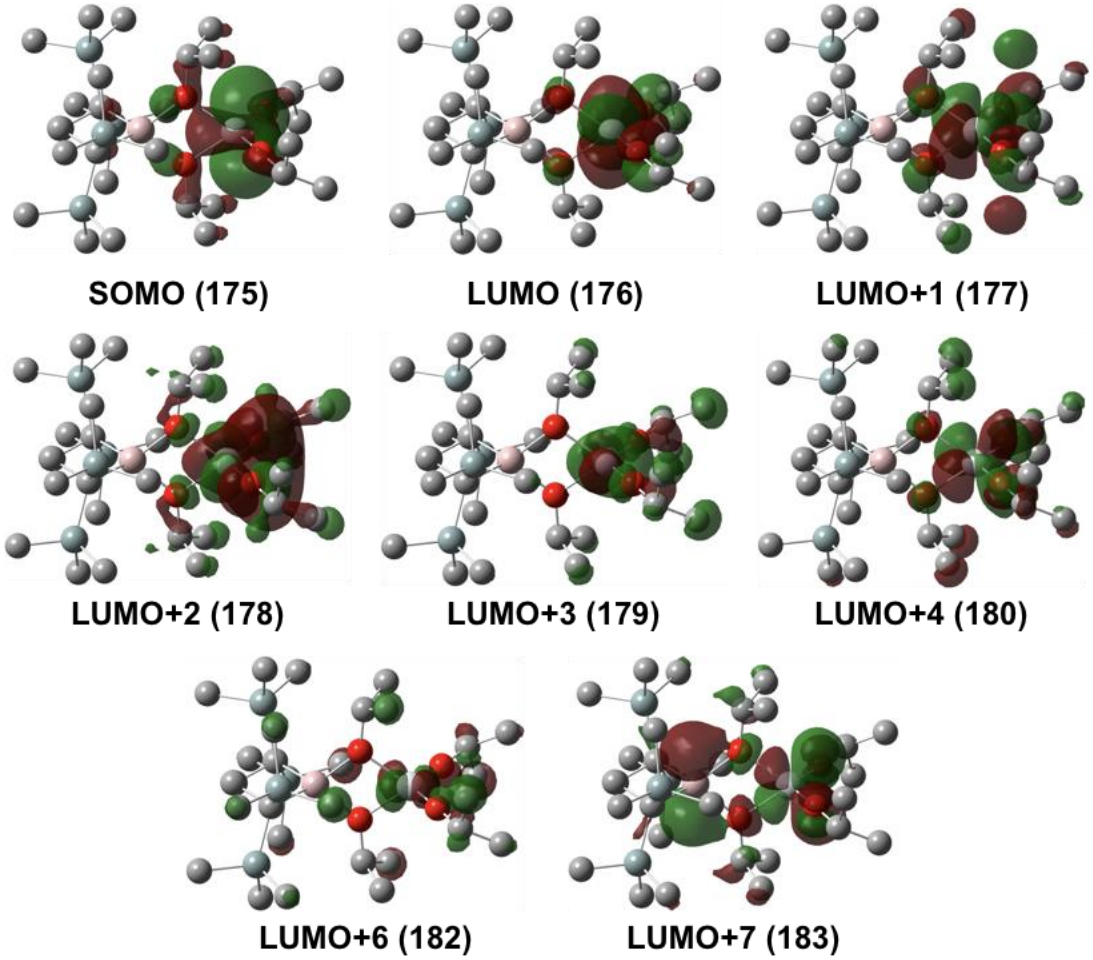

Figure 10. Transition-related orbitals of **2**

4.3. Conclusion

In conclusion, the reaction of dialkylalumanylpotassium **1** with titanium tetraisopropoxide was investigated. The alumanylanion **1** worked as a reducing reagent to afford the trivalent titanium complex **2** as a contact ion pair with aluminate anion via single electron transfer from **1** to titanium tetraisopropoxide. The ESR spectrum of **2** revealed the delocalization of an unpaired electron over Ti and Al atoms. The DFT calculations of **2** provided information about the ratio of unpaired electron on Ti and Al atoms and the UV-vis absorption spectrum. Similarly, the reaction of **1** with Cp_2ZrCl_2 gave dimeric zirconioum(III) complex **3** probably through a single-electron-transfer reaction. X-ray crystallographic analysis of **3** revealed the existence of a covalent bond between Zr(III)-Zr(III).

4.4. Experimental section

All manipulations involving the air- and moisture-sensitive compounds were carried out under an argon atmosphere using glovebox (Korea KIYON) technique. All glasswares were dried for 20 min in the 250 °C oven before use. Toluene were purified by passing through a solvent purification system (Grass Contour). Hexamethyldisiloxane (TCI) were dried over sodium/potassium alloy, followed by filtering through pad of activated neutral alumina. The nuclear magnetic resonance (NMR) spectra were recorded on JEOL ECS-400 (399 MHz for ^{1}H, 100 MHz for ^{13}C). Chemical shifts are reported in δ ppm relative to the residual protiated solvent for ^{1}H, deuterated solvent for ^{13}C used as references. The absolute values of the coupling constants are given in Hertz (Hz). Multiplicities are abbreviated as singlet (s), doublet (d), triplet (t), quartet (q), multiplet (m), and broad (br). ESR spectrum was recorded on a JEOL JES-TE200 spectrometer using screw glass tube. ESR simulations were carried out on Isotropic simulation program for JES-X3 series ESR. Melting points were determined on Optimelt (SRS) and were uncorrected. Elemental analyses were performed on a Perkin Elmer 2400 series II CHN analyzer. Tetraalkyldialane **6** was prepared by according to procedures.[10i] $Ti(O^{i}Pr)_4$, $Cp^*_2ZrCl_2$, $TiCl_4$, $ZrCl_4$, $HfCl_4$, $CpZrCl_3$, Cp^*ZrCl_3, were purchased and used as received.

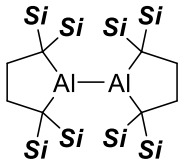

6

Si = $SiMe_3$

Synthesis of 2

In a glovebox, pre-cooled (–35 °C) crystalline tetraalkyldialumane **6** (40.0 mg, 59.3 μmol) and sodium/potassium alloy (41.0 mg, 298 μmol) were placed in a 3 mL vial with a glass stirring bar, then pre-cooled toluene/THF (1.50 mL, v/v = 100/1) was added to the mixture and the resulting suspension was stirred at –35 °C for 2 days. After the filtration by using a pre-cooled (–35 °C) plastic syringe with glass fiber filter, a red solution of **1** was obtained. To a precooled (–35 °C) toluene (1.00 mL) solution of $Ti(O^{i}Pr)_4$ (63.0 mg, 179 μmol) in a 15 mL vial the solution, the solution of **1** was added. The resulting dark-green suspension was stirred for 3 h at –35 °C. and then volatiles were evaporated under reduced pressure. Recrystallization from hexamethyldisiloxane afford bright blue crystal of **2** (10.1 mg, 15.3 μmol, 13% yield). Single crystal suitable for X-ray analysis were obtained from hexamethyldisiloxane solution at –35 °C. mp. 100.4-110.2 °C (decomp.); Anal. Calcd for $C_{28}H_{68}AlO_4Si_4Ti$: C, 51.26; H, 10.45; Found; C, 50.93; H, 10.23.

X-ray analysis of 3

In a glovebox, pre-cooled (–35 °C) crystalline tetraalkyldialumane **6** (40.0 mg, 53.8 μmol) and potassium graphite (40.0 mg, 320 μmol) were placed in a 3 mL vial with a glass stirring bar, then pre-cooled toluene/THF (1.50 mL, v/v = 100/1) was added to the mixture and the resulting suspension was stirred at –35 °C for 2 days. After the filtration by using a pre-cooled (–35 °C) plastic syringe with glass fiber filter, a red solution of **1** was obtained. To a precooled (–35 °C) toluene (1.00 mL) solution of Cp_2ZrCl_2 (7.90 mg, 26.9 μmol) in a 15 mL vial the solution, the solution of **1** was added. The resulting dark-red suspension was stirred for 10 min at room temperature. and then volatiles were evaporated under reduced pressure. Single crystal suitable for X-ray analysis were obtained from saturated cyclohexane solution at –35 °C.

Measurement and simulation of ESR spectrum of 2

In a glovebox, crystals of **2** were dissolved in hexane (1.0 mM) and the resulting solution was pipetted into a quarts ESR tube (5 mm ϕ). The ESR tube was brought out from glovebox and set to the probe of ESR spectrometer. The spectrum was measured at room temperature. Considering titanium has five stable isotopes [I = 0 for ^{46}Ti, ^{48}Ti, and ^{50}Ti (inactive for hyperfine coupling), total 87.2% abundance; I = 5/2 for ^{47}Ti (γ = –1.5105), 7.4% abundance; I = 7/2 for ^{49}Ti (γ = –1.51095), 5.2% abundance] and aluminum has only one isotope [I = 5/2 for ^{27}Al], the ESR spectral simulation was performed with an assumption of that ^{47}Ti and ^{49}Ti have same gyromagnetic ratio and the use of the following spin Hamiltonian.

$$H = \mu_B \boldsymbol{S}\cdot\boldsymbol{g}\cdot\boldsymbol{B}_0 + A_{Ti}\boldsymbol{S}\cdot\boldsymbol{I}_{Ti} + A_{Al}\boldsymbol{S}\cdot\boldsymbol{I}_{Al}$$

where μ_B, $\boldsymbol{S}$, $\mathbf{g}$, and $\boldsymbol{B}_0$ stand for the Bohr magneton, electron spin operator, g tensor, and static magnetic field, respectively. $\boldsymbol{I}_{Ti}$ and $\boldsymbol{I}_{Al}$ denote the nucleus spin operator. A_{Ti} and A_{Al} denote the hyperfine splitting parameter for these nuclei. The hyperfine splitting parameters were estimated by the spectral simulation. The best fitted parameters are shown in caption of Figure 4. The simulated spectrum shown in Figure 4 is in good agreement with the observed one. The DFT-calculated spin density on Ti and Al atoms (0.945 for Ti, 0.146 for Al; Ti:Al = 0.866:0.134) in **2** supported this observation of ESR spectrum (Figure 5).

Details for crystallography

Crystallographic data for **2** and **3** are summarized in Table 3. The crystal was coated with Paratone-N (Hampton Research) and put on a MicroMount^{TM} (MiTeGen, LLC), and then mounted on diffractometer. Diffraction data were collected on a Rigaku HyPix-6000 detector using Mo$K\alpha$ radiation (λ = 0.7103 Å). The Bragg spots were integrated using the CrysAlis^{Pro} program package.[17] Absorption corrections were applied. All structures were solved by the *SHELXT* program. Refinement on F^2 was carried out by full-matrix least-squares using the *SHELXL* in the *SHELX* software package[18] and expanded using Fourier techniques. All non-hydrogen atoms were refined using anisotropic thermal parameters. The hydrogen atoms were assigned to idealized geometric positions and included in the refinement with isotropic thermal parameters. The *SHELXL* was interfaced with Yadokari-XG 2009[19] for most of the refinement steps. The pictures of molecules were prepared using ORTEP-III for Windows.[20] The detailed crystallographic data have been deposited with the Cambridge Crystallographic Data Centre: Deposition code CCDC-1987277 (**2**). Data of compound **2** can be obtained free of charge from the Cambridge Crystallographic Data Centre via http://www.ccdc.cam.ac.uk/products/csd/request

Table 4. Crystallographic data for **2** and **3**.

	2	**3**
CCDC #	1987277	unpublished
Empirical formula	$C_{28}H_{68}AlO_4Si_4Ti$	$C_{76}H_{148}Al_2Si_8Zr_2$
Formula weight	656.06	1523.06
Crystal system	*Monoclinic*	*Monoclinic*
Space group	$P2_1/c$	$C2/_C$
T (K)	93(2)	93(2)
Color	blue	red
Habit	plate	plate
a (Å)	16.5554(6)	27.6821(11)
b (Å)	16.4771(6)	11.2505(3)
c (Å)	14.2768(5)	27.8448(9)
α (°)	90	90
β (°)	93.792(3)	108.263(4)°
γ (°)	90	90
V (Å^3)	3886.0(2)	8235.1(5)
Z	4	4
D_{calc} (g cm^{-3})	1.121	1.228
Abs. coeff (mm^{-1})	0.394	0.430
F(000)	1436	3288
Crystal size (mm)	0.18×0.12×0.01	0.15×0.07×0.04
θ range (°)	1.746–30.560°	1.969–30.932
Reflns collected	37595	34927
Indep reflns/R_{int}	9695/0.0695	10996/0.0562
Parameters	363	421
GOF on F^2	1.024	1.044
R_1, wR_2 [I>2σ(I)]	0.0563, 0.1154	0.0533, 0.1188
R_1, wR_2 (all data)	0.0977, 0.1282	0.1023, 0.1371

Computational Details

Gaussian 16 (rev. B.01)[21] software package was employed to perform all of the calculations. The full model of **2** was optimized from the crystallographically obtained structure at the UB3LYP[22] level of theory using LanL2DZ[23] (for Ti) and 6-31+g(d)[24] (for others) basis sets. The TD-DFT[25] calculations were performed to estimate UV-vis spectrum of **2** with UPBEh1PBE[26] level of theory using LanL2DZ[23] (for Ti) and 6-31+g(d)[24] (for others) basis sets.

4.5. References

1. Beaumier, E. P.; Pearce, A. J.; See, X. Y.; Tonks, I. A. *Nat. Rev. Chem.* **2019,** *3*, 15-34.

2. (a) Ziegler, K.; Holzkamp, E.; Breil, H.; Martin, H. *Angew. Chem.* **1955,** *67*, 541-547; (b) Natta, G.; Pino, P.; Mazzanti, G.; Giannini, U. A. *J. Am. Chem. Soc.* **1957,** *79*, 2975-2976; (c) Sinn, H.; Kaminsky, W., Ziegler-Natta Catalysis. In *Advances in Organometallic Chemistry*, Stone, F. G. A.; West, R., Eds. Academic Press: 1980; Vol. 18, pp 99-149.

3. (a) Tebbe, F. N.; Parshall, G. W.; Reddy, G. S. *J. Am. Chem. Soc.* **1978,** *100*, 3611-3613; (b) Petasis, N. A.; Bzowej, E. I. *J. Am. Chem. Soc.* **1990,** *112*, 6392-6394.

4. (a) Mukaiyama, T.; Sato, T.; Hanna, J. *Chem. Lett.* **1973,** *2*, 1041-1044; (b) McMurry, J. E.; Fleming, M. P. *J. Am. Chem. Soc.* **1974,** *96*, 4708-4709; (c) McMurry, J. E. *Chem. Rev.* **1989,** *89*, 1513-1524.

5. (a) Fachinetti, G.; Floriani, C. *J. Chem. Soc., Chem. Commun.* **1974**, 66-67; (b) Hill, J. E.; Fanwick, P. E.; Rothwell, I. P. *Organometallics* **1990,** *9*, 2211-2213; (c) Li, S.; Takahashi, T., Aromatic Ring Construction from Zirconocenes and Titanocenes. In *Transition-Metal-Mediated Aromatic Ring Construction*, Tanaka, K., Ed. John Wiley & Sons, Inc.: 2013; pp 299-320.

6. Mountford, P.; Hazari, N., 4.04 - Complexes of Titanium in Oxidation State iii. In *Comprehensive Organometallic Chemistry III*, Mingos, D. M. P.; Crabtree, R. H., Eds. Elsevier: Oxford, 2007; pp 281-322.

7. (a) Klabunde, U.; Tebbe, F. N.; Parshall, G. W.; Harlow, R. L. *J. Mol. Catal.* **1980,** *8*, 37-51; (b) Coles, S. J.; Hursthouse, M. B.; Kelly, D. G.; Toner, A. J.; Walker, N. M. *J. Organomet. Chem.* **1999,** *580*, 304-312; (c) Firth, A. V.; Stewart, J. C.; Hoskin, A. J.; Stephan, D. W. *J. Organomet. Chem.* **1999,** *591*, 185-193; (d) Yu, P.; Müller, P.; Said, M. A.; Roesky, H. W.; Usón, I.; Bai, G.; Noltemeyer, M. *Organometallics* **1999,** *18*, 1669-1674; (e) Thompson, R.; Nakamaru-Ogiso, E.; Chen, C.-H.; Pink, M.; Mindiola, D. J. *Organometallics* **2014,** *33*, 429-432; (f) Barr, J. L.; Kumar, A.; Lionetti, D.; Cruz, C. A.; Blakemore, J. D. *Organometallics* **2019,** *38*, 2150-2155.

8. (a) Lobkovskii, E. B.; Soloveichik, G. L.; Sisov, A. I.; Bulychev, B. M.; Gusev, A. I.; Kirillova, N. I. *J. Organomet. Chem.* **1984,** *265*, 167-173; (b) Lobkovskii, E. B.; Soloveichik, G. L.; Bulychev, B. M.; Gerr, R. G.; Struchkov, Y. T. *J. Organomet. Chem.* **1984,** *270*, 45-51; (c) Bel'sky, V. K.; Sizov, A. I.; Bulychev, B. M.; Soloveichik, G. L. *J. Organomet. Chem.* **1985,** *280*, 67-80; (d) Sizov, A. I.; Molodnitskaya, I. V.; Bulychev, B. M.; Evdokimova, E. V.; Soloveichik, G. L.; Gusev, A. I.; Chuklanova, E. B.; Andrianov, V. I. *J. Organomet. Chem.* **1987,** *335*, 323-330; (e) Sisov, A. I.; Molodnitskaya, I. V.; Bulychev, B. M.; Evdokimova, E. V.; Bel'skii, V. K.; Soloveichik, G. L. *J. Organomet. Chem.* **1988,** *344*, 293-301; (f) Thomas, J.; Klahn, M.; Spannenberg, A.; Beweries, T. *Dalton Trans.* **2013,** *42*, 14668-14672; (g) Sun, R.; Liu, J.; Yang, S.; Chen, M.; Sun, N.; Chen, H.; Xie, X.; You, X.; Li, S.; Liu, Y. *Chem. Commun.* **2015,** *51*, 6426-6429.

9. Liu, F. q.; Gornitzka, H.; Stalke, D.; Roesky, H. W. *Angew. Chem. Int. Ed. Engl.* **1993,** *32*, 442-444.

10. (a) Mach, K.; Antropiusová, H.; Polačekst, J. *J. Organomet. Chem.* **1979,** *172*, 325-329; (b) Schmid, G.; Thewalt, U.; Troyanov, S. I.; Mach, K. *J. Organomet. Chem.* **1993,** *453*, 185-191; (c) Horáček, M.; Kupfer, V.; Müller, B.; Thewalt, U.; Mach, K. *J. Organomet. Chem.* **1998,** *552*, 75-82.
11. (a) Hicks, J.; Vasko, P.; Goicoechea, J. M.; Aldridge, S. *Nature* **2018,** *557*, 92-95; (b) Hicks, J.; Mansikkamäki, A.; Vasko, P.; Goicoechea, J. M.; Aldridge, S. *Nat. Chem.* **2019,** *11*, 237-241; (c) Hicks, J.; Vasko, P.; Goicoechea, J. M.; Aldridge, S. *J. Am. Chem. Soc.* **2019,** *141*, 11000-11003; (d) Hicks, J.; Heilmann, A.; Vasko, P.; Goicoechea, J. M.; Aldridge, S. *Angew. Chem. Int. Ed.* **2019,** *58*, 17265-17268; (e) Schwamm, R. J.; Anker, M. D.; Lein, M.; Coles, M. P. *Angew. Chem. Int. Ed.* **2019,** *58*, 1489-1493; (f) Anker, M. D.; Coles, M. P. *Angew. Chem. Int. Ed.* **2019,** *58*, 18261-18265; (g) Schwamm, R. J.; Coles, M. P.; Hill, M. S.; Mahon, M. F.; McMullin, C. L.; Rajabi, N. A.; Wilson, A. S. S. *Angew. Chem. Int. Ed.* **2020,** *59*, 3928-3932.; (h) Anker, M. D.; Coles, M. P. *Angew. Chem. Int. Ed.* **2019,** *58*, 13452-13455; (i) Kurumada, S.; Takamori, S.; Yamashita, M. *Nat. Chem.* **2020,** *12*, 36-39; (j) Sugita, K.; Nakano, R.; Yamashita, M. *Chem. Eur. J.* **2020,** *26*, 2144-2147. (k) Sugita, K.; Yamashita, M. *Chem. Eur. J.* **2020,** *26*, *in press.* doi:10.1002/chem.202000752; (l) Heilmann, A.; Hicks, J.; Vasko, P.; Goicoechea, J. M.; Aldridge, S. *Angew. Chem. Int. Ed.* **2020,** *59*, doi: 10.1002/anie.201916073.
12. Stinghen, D.; Atzori, M.; Fernandes, C. M.; Ribeiro, R. R.; de Sá, E. L.; Back, D. F.; Giese, S. O. K.; Hughes, D. L.; Nunes, G. G.; Morra, E.; Chiesa, M.; Sessoli, R.; Soares, J. F. *Inorg. Chem.* **2018,** *57*, 11393-11403.
13. Tudyka, S. S.; Pflanz, K.; Brunner, H.; Aldinger, F.; Borrmann, H.; Fischer, P. *Z. Anorg. Allg. Chem.* **1997,** *623*, 1163-1167.
14. Rodriguez-Delgado, A.; Chen, E. Y. X. *Inorg. Chim. Acta* **2004,** *357*, 3911-3919.
15. (a) Cotton, A. F.; Diebold, P. M.; Kibala, A. P. *Inorg. Chem.* **1988,** *27,* 799-804.(b) Miyazaki, T.; Tanabe, Y.; Yuki, M.; Miyake, Y.; Nishibayashi, Y. *Organometallics* **2011,** *30,* 2394-2404.
16. (a) Maki, A. H.; Randall, E. W. *J. Am. Chem. Soc.* **1960,** *82*, 4109-4111; (b) Bartelink, H. J. M.; Bos, H.; Smidt, J.; Vrinssen, C. H.; Adema, E. H. *Recl. Trav. Chim. Pays-Bas* **1962,** *81*, 225-237; (c) Henrici-olivé, G.; Olivé, S. *Angew. Chem. Int. Ed. Engl.* **1967,** *6*, 790-798; (d) Zefirova, A. K.; Tikhomirova, N. N.; Shilov, A. E. *Dokl. Akad. Nauk SSSR* **1960,** *132*, 1082-1085; (e) Dzhabiev, T. S.; Shilov, A. E. *J. Struct. Chem.* **1965,** *6*, 279-280; (f) Henrici-Olivé, G.; Olivé, S. *Angew. Chem. Int. Ed. Engl.* **1968,** *7*, 821-822; (g) Henrici-olivé, V. G.; Olivé, S. *Makromol. Chem.* **1969,** *121*, 70-74; (h) Henrici-Olivé, G.; Olivé, S. *J. Organomet. Chem.* **1969,** *19*, 309-313; (i) Henrici-Olivé, G.; Olivé, S. *J. Organomet. Chem.* **1970,** *23*, 155-157; (j) Bulychev, B. M.; Tokareva, S. E.; Soloveichick, G. L.; Evdokimova, E. V. *J. Organomet. Chem.* **1979,** *179*, 263-273; (k) Mach, K.; Antropiusová, H.; Poláček, J. *J. Organomet. Chem.* **1980,** *194*, 285-295; (l) Bulychev, B. M.; Kostenko, A. L.; Yakovleva, N. y. A.; Soloveichik, G. L. *Transition Met. Chem.* **1981,** *6*, 32-36; (m) Mach, K.; Varga, V.; Antropiusová, H.; Poláček, J. *J. Organomet. Chem.* **1987,** *333*, 205-215; (n) Mach, K.; Hiller, J.; Thewalt, U.; Sivik, M. R.; Bzowej, E. I.; Paquette, L. A.; Zaegel, F.; Meunier, P.; Gautheron, B. *Organometallics* **1995,** *14*, 2609-2612.
17. CrysAlisPRO *CrysAlisPRO*, Oxford Diffraction/Agilent Technologies UK Ltd: Yarnton, England, 2015.
18. Sheldrick, G. *Act. Cryst. Sec. C* **2015,** *71*, 3-8.
19. Kabuto, C.; Akine, S.; Kwon, E. *J. Cryst. Soc. Jpn.* **2009,** *51*, 218-224.
20. Farrugi, L. J. *J. Appl. Crystallogr.* **1997,** *30*, 565-565.

21. Frisch, M. J.; Trucks, G. W.; Schlegel, H. B.; Scuseria, G. E.; Robb, M. A.; Cheeseman, J. R.; Scalmani, G.; Barone, V.; Petersson, G. A.; Nakatsuji, H.; Li, X.; Caricato, M.; Marenich, A. V.; Bloino, J.; Janesko, B. G.; Gomperts, R.; Mennucci, B.; Hratchian, H. P.; Ortiz, J. V.; Izmaylov, A. F.; Sonnenberg, J. L.; Williams; Ding, F.; Lipparini, F.; Egidi, F.; Goings, J.; Peng, B.; Petrone, A.; Henderson, T.; Ranasinghe, D.; Zakrzewski, V. G.; Gao, J.; Rega, N.; Zheng, G.; Liang, W.; Hada, M.; Ehara, M.; Toyota, K.; Fukuda, R.; Hasegawa, J.; Ishida, M.; Nakajima, T.; Honda, Y.; Kitao, O.; Nakai, H.; Vreven, T.; Throssell, K.; Montgomery Jr., J. A.; Peralta, J. E.; Ogliaro, F.; Bearpark, M. J.; Heyd, J. J.; Brothers, E. N.; Kudin, K. N.; Staroverov, V. N.; Keith, T. A.; Kobayashi, R.; Normand, J.; Raghavachari, K.; Rendell, A. P.; Burant, J. C.; Iyengar, S. S.; Tomasi, J.; Cossi, M.; Millam, J. M.; Klene, M.; Adamo, C.; Cammi, R.; Ochterski, J. W.; Martin, R. L.; Morokuma, K.; Farkas, O.; Foresman, J. B.; Fox, D. J. *Gaussian 16, Revision B.01*, Wallingford, CT, 2016.
22. (a) Lee, C.; Yang, W.; Parr, R. G. *Phys. Rev. B* **1988,** *37*, 785-789; (b) Becke, A. D. *Phys. Rev. A* **1988,** *38*, 3098-3100; (c) Miehlich, B.; Savin, A.; Stoll, H.; Preuss, H. *Chem. Phys. Lett.* **1989,** *157*, 200-206.
23. (a) Hay, P. J.; Wadt, W. R. *J. Chem. Phys.* **1985,** *82*, 270-283; (b) Wadt, W. R.; Hay, P. J. *J. Chem. Phys.* **1985,** *82*, 284-298; (c) Hay, P. J.; Wadt, W. R. *J. Chem. Phys.* **1985,** *82*, 299-310.
24. Huzinaga, S.; Andzelm, J.; Klobukowski, M.; Radzio-Andzelm, E.; Sakai, Y.; Tatewaki, H., *Gaussian basis sets for molecular calculations*. Elsevier: 1984.
25. (a) Adamo, C.; Jacquemin, D. *Chemical Society Reviews* **2013,** *42*, 845-856; (b) Laurent, A. D.; Adamo, C.; Jacquemin, D. *Phys. Chem. Chem. Phys.* **2014,** *16*, 14334-14356.
26. (a) Perdew, J. P.; Burke, K.; Ernzerhof, M. Generalized Gradient Approximation Made Simple. *Phys. Rev. Lett.* **1996,** *77*, 3865-3868; (b) Perdew, J. P.; Burke, K.; Ernzerhof, M. Generalized Gradient Approximation Made Simple [Phys. Rev. Lett. 77, 3865 (1996)]. *Phys. Rev. Lett.* **1997,** *78*, 1396-1396; (c) Adamo, C.; Barone, V. Toward reliable density functional methods without adjustable parameters: The PBE0 model. *J. Chem. Phys.* **1999,** *110*, 6158-6170; (d) Ernzerhof, M.; Scuseria, G. E. Assessment of the Perdew–Burke–Ernzerhof exchange-correlation functional. *J. Chem. Phys.* **1999,** *110*, 5029-5036; (e) Ernzerhof, M.; Perdew, J. P. Generalized gradient approximation to the angle- and system-averaged exchange hole. *J. Chem. Phys.* **1998,** *109*, 3313-3320.

Chapter 5

Conclusion

In summary, the author revealed new three-different reactivity of dialkylalumanyl anion (Scheme 1). In chapter 2, the alumanyl anion behaves as a low-oxidation-state aluminum species in the reaction with unsaturated hydrocarbons to furnish aluminum(III)-containing cycloadducts. The proposed mechanism by DFT calculations revealed the transition state has a carbanionic character. In chapter 3, the reaction of the alumanyl anion with cationic yttrium complex gave an alumanylyttrium possessing an unprecedented Al–Y bond. UV-Vis spectrum showed two absorptions 335 nm and 432 nm. The latter absorption was attributed to HOMO (Al–Y σ bond)-LUMO (overlapping vacant orbital between Al and Y atoms) transition based on the TD-DFT calculations. Dialkylalumanyl ligand in the alumanylyttrium complex contributed to the narrower HOMO-LUMO gap than that of the previously reported borylyttrium complex. In chapter 4, one-electron reduction from alumanyl anion to the substrate proceeded in the presence group 4 metal complexes. The structural property of the resulted Ti(III) and Zr(III) complexes were revealed by using X-ray analysis and ESR measurement.

Scheme 1. Summary of this thesis

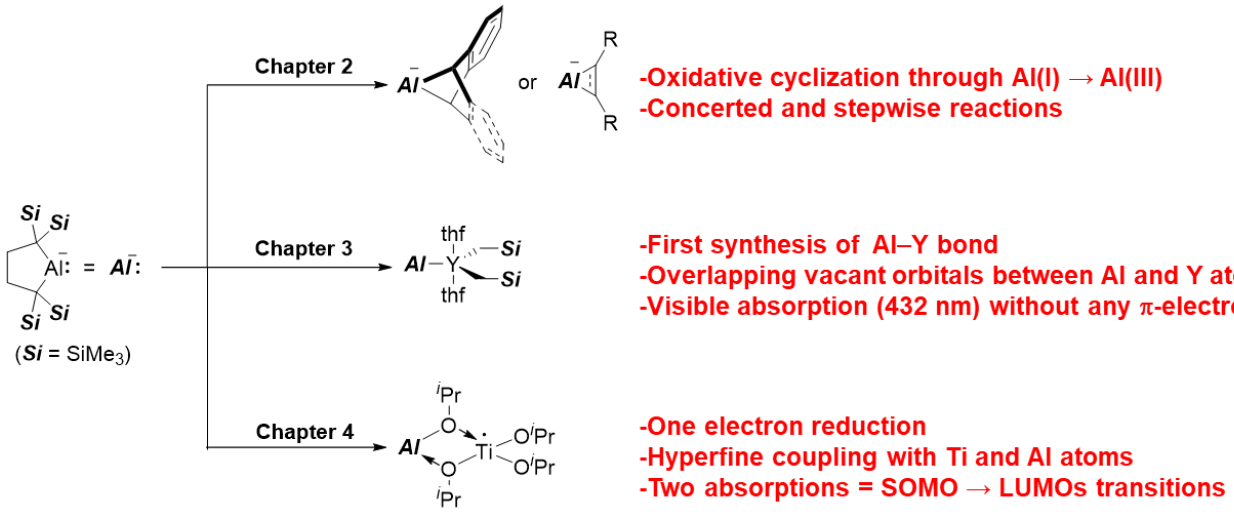

Finally, the author would like to envision the future of organometallic chemistry and main-group chemistry based on this thesis. In chapter 2, the author revealed the reaction of dialkylalumanylpotassium **1** with unsaturated hydrocarbons possessing benzene rings or oxygen substituents proceeded well, but **1** did not give cycloadducts with alkyl-substituted unsaturated hydrocarbons probably due to a lack of stabilization of K^+ center. In other words, in the reaction development of **1**, it is important to stabilize K^+ center of products.

On the other hand, it would be fundamentally important to achieve deprotonation of alkane C(sp^3)-H bond by using group 13 element compounds in the low-oxidation state, such as highly basic **1**. The author guesses that conducting the reaction of non-solvated **2**, which has recently been prepared in the Yamashita research group, with alkanes in the presence of crown ethers to stabilize K^+ center, giving a thermodynamically stable products, would be a key (Scheme 2).

Scheme 2. Deprotonation of alkanes with **2** in the presence of crown ethers

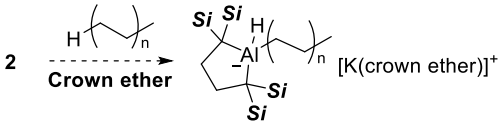

Considering the reactivity of **1** toward group 3 and 4 metal complexes disclosed in chapters 3 and 4, the desired alumanylmetal complex would be obtained by reaction with relatively electron-rich metal electrophile being resistant to reduction, while the electron transfer reaction would proceed in case of the reaction of **1** with relatively electron-poor metal electrophiles which is easily reduced. In the future, systematic synthesis of alumanyl metal complex having 2-center-2-electron Al-M bond would be achieved by using electron-rich metal precursor to avoid reduction of metal center. One can expect that the introduction of the dialkylalumanyl ligand to transition metal complex would make the metal center be electron-rich. Therefore, a dialkylalumanyl iridium complex would be used as a more active C-H borylation catalyst and it would be possible to achieve catalytic C-H borylation under milder reaction condition than that of well-known catalyst (Figure 1).[1,2] To estimate the electron donating ability of the alumanyl ligand, it would be important to synthesize carbonyl complexes having an alumanyl anion and to measure IR spectrum. If the alumanyl transition metal complexes could be synthesized systematically, they would be applied toward catalytic C-H functionalization of unactivated hydrocarbons such as benzene and alkanes.

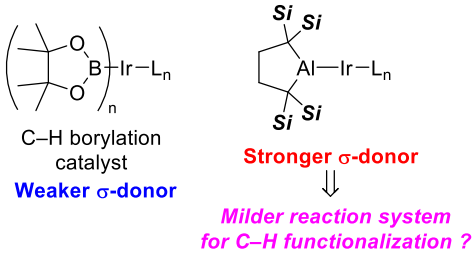

Figure 1. Alumanyl ligated iridium complex for C-H functionalization of unactivated hydrocarbons

In this thesis, the authors revealed the reactivity of dialkylalumanyl anion **1**, application as a ligand for transition metal complexes, and its properties. Further additional trials above would contribute to organometallic chemistry and main group chemistry in future.

reference

1. Cho, J.-Y.; Tse, M. K.; Holmes D.; Maleczka, E. R.; Smith R. M.; *Science* **2002,** 295, 305-308.
2. Ishiyama, T.; Takagi, J.; Ishida, K.; Miyaura, T.; Anastasi, R. N.; Hartwig, F. J. *J. Am. Chem. Soc.* **2002,** *124,* 390-391.

Full Publication List (Since 2015)

(At Chuo University: B4-M2)

1. Synthesis of Silaphenalenes by Ruthenium-Catalyzed Annulation between 1-Naphthylsilanes and Internal Alkynes through C–H Bond Cleavage
Yuichiro Tokoro, Kengo Sugita, Shin-ichi Fukuzawa
Chem. Eur. J. **2015,** *21,* 13229-13232.

2. Synthesis of Ferrocene-Fused Pyrans through Alkynoxy-Directed C–H Activation/Cyclization
Takashi Mitsui, Yuichiro Tokoro, Ryosuke Haraguchi, Kengo Sugita, Masato Harada, Yasunori Minami, Shin-ichi Fukuzawa, Tamejiro Hiyama
Bulletin. Chem. Soc. Jpn. **2018,** *91,* 839-845.

(At Nagoya University: D1-D3)

3. Cycloaddition of Dialkylalumanyl Anion toward Unsaturated Hydrocarbons in (1+2) and (1+4) Modes
Kengo Sugita, Ryo Nakano, Makoto Yamashita
Chem. Eur. J. **2020,** *26,* 2144-2147.

4. An Alumanylyttrium Complex with an Absorption due to a Transition from the Al–Y Bond to an Unoccupied d-orbital
Kengo Sugita, Makoto Yamashita
Chem. Eur. J. **2020,** *26,* 4520-4523.

5. One-Electron Reduction of Ti(IV) Complex by Dialkylaluminum(I) Anion Giving the Ti(III) Species
Kengo Sugita, Makoto Yamashita
Organomelltalics **2020,** *39,* Accepted.

Chapter 6

Acknowledgement

All the works have been done under supervision of Prof. Dr. Makoto Yamashita from 2017 to 2020 in Nagoya University. First of all, the author wants to thank Professor Dr. Makoto Yamashita for his persistent discussion, ideas, funding, and encouragement.

The author is very grateful to vice reviewer Prof. Dr. Takashi Ooi and Prof. Dr. Susumu Saito

The author would like to thank Lecturer Senior Lecture Dr. Jun-ichi Ito and Assist. Prof. Dr. Katsunori Suzuki, Assist. Prof. Dr. Ryo Nakano and Postdoctoral Fellow Dr. Shogo Morisako for the usual discussion and encouragement.

The authors would like to thank Ms. Shiho Takeyasu for the assistance of the office procedures.

The author would like to thank Mr. Satoshi Kurumada (Yamashita group) who firstly isolated dialkylalumanylpotassium that is used in the thesis for the usual discussion.

The author appreciates for Prof. Dr. Kenichiro Itami, Prof. Dr. Kei Murakami (Graduate School of Science in Nagoya University & Institute of Transformative Bio-Molecules, ITbM) for the GC-MS measurement, Prof. Dr. Hiroshi Shinokubo, Assist.Prof. Dr. Norihito Fukui, Mr. Keita Tajima (Graduate School of Engineering, Nagoya University) for the kind assistance of quantum yield estimation. Dr. Yukio Mizuta (JEOL Ltd.) for ESR simulation

The author also thanks Prof. Dr. Shin-ichi Fukuzawa (Graduate School of Science and engineering, Chuo University), Assist. Prof. Dr. Yuichiro Tokoro (Current; Yokohama National University), Assist. Prof. Dr. Ryosuke Haraguchi (Current; Chiba Insitute Technology) for their basic instruction by Master degree at Chuo University.

The author would like to acknowledge to Dr. Seiji Akiyama (Yamashita group) for the assistance of technical (mainly about DFT calculation) and mental support as a same period member for 3 years.

The author would like to thank all awesome Yamashita group members

Mr. Haruki Kisu, Mr. Tao Ding, Mr. Kuno Masaki, Ms. Wakano Taniguchi, Ms. Yasuho Nanba, Mr. Kaito Yamada, Ms. Ming Min Lee, Mr. Kazuyoshi Asaka, Ms. Aoi Okamura, Ms. Akemi, Kobayashi, Ms. Akane Suzuki, Ms. Yuna Yonekawa, Ms. Hyejin Lee, Ms. Yuria Otsuka, Mr. Katsumi, Sato, Mr. Ryotaro Yamanashi and all alumni members

The author thanks my buddies, Dr. Satoshi Nakane (Kitamura group, Graduate School of Pharmaceutical Sciences, Nagoya University) and Dr. Shuya Yamada (Itami group, Graduate School of Science, Nagoya University) for the support of the author’s research outside the Yamashita group.

The author also thanks same period friend in organic chemistry, Mr. Akio Urushima, (Yashima group) Mr. Yusuke Morita (Ooi group), Mr. Kohsuke Kato (Ooi group), Dr. Ryotaro Yamada (Itami group), Dr. Naoto Sahara, Dr. Takuya Mochizuki (Ishihara group), Dr. Shotaro Iwase (Kitamura group).

Finally, the author appreciates Ikuo Sugita, Junko Sugita, Mayu Sugita, Hideshiro Sugita, Reiko Sugita, Tokikatsu Suzuki, Chika Suzuki, Sugita family, Suzuki family, Yokoo family, Kawashimo family for kind assistance and financial supports for a long student life.

May 2020

Kengo Sugita